GEOMAR REPORT

GEOMAR

Helmholtz-Zentrum für Ozeanforschung Kiel

RV SONNE Fahrtbericht / Cruise Report SO244/2

GeoSEA: Geodetic Earthquake Observatory on the Seafloor

Antofagasta (Chile) – Antofagasta (Chile)
27.11.-13.12.2015

Berichte aus dem GEOMAR
Helmholtz-Zentrum für Ozeanforschung Kiel

Nr. 34 (N. Ser.)

Dezember 2016

GEOMAR

Helmholtz-Zentrum für Ozeanforschung Kiel

RV SONNE Fahrtbericht / Cruise Report SO244/2

GeoSEA: Geodetic Earthquake Observatory on the Seafloor

Antofagasta (Chile) – Antofagasta (Chile)
27.11.-13.12.2015

Berichte aus dem GEOMAR
Helmholtz-Zentrum für Ozeanforschung Kiel

Nr. 34 (N. Ser.)

Dezember 2016

GEOMAR
Helmholtz-Zentrum für Ozeanforschung Kiel

Das GEOMAR Helmholtz-Zentrum für Ozeanforschung Kiel ist Mitglied der Helmholtz-Gemeinschaft Deutscher Forschungszentren e.V.

The GEOMAR Helmholtz Centre for Ocean Research Kiel is a member of the Helmholtz Association of German Research Centres

Herausgeber / Editor:
Heidrun Kopp, Dietrich Lange, Katrin Hannemann, Anne Krabbenhoeft, Florian Petersen, Anina Timmermann and Scientific Crew SO244/2

GEOMAR Report
ISSN Nr.. 2193-8113, DOI 10.3289/GEOMAR_REP_NS_34_2016

Helmholtz-Zentrum für Ozeanforschung Kiel / Helmholtz Centre for Ocean Research Kiel
GEOMAR
Dienstgebäude Westufer / West Shore Building
Düsternbrooker Weg 20
D-24105 Kiel
Germany

Helmholtz-Zentrum für Ozeanforschung Kiel / Helmholtz Centre for Ocean Research Kiel
GEOMAR
Dienstgebäude Ostufer / East Shore Building
Wischhofstr. 1-3
D-24148 Kiel
Germany

Tel.: +49 431 600-0
Fax: +49 431 600-2805
www.geomar.de

Table of Content / Inhaltsverzeichnis

1. Cruise summary / Zusammenfassung

1.1 German / Deutsch

Die Reise SO244-2 des FS SONNE fand vom 27. November bis 13. Dezember 2015 vor der Küste Nordchiles statt. Ziel der Ausfahrt war es, das geodätische Meeresbodennetzwerk GeoSEA (**G**eodetic **E**arthquake **O**bservatory on the **SEA**floor) auf dem Kontinentalhang und der ozeanischen Platte im Bereich der südamerikanischen Plattengrenze um 21°S zu installieren. Dieses Segment der Subduktionszone zwischen der Nazca-Platte und Südamerika ist zuletzt im Jahre 1877 während eines Erdbebens gebrochen und wurde vor dem Iquique/Pisagua-Erdbeben im Jahr 2014 (Mw=8.1) als seismische Lücke identifiziert. Der südliche Abschnitt ist bisher nicht in einem rezenten Erdbeben gebrochen und befindet sich somit in der letzten Phase der interseismischen Periode des seismischen Zyklus. Die Methode der Meeresbodengeodäsie bietet eine Möglichkeit, Krustendeformationen in hoher Auflösung zu erfassen, was im marinen Bereich quasi das Analogon zu der an Land genutzten satellitengestützten GPS-Technologie darstellt. Das GeoSEA Netzwerk besteht aus autonomen Meeresboden-Transpondern, die auf etwa 4 m hohen Stahltripoden mit Hilfe des Geodrahtes des FS SONNE auf den Meeresboden abgefiert werden und mittels akustischer Signale für einen Zeitraum von bis zu 3.5 Jahren miteinander kommunizieren. Ein weitere Komponente des Netzwerkes ist GeoSURF: mit Hilfe dieses Wellengleiters kann sowohl die Funktionalität des Netzwerkes in der Tiefe überprüft werden, als auch die Daten zur Oberfläche transferiert werden, von wo aus sie per Satellitenverbindung weitergeleitet werden. Für die Installationen wurden drei Gebiete am mittleren und unteren Kontinentalhang sowie seewärts des Tiefseegrabens identifiziert, die während des ersten Fahrtabschnittes Leg I von SO244 mit einem autonomen Unterwasserfahrzeug (AUV) mit einer Auflösung von 2 m kartiert wurden. Das Netzwerk in Gebiet 1 (Area 1) auf dem mittleren Hang besteht aus 8 Transponderstationen, die paarweise auf vier topographischen Rücken stehen, die den Verlauf von Verwerfungen markieren. In Gebiet 2 (Area 2) auf der ozeanischen Platte seewärts der Deformationsfront (‚outer rise') messen fünf Transponder die Öffnung von Extensionsbrüchen. Das dritte Messgebiet (Area 3) befindet sich in Wassertiefen von über 5000 m auf dem unteren Kontinentalhang, wo insgesamt 10 Stationen den diffusen tektonischen Spannungsaufbau verfolgen. Daten aller drei Netzwerke und aller Stationen konnten erfolgreich von GeoSURF bzw. von einem HPT Modem, das vom FS SONNE zu

Wasser gelassen wurde, geladen und gesichert werden. Die Netzwerkinstallation bestehend aus insgesamt 23 Meeresbodenstationen wurde am 7. Dezember erfolgreich abgeschlossen. Anschließend wurden 14 Ozeanbodenseismometer (OBS) in der Region ausgebracht, um die seismische Aktivität aufzuzeichnen. Diese Geräte sollen im Frühjahr/Sommer 2016 von Bord des U.S.-amerikanischen Forschungsschiffes RV LANGSETH geborgen werden.

1.2 English / Englisch

RV SONNE cruise SO244-2 sailed offshore northern Chile from Nov. 27 to Dec. 13, 2015 to install the seafloor geodetic network GeoSEA (**G**eodetic **E**arthquake **O**bservatory on the **SEA**floor) on the marine forearc and outer rise of the South American subduction system around 21°S. This segment of the Nazca-South American plate boundary has last ruptured in an earthquake in 1877 and was identified as a seismic gap prior to the 2014 Iquique/Pisagua earthquake (Mw=8.1). The southern portion of the segment remains unbroken by a recent earthquake and is currently in the latest stage of the interseismic phase of the seismic cycle. Seafloor geodetic measurements provide a way to monitor crustal deformation at high resolution comparable to the satellite-based GPS technique upon which terrestrial geodesy is largely based. The GeoSEA Network consists of autonomous seafloor transponders installed on 4 m high tripods, which were lowered to the seabed on the deep-sea cable of RV SONNE. The transponders within an array intercommunicate via acoustic signals for a period of up to 3.5 years. An additional component of the network is GeoSURF, a self-steering autonomous surface vehicle (Wave Glider), which monitors system health and is capable to upload the seafloor data to the sea surface and to transfer it via satellite. We have chosen three areas on the middle and lower slope and the outer rise for the set-up of three sub-arrays. The array in Area 1 on the middle continental slope consists of 8 transponders located in pairs on four topographic ridges, which are surface expressions of faults at depth. Area 2 is located on the outer rise seaward of the trench where 5 stations monitor extension across plate-bending related normal faults. The third area is located at water depth >5000 m on the lower continental slope where an array of 10 stations measures diffuse strain build-up. Data from all networks and all stations were successfully uploaded to GeoSURF and/or a HPT modem lowered into the water from RV SONNE. The seabed installation of a total of 23 transponders was completed by

December 07, when we proceeded to deploy a total of 14 ocean bottom seismometers (OBS) on the forearc between 19.2°-21.6°S. These instruments will be recovered by RV LANGSETH in Spring/Summer 2016.

2. Participants / Teilnehmer

2.1 Principal investigators / Leitende Wissenschaftler

Name		Institution
Prof. Dr. Heidrun Kopp	Chief Scientist	GEOMAR
Dr. Dietrich Lange	Co-Chief Scientist	GEOMAR

2.2 Scientific party / wissenschaftliche Fahrtteilnehmer

Name		Institution
Katrin Hannemann	Geodesy	GEOMAR
Florian Petersen	Geodesy	CAU
Dr. Anne Krabbenhöft	Geodesy Array, OBS	GEOMAR
Darren Murphy	Telemetry	Sonardyne Ltd.
Henning Schröder	OBS	GEOMAR
Klaus-Peter Steffen	Transducer Deployment	GEOMAR
Torge Matthiesen	Transducer Deployment	GEOMAR
Patrick Schröder	Telemetry	GEOMAR
Lina Buchmann	Technician	GEOMAR
Margit Wieprich	OBS	GEOMAR
Ann-Marie Völsch	Watch keeper	GEOMAR
Florian Gausepohl	Watch keeper	GEOMAR
Manuel Moser	Watch keeper	CAU
Eduardo Contreras-Reyes	Seismology	Universidad de Chile
Jose Mieres	Seismology	Universidad de Chile
Prof. Dr. Jan Behrmann	Bathymetry	GEOMAR
Tanja-Anina Timmermann	Watch keeper	CAU
Jan Steffen	Watch keeper & PR	GEOMAR
Frank Benitsch	Watch keeper	GEOMAR
Jasna Haro Gomez	Observer	SHOA

2.3 Crew / Mannschaft

Name	
Lutz Mallon	Master
Nils Aden	Chiefmate
Jens Göbel	2. Mate
Ulrich Büchele	2. Mate
Dr. Sabine Heuser	Surgeon
Achim Schüler	Chief Engineer
Tim Stegmann	2nd Engineer
Steffen Genschow	2nd Engineer
Jörg Leppin	Chief Electrician
Hermann Pregler	System Operator
Matthias Grossmann	System Operator
Thomas Beyer	Electrician
Henning De Buhr	Electrician
Volker Blohm	Fitter
Lothar Münch	Motorman
Matyas Talpay	Motorman
Sebastian Thimm	Motorman
Andreas Schrapel	Bosum
Arnold Ernst	Ship Mechanic
Benjamin Brüdigam	Ship Mechanic.
Ingo Fricke	Ship Mechanic
Oliver Eidam	Ship Mechanic
Sascha Fischer	Ship Mechanic
Stefan Burzlaff	Ship Mechanic
Torsten Kruszona	Ship Mechanic
Frank Tiemann	Chief Cook
Andre Garnitz	Cook
Andreas Pohl	Chief Steward
Maik Steep	Steward
Rene Lemm	Steward
Sylvia Kluge	Stewardess

Figure 2.1: Group photo of the SO244-2 scientific crew.

3. Narrative of the cruise / Ablauf der Forschungsfahrt

Cruise SO244-2 commenced in Antofagasta, Chile, on November 27, 2015, where 24 scientists from Chile, Germany and Great Britain embarked on RV SONNE. The vessel left port at 09:30 h local time to start on the transit north to 21°S/71°W. The previous days in port as well as the transit were used to prepare our gear, in particular to set up the first eight 4 m high steel tripods on the aft working deck and to synthetically model the GeoSEA array layout and geometry for working area 1 based on the AUV seafloor bathymetry maps acquired during Leg I of SO244. We arrived at the first deployment site on Nov. 28, 2015 at 05:30 h to map a 2 nm short profile across the planned deployment sites with the EM122 multibeam system set to a beam width of 90°. This was followed by a CTD deployment to a water depth of 2500 m to compare the variations in time of the sound speed profile to the AUV-based CTD measurements conducted during Leg I. At 10:00h and 20°47,943'S/70°48,910'W, station A 301 was veered from the aft deck with the deep-sea cable to an initial water depth of 200 m when the cable was put on hold to deploy a HPT dunker modem over the starboard side of RV SONNE. While on hold,

tension on the deep-sea cable suddenly decreased, indicating that the tripod was in a free-fall mode towards the seafloor at 2733 m water depth. Due to the quick response of the deck's crew and the scientific crew the hook of the heavy weight releaser to which the tripod is attached could be released and the instrument as well as the floats were rescued. With the dunker modem we could monitor the decent (~1 m/s with float vs. 2 m/s without) and touch down of the tripod on the seafloor. As the barycenter of the tripod is located at its base, the instrument landed upright and could be pinged immediately. It was released approximately 60 m away from its planned position and could later be included in the network as a full-scale node. After some modifications to the suspension bracket we continued with the deployment of station A102 at 16:00 h at 20°47,677'S/70°48,460'W in a water depth of 2603 m. At 19:30h we received confirmation that both beacons respond and communicate properly with each other.

On November 29 we deployed stations A103, A104, and A105 to water depths ranging from 2620 m to 2865 m. All five stations respond properly to the acoustic interrogation sent via dunker modem from RV SONNE. The line-of-sight between all instruments is clear. We left the first working area to return towards the end of the cruise for the deployment of the remaining three stations. On the transit to Area 2 on the outer rise seaward of the trench we conducted an EM122 survey to increase the data quality of the existing map acquired during Leg I.

We arrived in working area 2 on November 30 and started to deploy station A201 at 06:00h at 21°03,370'S/71°43,846'W at a water depth of 4105 m. After sending the release command when the station had reached the seafloor, we did not receive an answer from the release unit and hence heaved the tripod by 30 m off the seafloor. After repeatedly sending release commands from the ship's Posidonia system as well as from IXSEA's release box and hydrophone, the station released and was safely installed on the seafloor. After swopping the IXSEA release unit for the following station A202, it was lowered into the water at 12:00h and reached the seafloor at 13:45h. We only succeeded to release it after several hours at 16:00h after conducting an acoustic reset of the release unit. We still did not receive a reply, but could see from the Posidonia tracker that the station had released. Both stations communicate with the dunker modem as well as with each other. We continued to

deploy station A203, which was veered into the water column at 18:15h. However, we could not establish communication with this station once it was on the seafloor and hence heaved it back onto the working deck of RV SONNE where it was safely recovered on…

…December 1, 2015 at 04:00h. We exchanged the releaser for a heavy weight IXSEA RT8 unit and again lowered station A203. While veering, we deployed the wave glider GeoSURF at 07:30h and commanded it to sail above station A202 to establish a data connection with the station. Station A203 was released at a water depth of 4065 m at 10:20h, however, we only could confirm the release after heaving the cable by 30 m and confirming that the station remained on the seafloor. After the gear was safely recovered, we could see that the release unit was covered by sediment and hence must have fallen to the seafloor. This led us to test the capacity of the float, which turned out to be too low to keep the release unit floating in the water column. We added a second Benthos sphere to the system. At 13:10h we prepared the deployment of station A204, which however slipped from the heavy weight release and hence was deployed in free-fall mode to a water depth of 4034 m where it landed upright with a tilt of 2°. We continued with the deployment of station A205, which was lowered to the seafloor at 15:20h and released two hours later using the ship's Posidonia system. Communication to all stations and within the network was confirmed. GeoSURF successfully uploaded data from stations A201, A202 and A204 before we had to recover it using the rescue boat of RV SONNE before night fell.

Over night we started our transit to working area 3, again mapping the transit path using the EM122 system. We arrived in our last working area in the morning of December 2, and started to deploy station A301 at 20°47,034'S/71°04.011'W at a depth of 5243 m. Due to the great water depth of >5000 m in this area, we could only achieve two deployments and installed station A302 at 20°47,561'S/71°04,945'W at a water depth of 5367 m in the afternoon.

Deployment continued the next day, December 3, 2015, with stations A303 in the morning at 20°46,853'S/71°03,520'W at a depth of 5200 m and station A304 in the afternoon at 20°46,565'S/71°04,635'W at a depth of 5336 m in the afternoon.

Deployment of both stations went smoothly; both were released by Posidonia after confirming their line-of-sights to the neighboring stations. Each deployment lasts approximately 5 hours, which led us to deploy three stations on…

…December 4, 2015 after using the night hours to acquire additional bathymetry data in the deep-sea trench. Installation of stations A305 through A307 went without any problems from 06:00h to 20:30h. Communication between stations and with the dunker modem on board RV SONNE was trouble-free and the stations have free line-of-sight and a maximum tilt of 5°.

Deployment of the last stations in area 3 (A308 – A310) in water depth of 5095 m to 5220 m was successfully completed on December 5 at 21:00 h. During recovery of the releaser of station A310 the connecting line ripped apart above the Benthos spheres. Both floatation spheres as well as the heavy weight release unit got entangled in the portside propeller of RV SONNE, as could be verified by video. RV SONNE turned off the propellers as night fell and drifted slowly northwards carried by the Humboldt current.

On the morning of December 6 in the daylight we tried to free the propeller from the entangled material, however we did not succeed. We commenced our 12 nm long transit back to working area 1 to install the first of the remaining three stations (A106). This station immediately responded to the pings from the five stations already deployed in the network as well as to RV SONNE. This success was a vague consolation for the fact that one or both of the Benthos spheres must have imploded during transit. Fortunately the heavy-weight release unit pulled both spheres as well as the remaining line to depth, setting the portside propeller free so that it could be utilized unconditionally. In the afternoon of December 6 we deployed station A107 before heading to shallower water depth for a high-resolution mapping survey in the area between 20°40’S/70°32’W and 21°01’S/70°39’W using Kongsberg’s multibeam EM710 system, which is permanently installed on RV SONNE.

We returned to working area 1 on December 7 to deploy the last GeoSEA station A108 at 08:00h. At 14:30h we deployed the first of a total of 14 ocean bottom seismometers (OBS), which will record the seismic activity on the northern Chilean

forearc until spring/summer 2016, when they will be recovered from RV LANGSETH. OBS deployment for stations OBS02-OBS13 continued until 08:45h the next day.

On December 8 we returned to working area 1 to deploy GeoSURF here, which traveled autonomously until the next day. After deployment of GeoSURF we continued to working area 3 where we deployed OBS01. In addition, we retrieved data from the GeoSEA stations using the HPT dunker modem and re-configured the logging settings for the sub array.

We recovered GeoSURF in the morning of December 9 after it successfully uploaded data from the GeoSEA stations in working area 1. At 13.00h we returned to working area 3 to verify that the re-configuration of the array has executed properly. We left here at 16:30 to begin our transit west to working area 2, where we arrived at 20.30h to again deploy GeoSURF for the night while RV SONNE mapped previously uncharted seafloor west of the trench.

By 09:00h on December 10, GeoSURF was safely back on deck and all data were uploaded and secured. We now headed on our final bathymetry grid south of working area 2. Mapping continued until 24:00h on Dec. 11, covering a total of 8814 km^2 in this area. RV SONNE then headed south to commence our transit towards the port of Antofagasta. During transit, we deployed our final OBS south of the Iquique/Pisagua earthquake aftershock region. RV SONNE safely reached the pilot station at Antofagasta harbor on Dec. 13 at 08:00h and berthed at 08:30h, terminating cruise SO244-2. Throughout the cruise weather conditions were optimal, always calm seas and no rain.

Figure 3.1 shows a track plot of SO244-2.

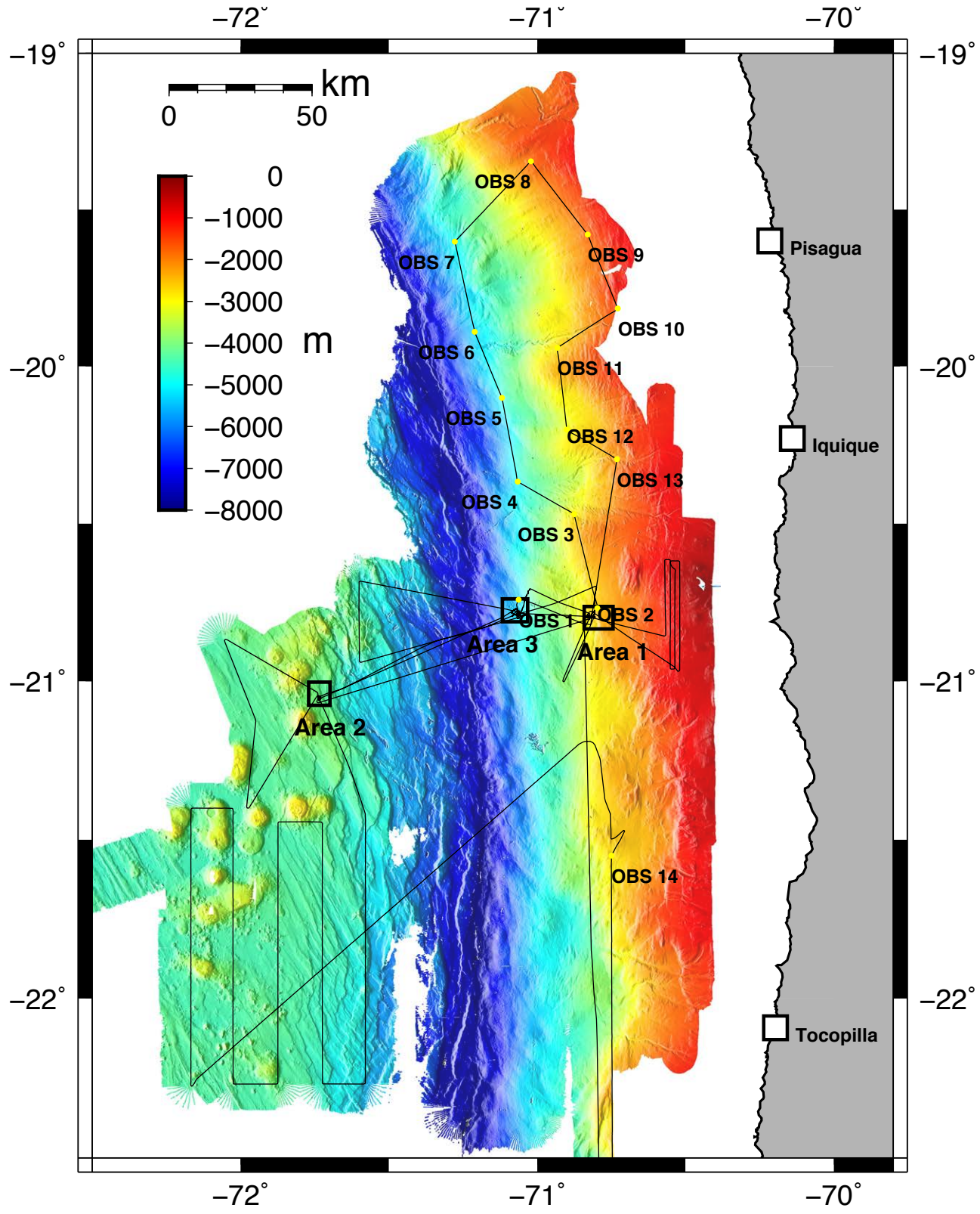

Figure 3.1: Ship track of RV SONNE cruise SO244 Leg II.

4. Aims of the Cruise / Zielsetzung der Forschungsfahrt

The primary aim of cruise SO244-2 was to install an autonomous seafloor geodetic array to record deformation on the northern Chilean continental margin. The motivation for seafloor geodetic measurements lies in the fact that our understanding of earthquake processes in the framework of classic elasticity theory is well developed (e.g. Kanamori and Brodsky, 2005), while the evolution of strain through the interseismic and co-seismic phases remains poorly understood. The ability of terrestrial geodetic networks to precisely measure crustal deformation with millimeter accuracy in the form of lateral movement and/or vertical displacement has enormously advanced our knowledge of fault slip and earthquake rupture propagation over the past decade (e.g. Hsu et al., 2006; Briggs et al., 2006; Liu et al., 2010; Lay et al., 2012). They have documented the active accumulation of interseismic strain, and subsequent strain release associated with devastating earthquakes (Heki, 2011). Much of the elastic strain build-up and release associated with large subduction zone earthquakes, however, occurs offshore (Kopp, 2013). The satellite-based GPS technique upon which terrestrial geodesy is largely based is not applicable in oceanic areas due to the opacity of seawater to electromagnetic radiation. As a result, our knowledge of the real-time crustal deformation has so far ended at the global shorelines, imposing severe limitations on the effectiveness of present-day models. Seafloor geodetic measurements provide perhaps the only way to successfully deal with these problems (Newman, 2011), allowing us to directly measure deformation in some of the most active (and potentially destructive) places on Earth. The seafloor represents the critical interface between the ocean and the geosphere where processes occurring at depth are transferred and manifested in seafloor deformation. The ability to observe and monitor seafloor deformation using newly developed marine technology and vastly improved resolution will advance our understanding of subduction zone seismicity and will improve spatial and temporal hazard assessment. The technological developments in the past ~10 years have led to a new generation of submarine transducers, which are now capable of rendering an improved resolution that makes seafloor geodetic measurements feasible for tectonic investigations.

Seafloor displacement occurs in the horizontal (x,y) and vertical direction (z) as a function of time (t). The vertical displacement is measured by monitoring

pressure variations at the seafloor. Horizontal seafloor displacement can be measured either using an acoustic/GPS combination to provide absolute positioning or by long-term acoustic telemetry between different beacons fixed on the seafloor to determine relative distances by using the travel time observations to each other, which is the technique used in the current GeoSEA array set-up (Figure 4.1). The scientific target is to measure seafloor deformation as a function of elastic strain above the submerged up-dip region of the seismogenic locked zone off northern Chile. In this approach the overarching goal is to identify the extent of the locked zone. Elastic strain is a function of convergence rate, fault geometry and locked zone. Elastic strain on the continent is observed with land-based geodetics, convergence rate is obtained from far-field GPS, thrust-fault geometry is known from deep-sounding seismics and seismology and seafloor geodesy is needed to solve for the locked zone (deformation measurement of up-dip region).

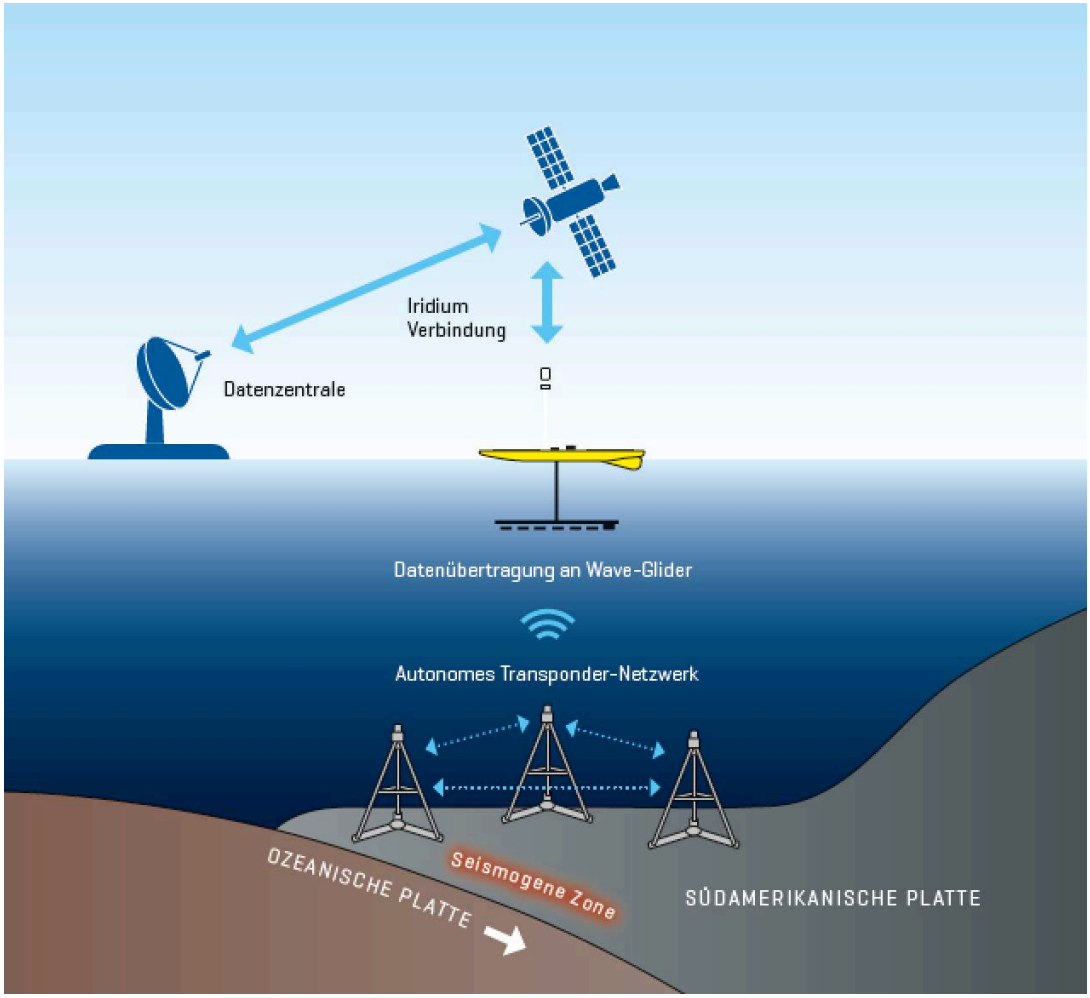

Figure 4.1: Sketch of the GeoSEA array and GeoSURF (C. Kersten, GEOMAR).

In addition to the installation of the GeoSEA array and the set up of communication with GeoSURF, monitoring of seismic activity in the survey region was defined as a secondary goal in order to later merge the geodetic and seismological data. To this end, a total of 14 OBS were installed on the forearc between 19°-22°S in November 2014 from the Chilean navy vessel OPV Comandante TORO (Armada de Chile) and recovered during Leg I of SO244. These instruments were re-deployed during Leg II in the aftershock region of the April 1, 2014 Iquique/Pisagua earthquake to be recovered in 2016 by the RV LANGSETH.

5. Setting of the working area / Beschreibung des Arbeitsgebiets

The Chilean convergent margin forms part of the global subduction zone system where the majority of global earthquakes occur. During great earthquakes (M>8) along these convergent plate boundaries the shallow interface between the plates ruptures and rupture propagates down to depths of ~50 km. The Chilean deep-sea trench marks the onset of subduction underneath the South American continent and the seismogenic zone where large ruptures occur is almost exclusively located beneath the marine forearc. The Nazca-South American plate boundary system which includes our working area has been the site of a number of recent large earthquakes, including the April 1, 2014 Iquique/Pisagua event with a magnitude of M_w=8.1 (e.g. Lay et al., 2014). This earthquake ruptured a portion of the Iquique segment. Segments sometimes fail in numerous smaller events over a time period of decades and at other times in large events that span the entire segment. Plate convergence between the Nazca and South America plates occurs at a rate of 65 mm/yr (Béjar-Pizarro et al., 2010) and approximately 8.5 m of slip has accumulated over the last ~130 years. Although the northern Chile subduction zone failed in "moderate" M_w 7.7 and 8.3 events in 2007 and 2014 (Figure 5.1 A), these have not fully released the strain accumulated due to plate convergence since 1877 (e.g. Schurr et al., 2014). The temporal and spatial history of the Iquique earthquake sequence and its correlation to the pre-earthquake locking pattern as recorded by geodetic and seismological instrumentation onshore has recently been described in detail by Ruiz et al. (2014), Lay et al. (2014), and Schurr et al. (2014).

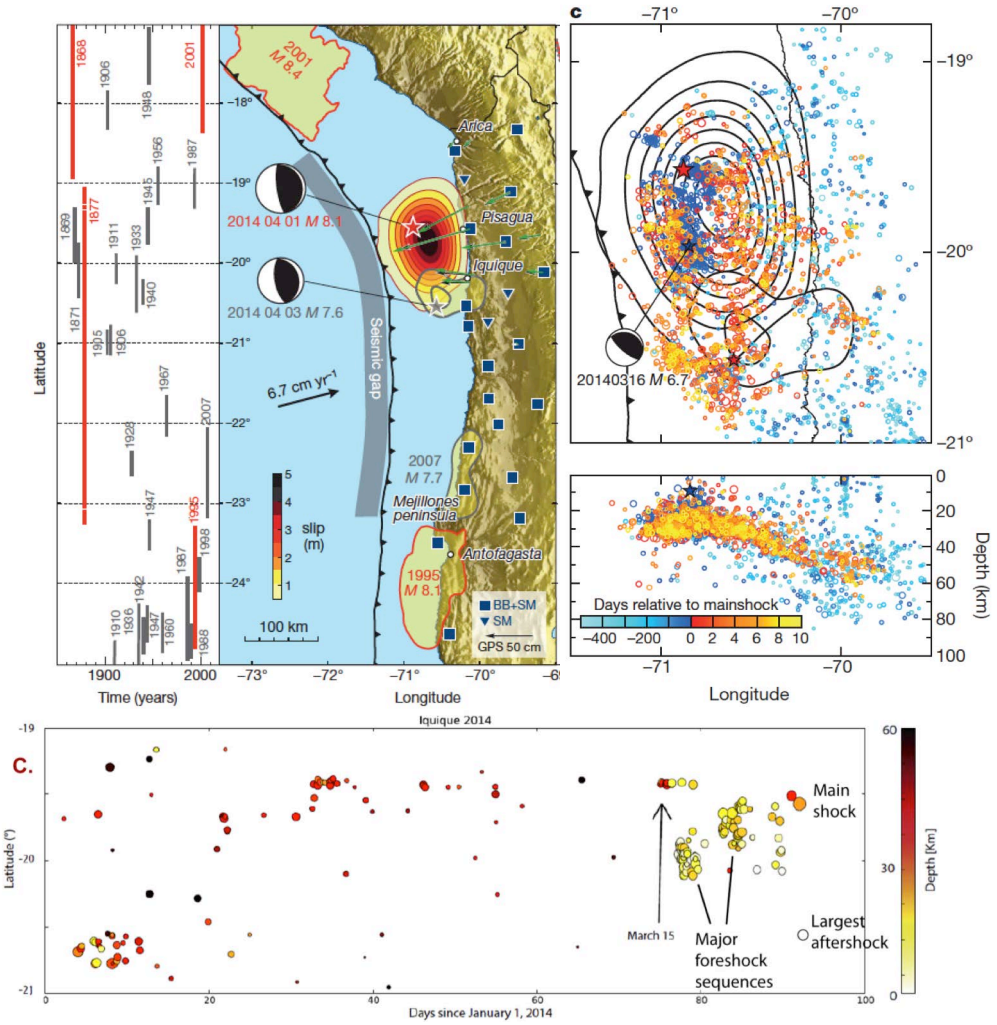

Figure 5.1: Top left (A): Map of the northern Chilean subduction zone and adjacent Nazca plate showing the seismic gap and the location of the 2014 Iquique earthquake and the rupture areas of the 1995 Antofagasta (red, ~24°S), 2001 Peru and 2007 Tocopilla (grey, 22.5°S) earthquakes (from Schurr et al., 2014). Top right (B): Fore- and aftershock seismicity of the Iquique event (Schurr et al., 2014). Lower panel (C): Time/space history of precursory activity (from Ruiz et al., 2014, supplementary material; labels and largest aftershock were added).

Seismicity in the region started increasing around 2008, with several clusters of small (M>4) earthquakes on the plate boundary in this region, including a cluster near the April 1, 2014 hypocentre. The current sequence started with two M_w 5.7 events in January 2014 near the southern boundary of the April 1 rupture zone (Figure 5.1 C). A major foreshock with M_w 6.7 occurred on March 16 (Figure 5.1 B) followed a week later by two M_w 6.2 foreshocks on a patch distinctly north of the March 16 sequence and near the epicentre of the April 1 earthquake. Both patches of foreshock activity were near the up-dip edge of the eventual rupture plane. The fault plane for the first foreshock was oriented ~70° to the NW relative to the plate motion direction and to the fault planes of the other foreshocks, the main shock, and

several of the large aftershocks (Ruiz et al., 2014). Subsequent events showed mechanisms consistent with the plate motion. This suggests the rupture of a structural heterogeneity that rotated the axes of the stress field for the first foreshock. There is also geodetic evidence that the March 16 event might have initiated slow slip on the portion of the fault that ruptured on April 1 (Ruiz et al., 2014) and a gradual unlocking of the plate boundary before the 2014 Iquique/Pisagua earthquake (Schurr et al., 2014).

For the installation of the GeoSEA array, we chose the forearc area around 21°S (south of the Iquique/Pisagua earthquake rupture zone). The GeoSEA array was installed on the lower and middle slope of the marine forearc, because it is here above the updip limit of the seismogenic zone that we expect the largest deformation (Wang et al., 2012) due to the episodic loading at the trench. The high-resolution bathymetry data acquired during Leg I of cruise SO244 using the ship-based EM122 multibeam system covered the area between 70.5°W-71.5°W, which includes the continental slope down to the deep sea trench (compare Cruise Report FS SONNE cruise SO244 Leg I). Landward to the trench and the deformation front, a small active frontal prism of 5-10 km width lies adjacent to the lower slope. Subducting seafloor-spreading fabric modulates the morphology of the frontal prism and the lower slope. Normal faulting is widely observed on the middle slope and has been attributed to subduction erosion. The deployment areas for the GeoSEA sub-arrays were chosen based on the following criteria: (1) water depth between 2000 m and 6000 m, (2) little to no sediment cover and no turbidite channels or evidence for mass wasting events, (3) fault scarps not exceeding 100 m height, (4) evidence for active deformation. Furthermore, the sub-arrays should be spread on the middle and lower slope as well as on the outer rise.

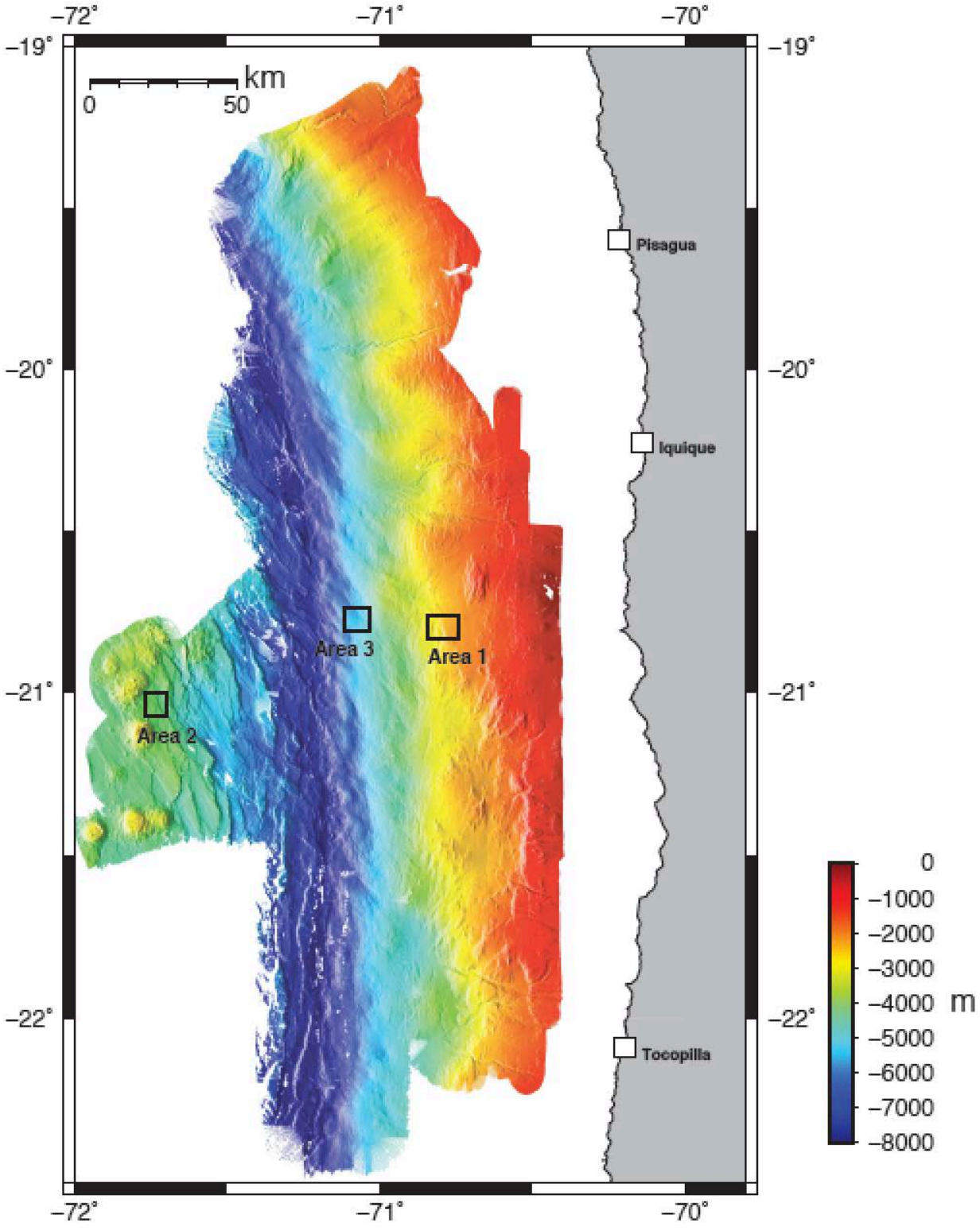

Figure 5.2: Bathymetry map with Areas 1-3. The three areas are described in detail below.

The installation of the GeoSEA seafloor geodetic array is complemented by onshore observations so that we are able to fully cover and record deformation affecting the forearc above the seismogenic zone in its entirety – regardless of whether it is offshore or onshore. This is possible because the Iquique segment is also the location of the onshore Integrated Plate Boundary Observatory Chile (IPOC), which is a distributed system of instrument networks run by a European-South American cluster of institutions dedicated to the study of earthquakes and deformation of the continental margin of Chile. IPOC is composed of a suite of onshore instrument arrays, including GPS, seismometers and tiltmeters (Figure 5.3). Offshore seismicity, however, is not well constrained due to a lack of offshore stations. The position of the megathrust is inferred from onshore stations and existing refraction data in its vicinity (e.g. Contreras-Reyes et al., 2012, Béjar-Pizarro et al., 2010).

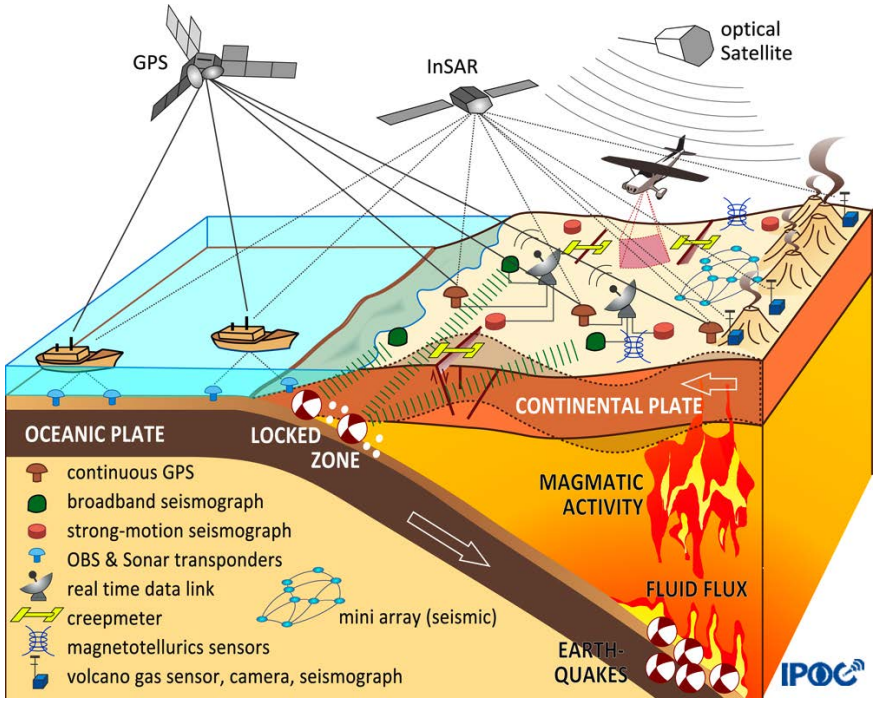

Figure 5.3: Location map of the IPOC observatory showing station distribution onshore in northern Chile (http://www.ipoc-network.org). The seafloor geodetic array extends the observations to the offshore domain around 21°S.

Working **Area 1** (Figure 5.4) is located on the middle slope of the continental margin in water depth of approximately 2500 m. An area of approximately 35 km^2 was mapped during Leg I of SO244 using the AUV ABYSS of GEOMAR focusing on a westward dipping normal fault. Several adjacent faults can also be identified in the

map, some of which terminate in an undisturbed sediment pond and show little evidence for recent activity. The main targeted fault is characterized by abundant mass wasting features generally not exceeding lengths of ~80 m across. Baselines across these faults will yield information on compressive trench perpendicular motion as well as any possible strike-slip component resulting from slip partitioning.

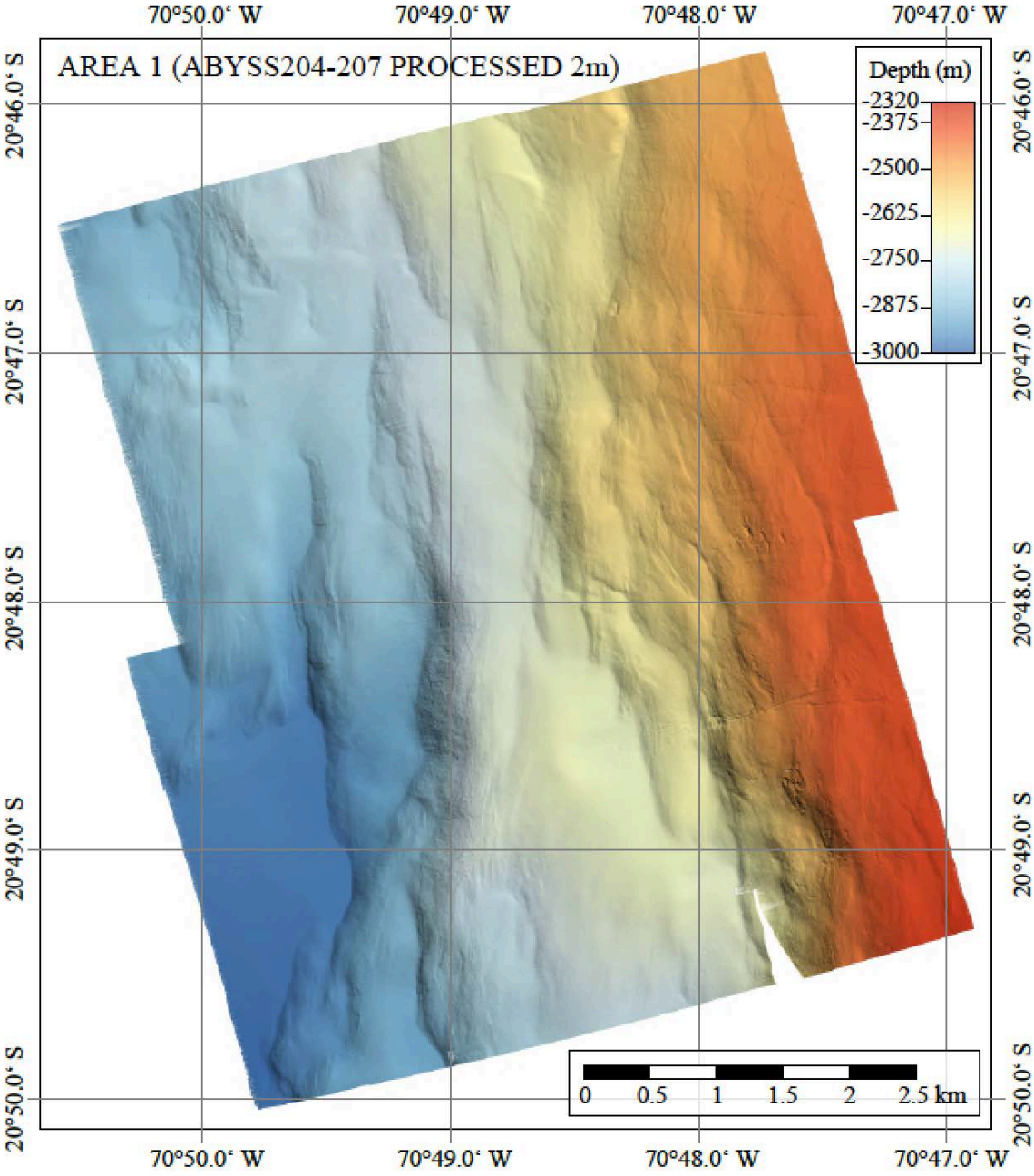

Figure 5.4: Working Area 1.

Area 2 is located on the outer rise of the Nazca plate about 100 km west of Area 1 and encompasses approximately 17 km^2 (Figure 5.5). Two eastward dipping

scarps are the dominant features in the area, which are interpreted to be normal faults that disturb the inherited volcanic features. The overall appearance of Area 2 is generally much smoother compared to Area 1, suggesting a drape of little disturbed sediment. This area was chosen because it offers the opportunity to measure the extension across bending-related trench-parallel normal faults, requiring only a minimal number of stations.

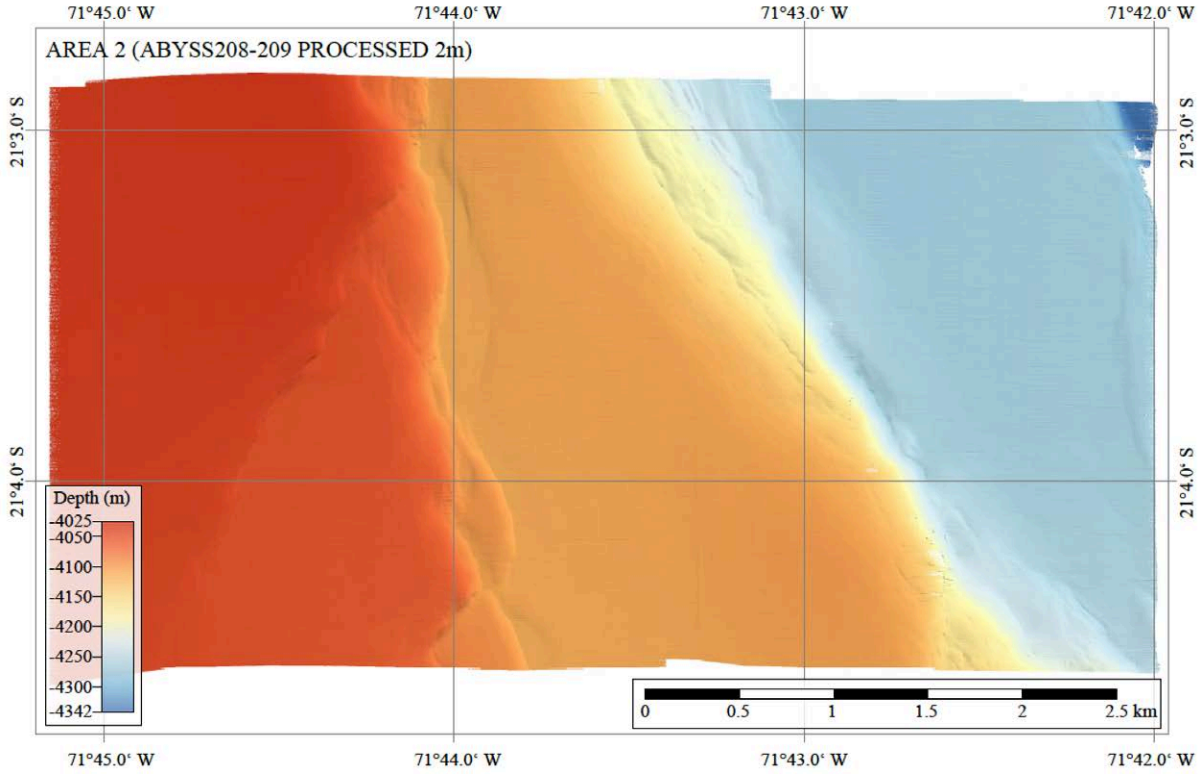

Figure 5.5: Working Area 2.

Area 3 is positioned on the lower continental plate at water depth exceeding 5000 m (Figure 5.6). The areal extent of the mapped region is approximately 35 km^2, located approximately 10 km east of the trench. The region is characterized by numerous ridges trending in a NW-SE direction of 140° with heights of up to 500 m and slopes exceeding 15°. A number of flat terraces and peaks are identified in the area, which are suitable for the installation of a GeoSEA tripod. The main target in this complex area is to measure diffuse strain over long baselines. The bathymetry and Parasound data collected during Leg I yield no indication for larger sediment accumulations.

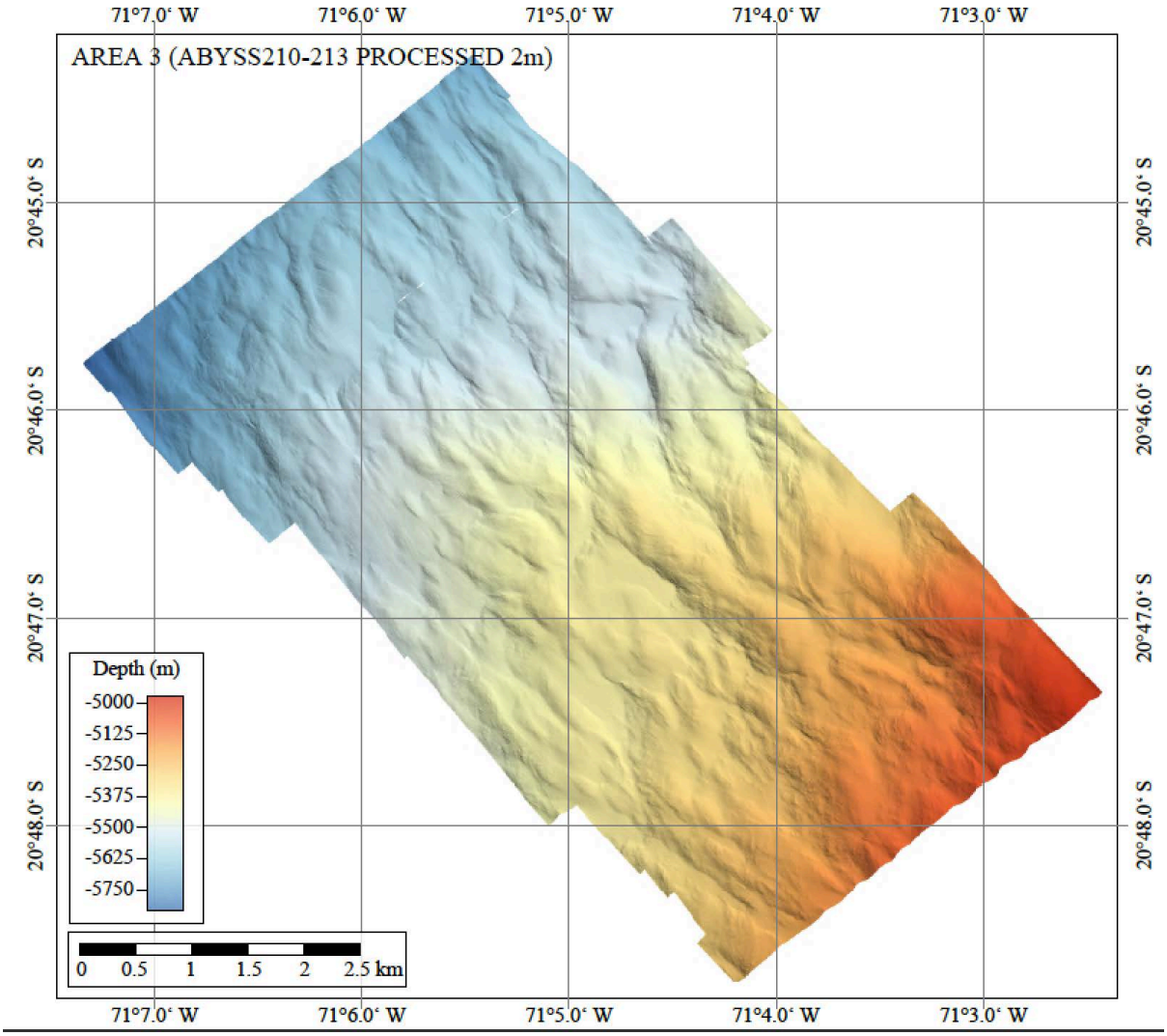

Figure 5.6: Working Area 3.

6. Work details and first results / Beschreibung der Arbeiten im Detail einschließlich erster Ergebnisse

6.1 Seafloor Geodesy

6.1.1 Method

The key problem in seafloor geodesy experiments is to minimize the errors in the distance measurements to be able to detect, over a reasonable time period, the relatively small seafloor displacements which are occurring. Seafloor acoustic ranging methods provide relative positioning by using precision acoustic transponders (Autonomous Monitoring Transponder, AMT) that include: high-precision pressure sensors (to monitor possible vertical movements as well as the tide effect (e.g., Ballu et al., 2009a, b)); tiltmeters in order to measure their inclination

as well as any change in the seafloor; and sound velocity (SV) sensors to correct sound speed variations. Acoustic signals (~13-18 kHz) are transmitted between seafloor reference points to provide two-way travel times in repeated interrogations over months to years to determine displacements (e.g., Chadwell and Sweeney, 2010) and, hence, deformation. This method is routinely used in industry, for oil field or pipeline monitoring for example. However, these studies target a much lower spatial resolution of baselines in the cm range and deployment times of much shorter time spans. As to gradiodynamic studies, results obtained by Osada et al., (2008) and Chadwell and Spiess (2008) proved satisfactory, with a repeatability of 2 mm over a baseline of 750 m. This method is the only one capable to continuously monitor horizontal and vertical ground displacement rates in the submarine environment and to characterize fault behavior (locked or aseismically creeping), as it is now routinely done on land along active deformation zones using InSAR technique and DGPS continuous monitoring (e.g., Michel and Avouac, 2002; Delacourt et al., 2009; Dzurisin, 2003). Vertical deformation using pressure sensors was documented at Axial Seamount at 15 cm/yr due to inflation/deflation using pressure gauges (Chadwick et al., 2012). Furthermore, Philips et al. (2008) reported an uplifting of Kilauea's south flank at ~9 cm/yr and offshore Sumatra, pressure gauges recorded fluctuations of 8 mbar concurrent with the Mw=7.7 2006 Java earthquake (Boebel et al, 2010).

The important measurement to be made is the change in the position of a set of points as a function of time, such as interseismic creep or the displacement due to an earthquake. The objective of cruise SO244-2 was to install a network which is designed to measure distance changes with a repeatability in the mm range for distances in the km range (strain~$1E^6$). Prior to the installation, high-resolution bathymetric maps of the seafloor are generated using the shipborne multibeam system, and, more importantly, an AUV, to allow the modeling of the line-of-sight within the array. These maps are instrumental in characterizing tectonically active fault scarps at the seafloor, and will help to interpret the results of the seafloor geodetic survey, as well as allowing inferences regarding the active tectonics of a much larger area. Bathymetric mapping also serves as a "base-line" characterization of the whole area, and is used as a reference data set for subsequent re-surveying

either to measure areal deformation based on interferometry or for precise ground movement studies following an earthquake.

The measurements take the form of two complementary components to allow errors between the different methods to be determined and corrected:

1. The relative positions of the benchmarks are determined by acoustic triangulation methods using transponders/transmitters mounted on each benchmark. This is essentially an inverted form of long-baseline navigation. These measurements involve only the propagation of acoustic signals in the lowermost portions of the water column and along a ray path, they consequently profit from the fact that the expected temporal variability in the sound speed structure is minimal at great water depth and any effects can be minimized using signal processing techniques. The time of flight of acoustic signals between the transponders is combined with the depth information received form the pressure data and the AUV mapping and the speed of sound in water in the local area to determine the distance between the transponders.

2. Measuring absolute height changes by acoustic methods is substantially more difficult because of the variable deep ocean sound velocity structure. Measuring relative vertical displacements is also somewhat more complicated as variations in water pressure related to tides, ocean currents etc. introduce systematic errors. By measuring hydrostatic pressure, height changes such as uplift or subsidence might be resolved.

6.1.2 Instrumentation: GeoSEA Array and GeoSURF Wave Glider

In 2012 GEOMAR purchased the GeoSEA array consisting of 35 autonomous acoustic monitoring transponder (AMT) platforms and the autonomous surface vehicle GeoSURF (BMBF project 03F0658I). AMT Type 3505-6315 is manufactured by Sonardyne International Ltd., UK; the GeoSURF wave glider is manufactured by LiquidRobotics, USA. The AMTs include acoustic transponders/transmitters, acoustic modems, tiltmeters, and pressure gauges rated for 6000 m water depth (Figure 6.1.2).

Figure 6.1.2.1: Autonomous Monitoring Transponder (AMT) installed in tripod frame (J. Steffen).

For horizontal direct path measurements, the system utilizes acoustic ranging techniques with a ranging precision better than 15 mm (Sensor specifications for Sonardyne AMT Type 8305-6315) and long term stability over 3 km distances. Vertical motion is obtained from pressure gauges (Sensor specifications: PreSens pressure sensor, precision: ±0.0001%). Integrated inclinometers to monitor station settlement have an accuracy of ±1°. Data are acquired and recorded autonomously subsea without system or human intervention at sample rates between 90 and 180 minutes. These data can then be recovered via the integrated high-speed acoustic telemetry link without recovering the AMTs. When requested to do so, the stored data will be transmitted wirelessly up to GeoSURF for onward transmission via a satellite link to the shore for near-real time assessment. Alternatively, the data can be downloaded using a HPT dunker modem lowered to ~80 m from a vessel.

Transponders can be pre-configured with the chosen log regime prior to deployment using a laptop with a serial test cable set up. Once programmed, the transponders are deployed in frames and lowered to the seabed. The frames are 4 m high galvanized steel tripods (Figure 6.1.2.2) with a low barycenter and spikes attached to the base ‘arms’ (weight in water: approximately 300 kg). The AMT unit is installed at the top and may be retrieved using a ROV without recovering the frame. This would allow changing AMT transponders for longer recording periods exceeding 6 years. Alternatively, the entire frame may be recovered.

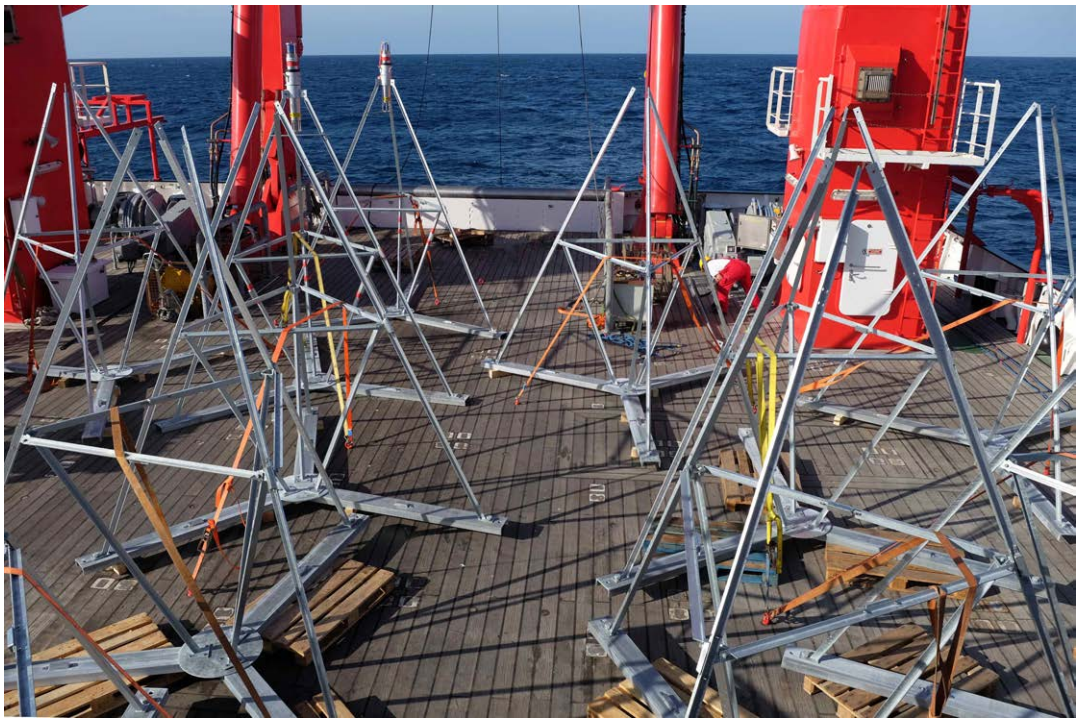

Figure 6.1.2.2: Galvanized steel tripod frames on the working deck of RV SONNE (J. Steffen).

Deployment of the frames is achieved using the deep-sea cable of RV SONNE and lowering the instrument through the A-frame (Figure 6.1.2.4).

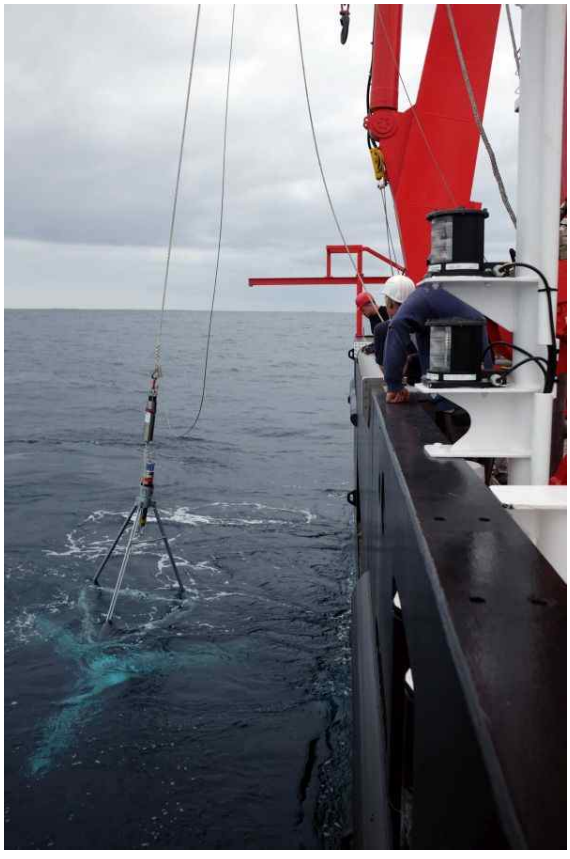

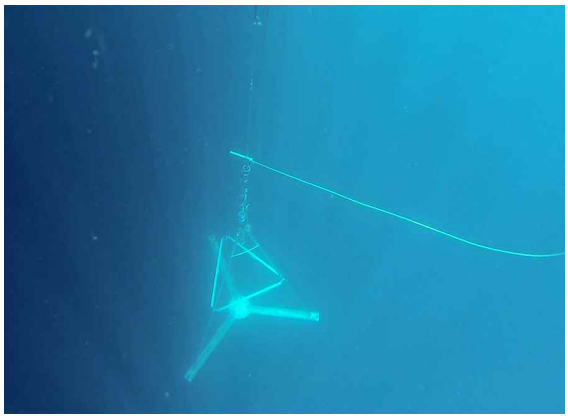

Figure 6.1.2.4: The tripod on the deep-sea cable above and below the water (J. Steffen).

During deployment, a number of quality assessment checks are run from the vessel to ensure that the unit is operating successfully. Precision pressure, temperature, sound velocity and dual-axis inclinometer sensors are integrated and are powered up at the requested time and sampling period, providing a low power platform for long-term surveys. Lithium battery packs provide sufficient power for the estimated 3.5 years duration of the project. The data is time stamped and logged internally for recovery via integrated high-speed acoustic telemetry, allowing measurements to be made over a period of more than 3 years without requiring a surface vessel or ROV to be present to command the process. Each AMT is fitted with a 1 GB SD memory card that can store up to 2 Mio 512 byte pages in total. In addition, the telemetry transceiver integrated in GeoSURF provides an acoustic gateway capability to enable it to communicate with, and extract data acoustically from, the seafloor array and to forward this data via the iridium satellite communications system (Figure 4.1). This approach obviates the requirement of a surface vessel to upload the acoustic data once GeoSURF is installed. Acoustic data upload is supported at a maximum of 900 bits per second to the WaveGlider transceiver (i.e. ~15 pages / minute). If GeoSURF is not available (e.g. in case of loss), internal data capacity in the AMTs is sufficient to store all acquired data over any possible deployment time, but can then only be retrieved after recovery of the AMT or alternatively be uploaded to a vessel via the HPT transceiver (dunker modem; Figure 6.1.2.5) (9000 bits/sec equivalent to 100 pages/minute).

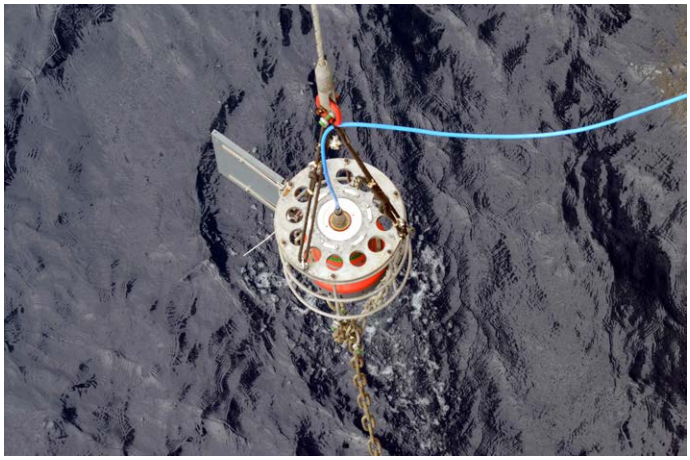

Figure 6.1.2.5: The HPT dunker modem deployed over the starboard side of RV SONNE (J. Steffen).

GeoSURF is an autonomous, environmentally powered ocean-going platform by Liquid Robotics that uses renewable energy sources to keep station and provides

a communications gateway between the benchmarks (communicating with the benchmarks via acoustic modem) and the home lab (via a satellite link) (Figure 6.1.2.6). This allows us, for example, to have regular information from the sensors mounted on the benchmarks and so rapidly respond to changes in the deformation pattern, to monitor the health of the system and, in the event of a major earthquake rupture, rapidly acquire information on the processes that occurred. At all other times, GeoSURF is not required to hold a continuous communication with the seafloor array. The integrated solar panels provide sufficient energy for this procedure and are designed to recharge the integrated Li-batteries. GeoSURF may be programmed for autonomous operation or it may alternatively be controlled by a pilot over the internet using a web interface.

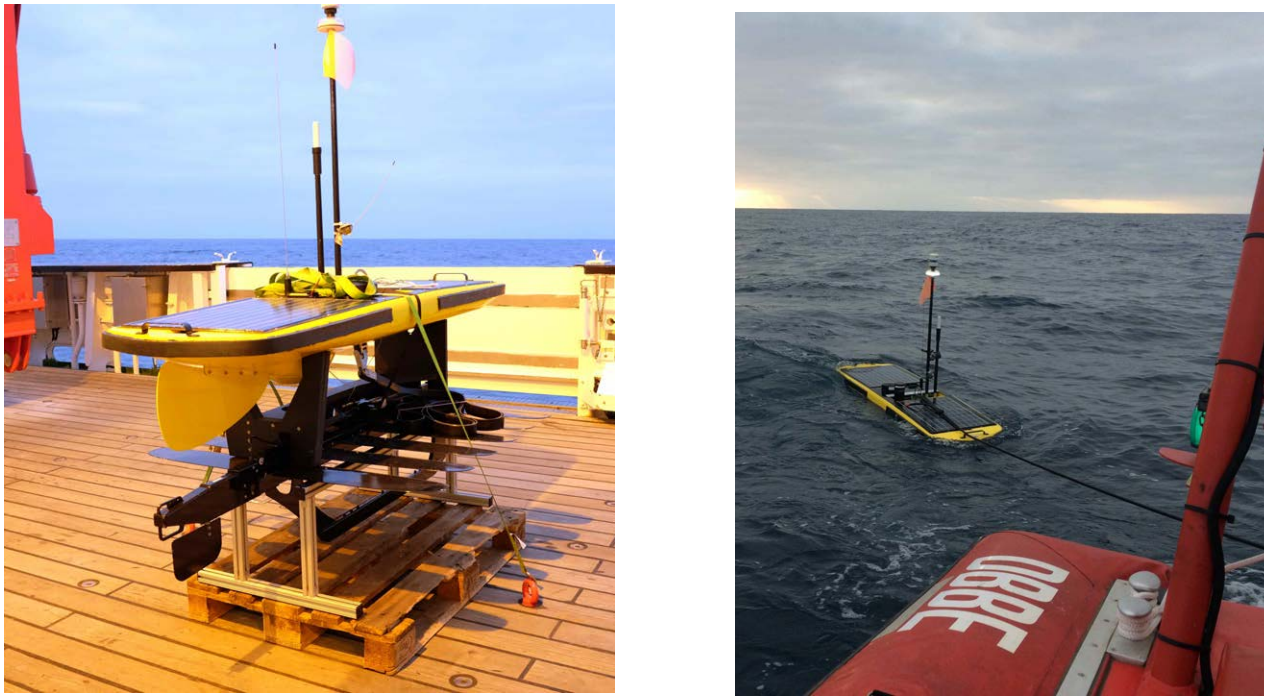

Figure 6.1.2.6: The GeoSURF wave glider ready for deployment on the deck and during recovery using RV SONNE's rescue boat (J. Steffen).

GeoSURF is composed of two parts (see Figure 6.1.2.6): the float containing all sensors and communication units and the sub hanging 6 meters below the float. The design of the separation allows the float to experience more wave motion than the sub. This difference allows wave energy to be harvested to produce forward thrust without requiring further energy for propulsion.

6.1.3 Working Area 1: Middle Continental Slope

Working area 1 is located on the middle continental slope where a network of eight transponders was deployed in water depths ranging from 2603 m to 2863 m. In order to accurately estimate the positions of the Posidonia transponders during installation of the geodetic stations we estimated the water sound velocity with a CTD. The vessel's CTD rosette was lowered to a water depth of 2500 m at 1 m/s to continuously measure sound speed in-situ at 20°47.98'S/70°48.93W (Figure 6.1.3.1).

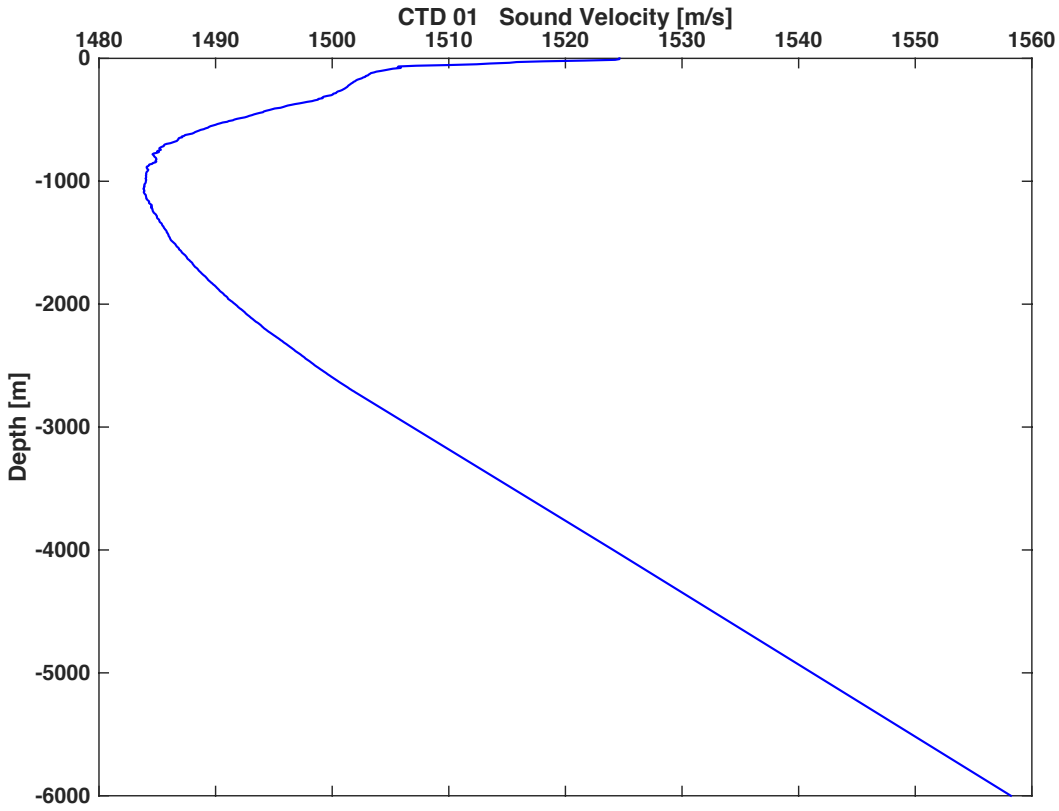

Figure 6.1.3.1: CTD sound velocity profile acquired in working area 1 prior to installation of the first geodetic station.

The eight transponders (A101-A108) were lowered to rest on topographic ridges (Figure 6.1.3.2) in pairs of two in order to have optimal lines-of-sight between the instruments (Figure 6.1.3.3). The line-of-sight was modeled prior to deployment (Figure 6.1.3.4) by comparing the AUV bathymetry with to the curved path (using the sound speed from the CTD measurement) between instruments installed on 3.5 m high tripods (instead of the 4.3 m high stands of the GeoSEA stations). Positions where the direct path was too close to or even interfered with the seafloor were

avoided during deployment. The target sites that allow visibility to all neighboring transponders is approx. 50 m X 50 m for most of the stations.

Figure 6.1.3.5 shows the relative location of the deployment sites from the initially planned site for stations A101-A108. Deployment sites for instruments lowered on the deep-sea cable in water depths between 2500 m - 3000 m deviated by up to 20 m from the originally planned positions. The position of station A101 deviates by more than 60 m from the planned site. This is due to the fact that A101 was deployed in 'free-fall' mode and not on the cable. In addition, the position for A101 shown here and in the station protocol is the position of the ship's GPS station at the time A101 reached the seafloor. RV SONNE's GPS station is located midship, approximately 60 m away from the aft working deck where the station was deployed.

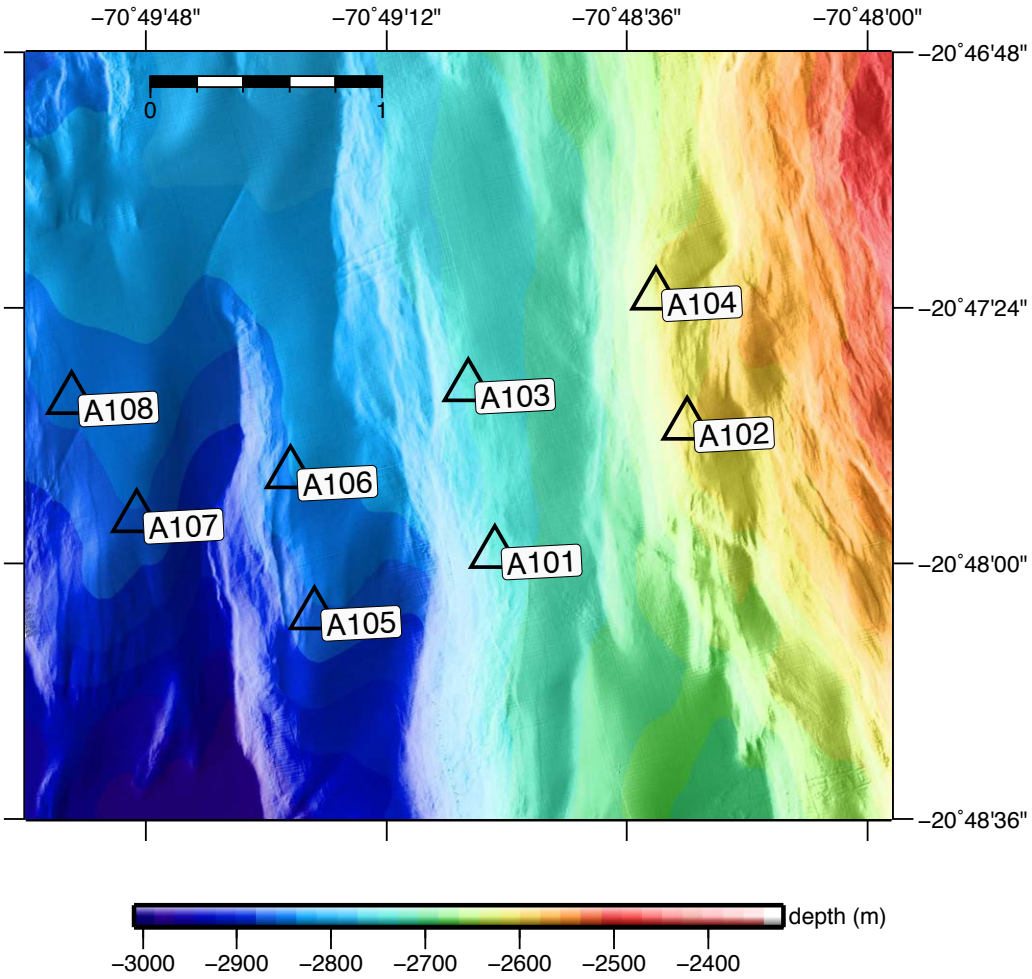

Figure 6.1.3.2: Location map of GeoSEA sub array 1 lcoated on the middle continental slope of northern Chile. The stations are deployed in pairs (A101-A103; A102-A104; A105-A106; A107-A108) on four topographic ridges, which are surface expressions of faults at depth. Scale at the top of the image is in km.

Station A102 landed approximately 20 m off (water depth: 2603 m), station A104 through A106 are within the 10 m range from their planned positions (water depths of 2615 m, 2863 m, and 2836 m, respectively). A103, A107 and A108 are between 12m and 17 m off (water depth: 2744 m, 2860 m, and 2852 m, respectively).

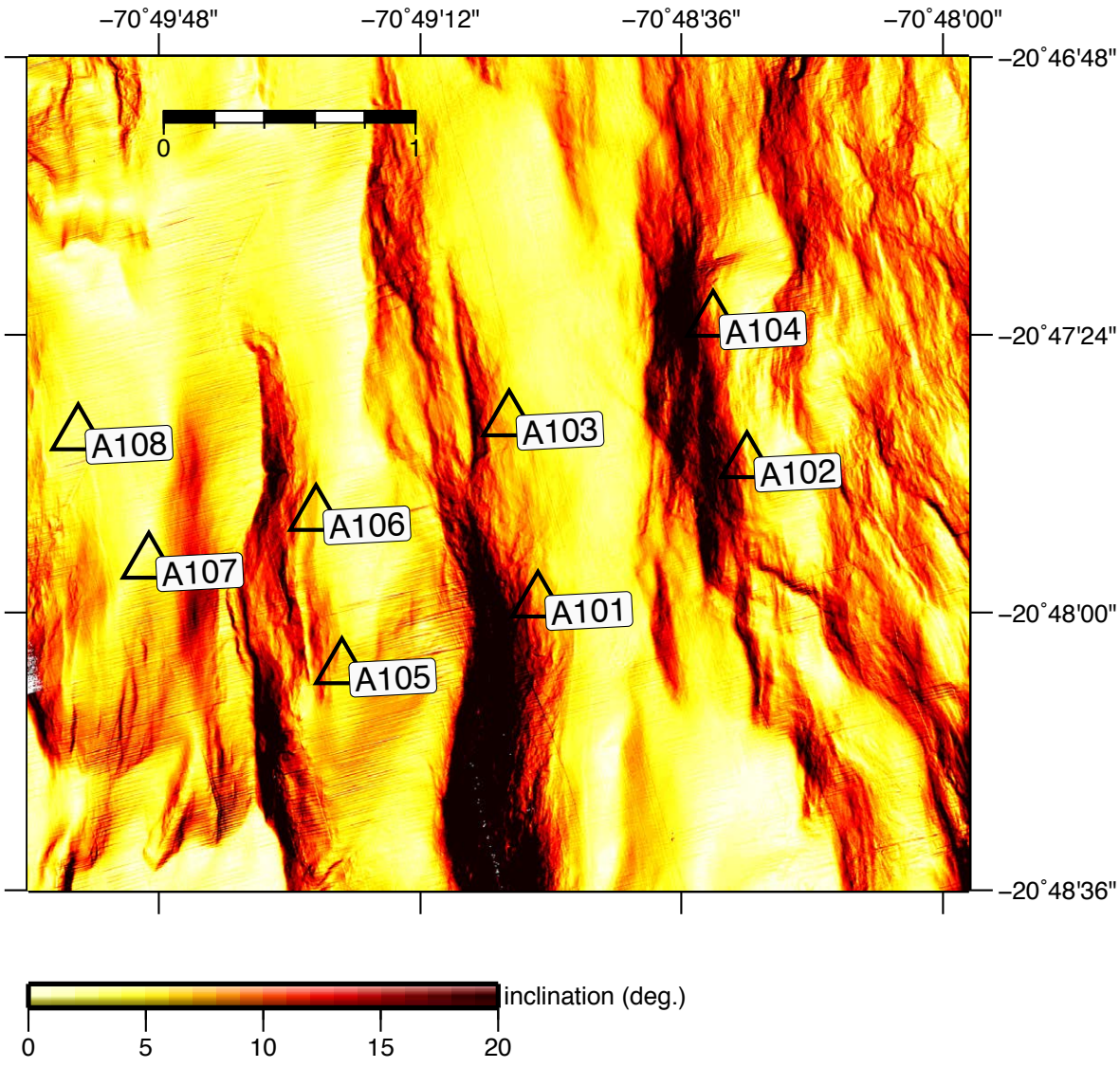

Figure 6.1.3.3: Slope map of GeoSEA sub array 1 showing the inclination of the study area. Steep slopes of more than 15° pose a challenge to the deployment on the deep-sea cable as the stations were required to the placed on the ridge crests to insure clear line-of-sight. Scale at the top of the image is in km.

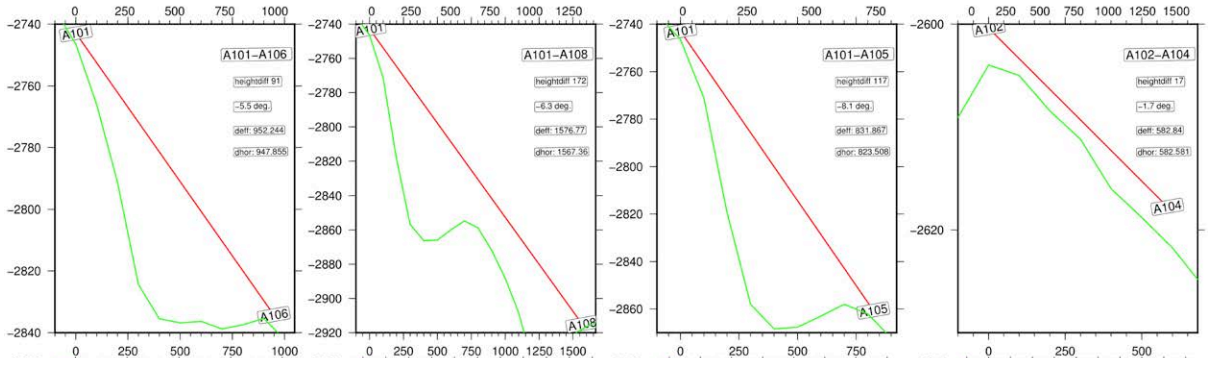

Figure 6.1.3.4: Modeled baselines. Example shown for station pairs A101-A106, A101-A108; A101-A105, A102-A104. Red line: direct path between stations, green line: seafloor. Heightdiff indicates the relative difference in elevation between the stations. The expected slope between the stations are indicated.

Baselines are measured with a logging rate of 160 minutes between each pair of stations and forward and backward direction. Accustic visibility was achieved for all pair except between the westernmost and easternmost pair (Table 6.1.3.1). As is evident from the overview of baselines provided in the table below, the longest baseline in the network is 2455 m. For stations placed further apart (A107 to A102 and A104) line-of-sight is limited due to the high topographic elevations between the stations. Station A108, however, has a clear line-of-sight to the easternmost pair A102/A104 and baselines are measured in both directions over a distance of 2455 m.

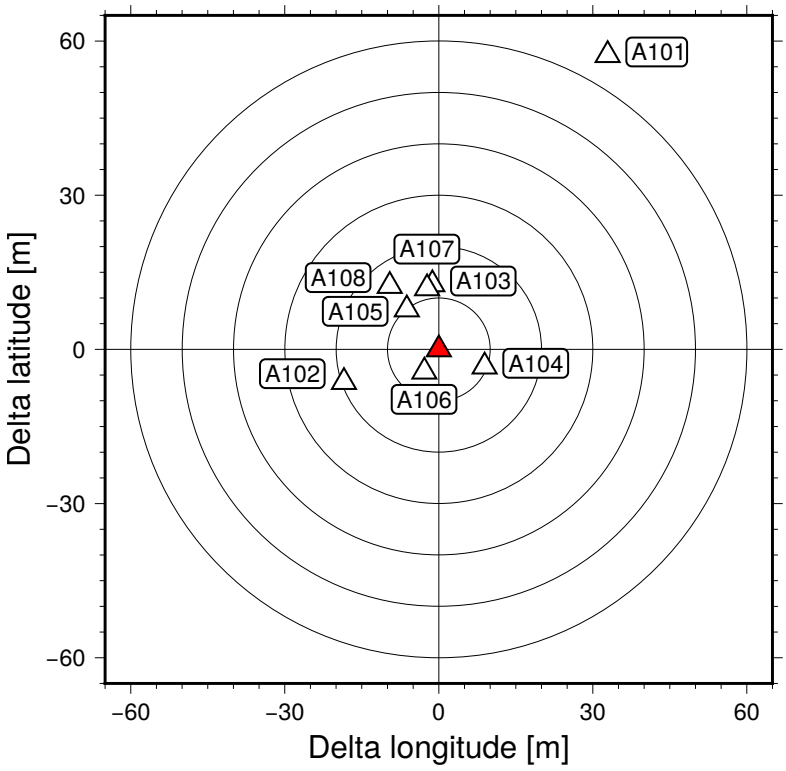

Figure 6.1.3.5: Deployment precision plot for GeoSEA sub array 1. The red triangle represents the planned location for each station. Circles are spaced at 10 m, indicating the discrepancy between the final deployment site (from Posidonia transponders) and the originally planned location. Station A101 was not lowered on the deep-sea cable, but was deployed in 'free-fall' mode. See text for details regarding positioning of A101.

To

From	A101 2701	A102 2702	A103 2703	A104 2704	A105 2705	A106 2706	A107 2707	A108 2708	
A101 2701	0.0	1009.3 883.2	728.2 657.2	1321.9 1208.1	832.6 935.0	953.0 1002.0	1562.0 1622.0	1950.6 1996.7	7
A102 2702	1009.3 883.2	0.0	971.7 966.4	580.9 575.2	1827.1 1814.5	1745.2 1742.0	2429.0 2409.0	2677.2	6
A103 2703	728.2 657.2	971.7 966.4	0.0	911.3 925.5	1194.4 1199.9	861.7 869.0	1546.8 1535.0	1720.8 1724.0	7
A104 2704	1321.9 1208.2	580.9 575.2	911.3 925.5	0.0	2036.9 2048.0	1772.9 1794.0	2455.4 2458.8	2578.1	6
A105 2705	832.6 935.0	1827.1 1814.5	1194.4 1199.9	2036.9 2048.0	0.0	617.9 623.0	877.2 879.0	1402.7 1412.2	7
A106 2706	953.0 1002.0	1745.2 1742.0	861.7 869.0	1772.9 1794.0	617.9 623.0	0.0	692.2 673.0	999.7 997.5	7
A107 2707	1562.0 1622.0	2429.0 2409.0	1546.8 1535.0	2455.4 2458.8	877.2 879.0	692.2 673.0	0.0	581.4 579.9	7
A108 2708	1950.6 1996.7	2677.2	1720.8 1724.0	2578.1	1402.7 1412.2	999.7 997.5	581.4 579.9	0.0	5
	7	6	7	6	7	7	7	5	

Table 6.1.3.1: Overview of expected (green, distances from planned coordinates) and measured (black) baselines.

All stations in this network log with a logging period of 160 minutes, beside of 2708, which was configured to log every 80 minutes. At these intervals, baselines, hydrostatic pressure, sound speed and high-resolution temperature measurements are conducted. Instrument inclination and battery status are only measured at a rate of 100 of the logging period (i.e. every 11.1 days).

Figure 6.1.3.6 shows all visible baselines between stations projected on the seafloor in a plain view (top panel) and perspective view (bottom panel). The central stations successfully send as well as receive baseline interrogations from all stations in the network; the outer stations were configured not to answer for incoming long baseline signals (e.g. baselines longer than 2500 m).

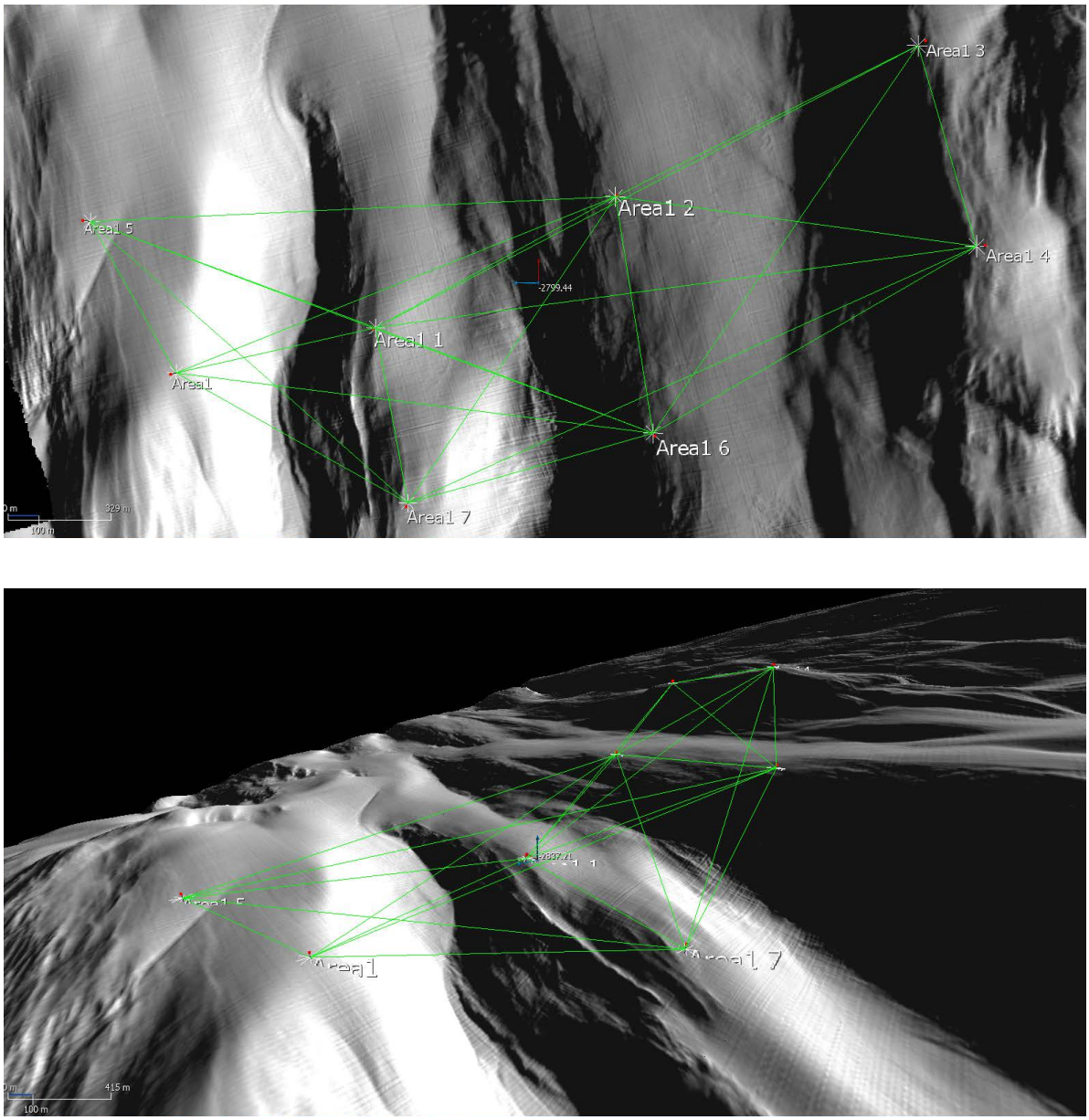

Figure 6.1.3.6: Seafloor view for GeoSEA sub array 1 on the middle continental slope. A total of 8 stations were placed on four N-S trending ridges. Green lines show all the measured baselines between the stations. Bottom image shows the array in a perspective view. North is located to the top right.

After the installation of the entire array was completed, we returned to area 1 to deploy GeoSURF for data upload. In addition, the data were also secured via the HPT dunker modem. Figure 6.1.3.7 shows a screenshot of Liquid's piloting webinterface for GeoSURF with the waypoints for navigation above the stations in area 1. Figure 6.1.3.8 shows the sound velocity, temperature and pressure loggings of station A101 and A108 for the time period between Dec. 6 and Dec. 9, after the station had mechanically settled into the seafloor.

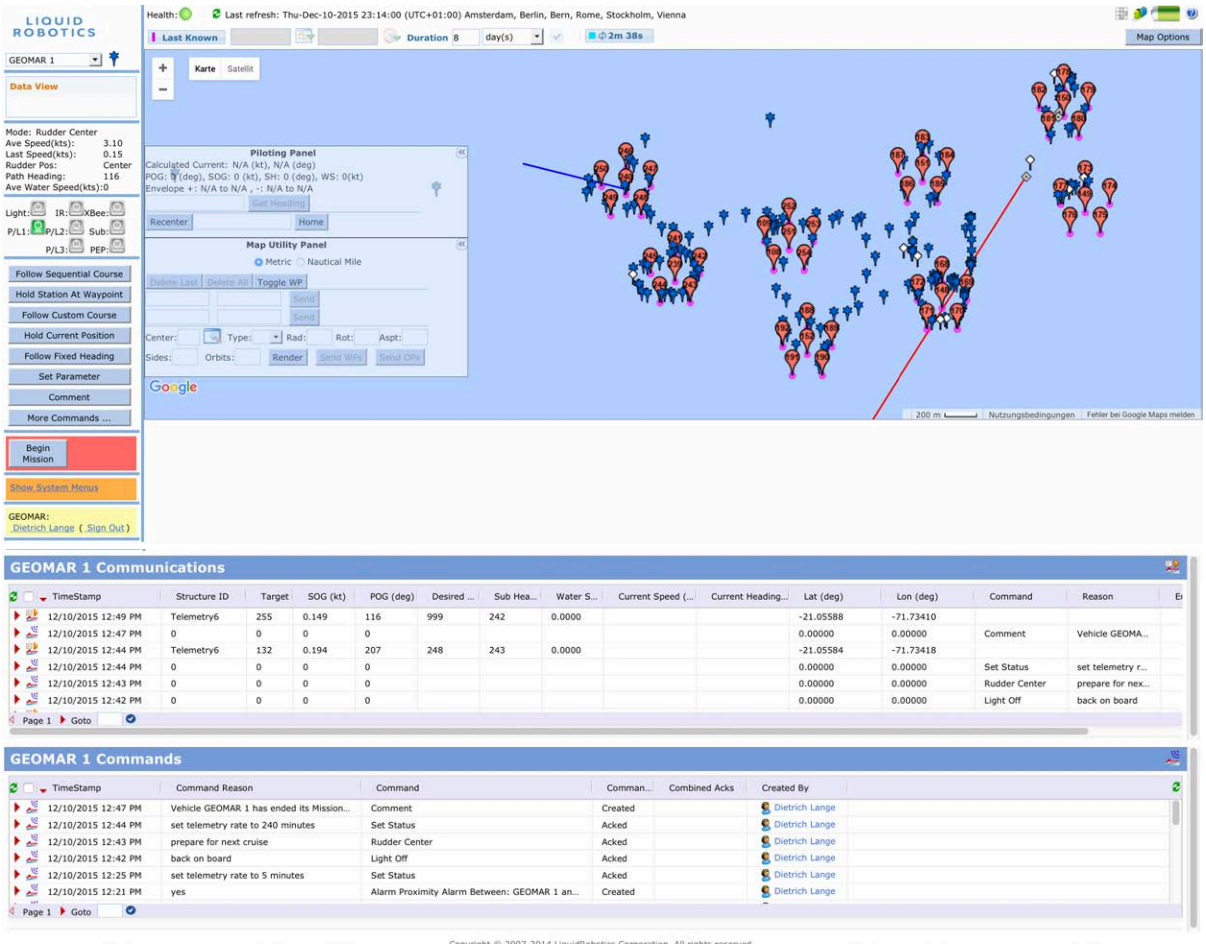

Figure 6.1.3.7: Upper part of the Liquid robotics piloting webinterface showing the command panels and the map-view for the vehicle GEOMAR1 (GeoSURF). Position reports of GeoSURF (5 minute repeat rate) are shown with blue pins. The waveglider holds position above the AMT's by cycling clockwise around waypoints (shown with red pins) distributed in pentagons with 300 m radius. The position of RV Sonne from AIS is shown with a grey upright square. GeoSURF is equipped with an redundant satellite tracker, which is indicated by white pins (two hours repeat time). The left panel shows the command options; the uppermost line indicates the vehicle health. In the central part the Piloting Panel and Map Utility Panel are shown. The lower part shows the incoming communication from the waveglider (upper panel) and the commands sent from the user to the waveglider (lower panel).

Sound velocity was measured as well as computed from pressure and temperature assuming constant salinity for comparison. Variations in sound velocity for area 1 are greater than for areas 2 or 3, likely related to the shallower position on the continental margin where active upwelling of water masses is occurring. Dominating low-frequency variations in pressure data are due to tides.

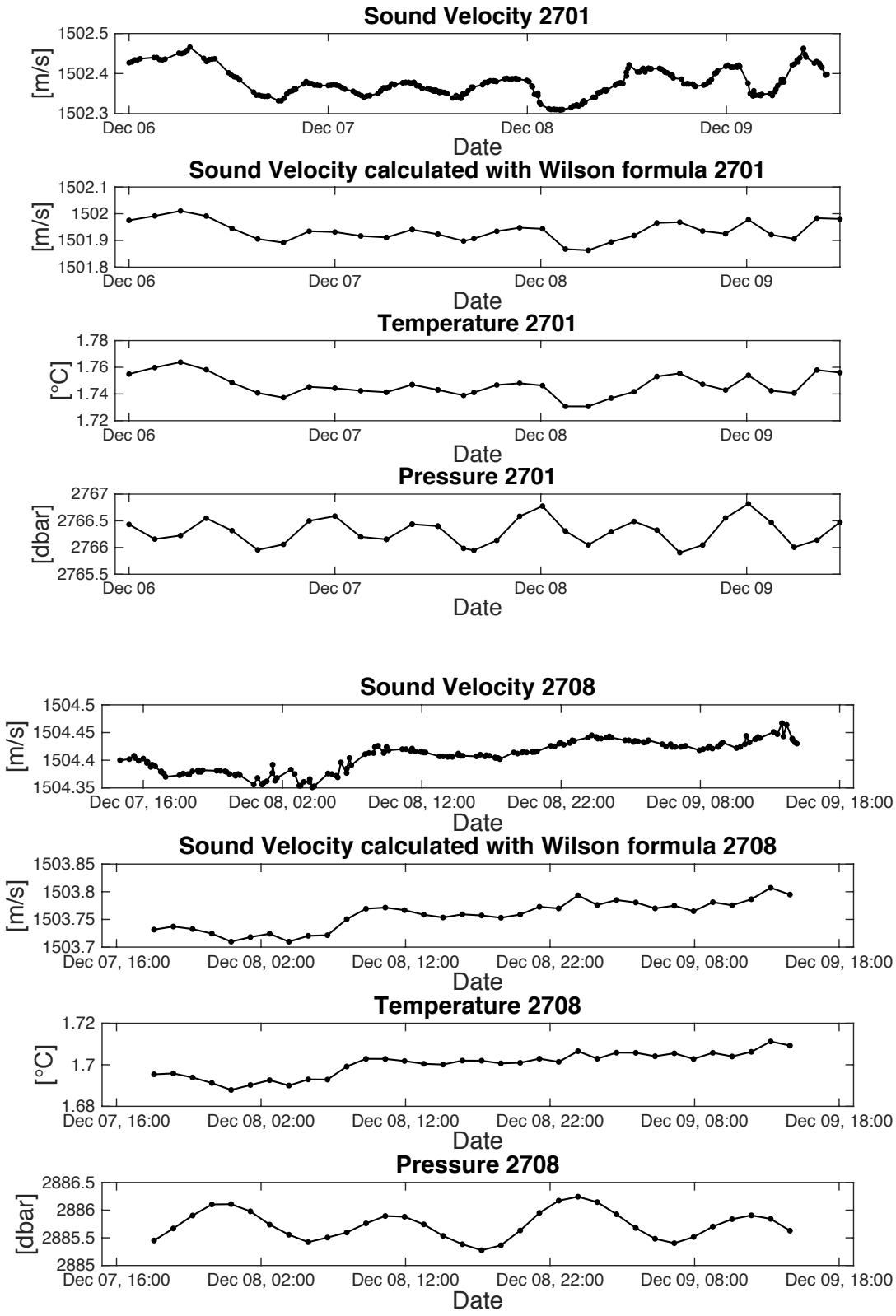

Figure 6.1.3.8: Logging data plotted against time for stations A101 (2701, upper panels) and A108 (2708, lower panels). The uppermost panel shows the sound velocity derived from direct measurements, the panel below shows sound velocity retrieved from pressure and temperature data assuming a constant salinity.

A baseline example is provided in Figure 6.1.3.9, showing the distance between stations A101 (2701) and A102 (2702), which are located 882.7 m apart. The baseline is computed from the travel times of the acoustic ping between the instruments, taking into account the measured sound velocities from the instruments at both sides. This preliminary baseline suggests a repeatability of 4 mm.

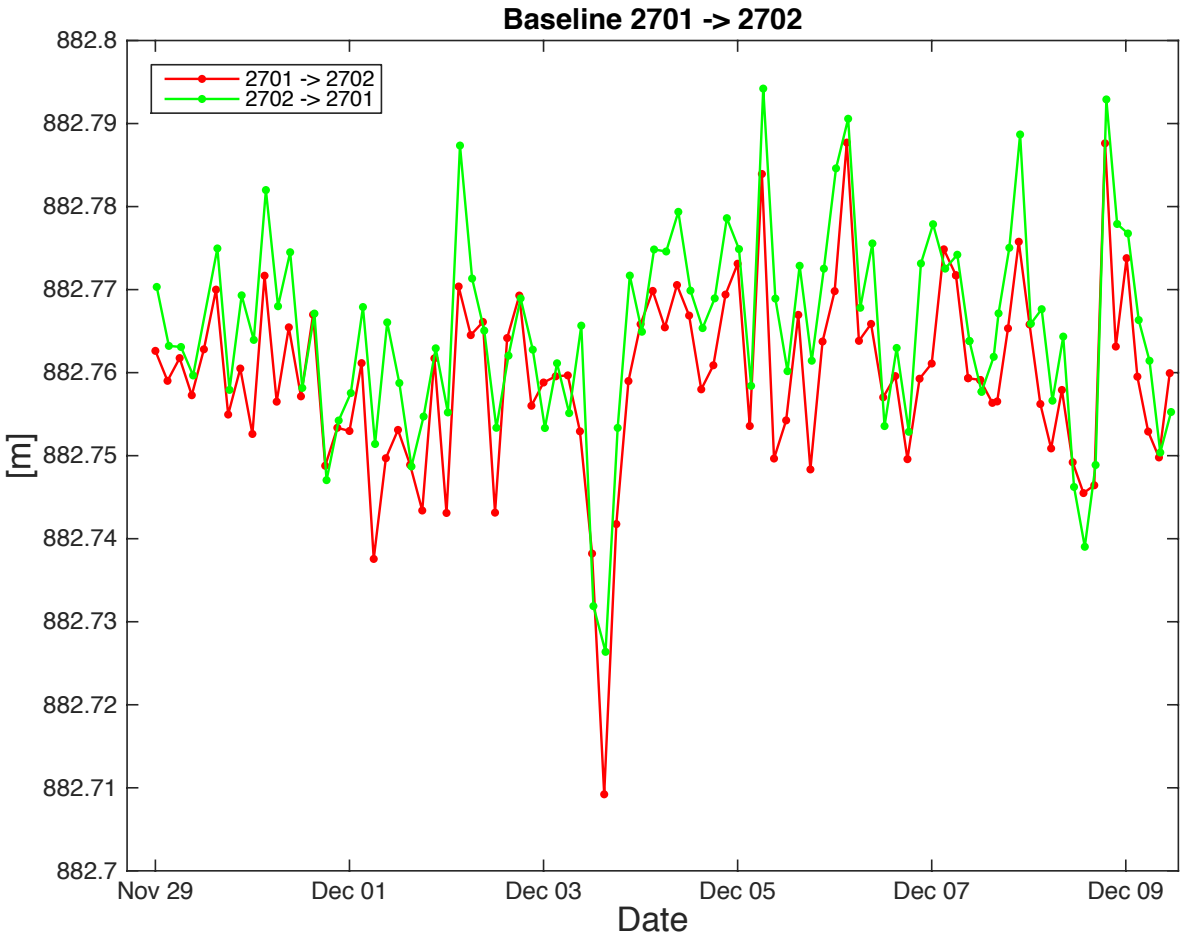

Figure 6.1.3.9: Baseline computation between stations A101 (2701) and A102 (2702). Red line represent baseline from A101 → A102; green line shows raypath length between A102 and A101. Note: these data have not been fully processed yet and are only allow preliminary estimates about precision.

6.1.4 Working Area 2: Outer Rise

A total number of five GeoSEA stations (A201-A205) was deployed in area 2 on the outer rise in water depths ranging from 4034 m – 4104 m (Figure 6.1.4.1). Even though water depth is significantly larger compared to area 1, the network configuration is comparatively simpler because of the limited variation in water depth of only 70 m between the five stations. Changes in the inclination are strongly focused on a N-S trending normal fault at around 71°44'10''W (Figure 6.1.4.2). The stations are positioned on both sides of this extensional fault and all possible baselines between the stations are achieved.

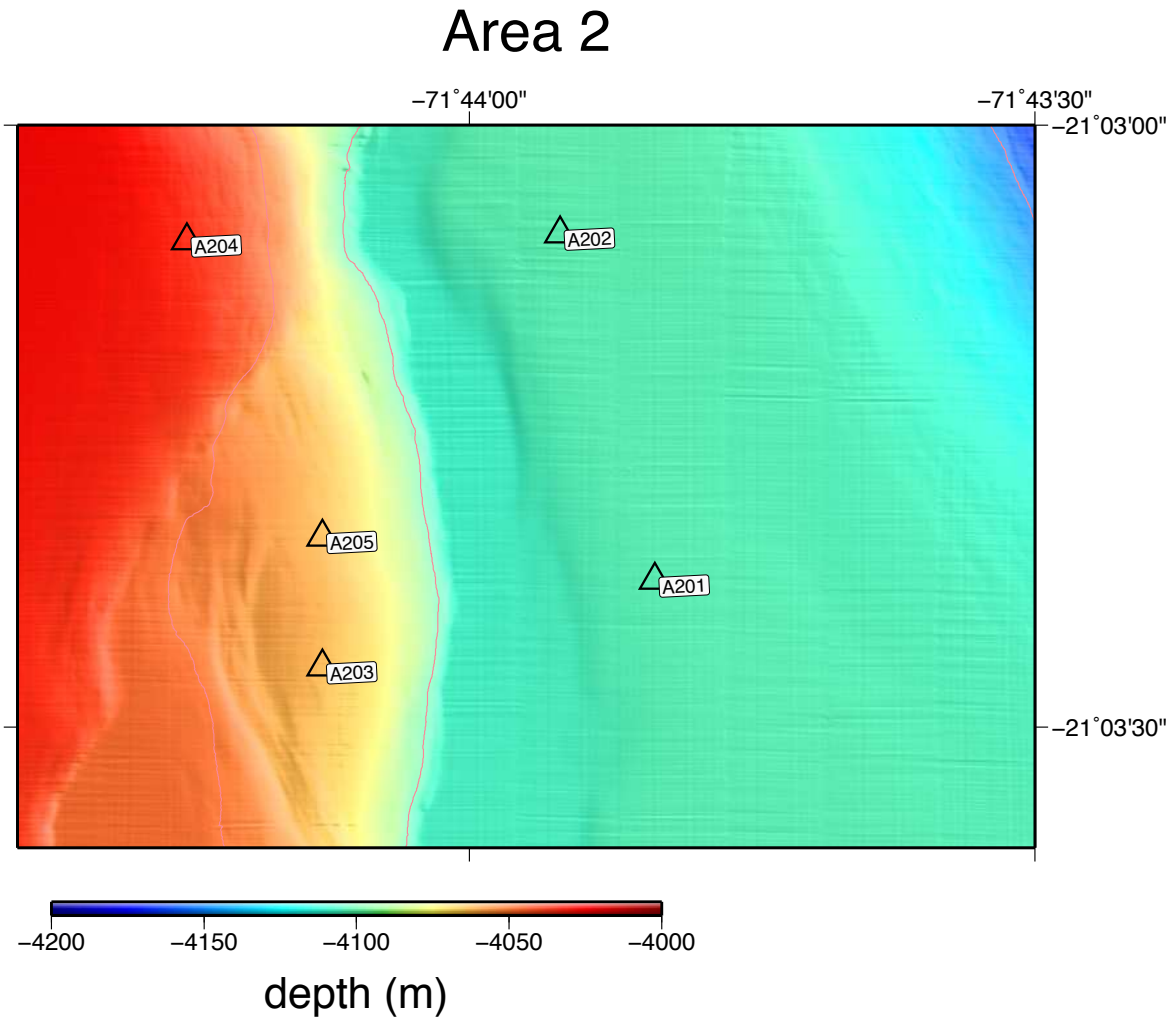

Figure 6.1.4.1: Location map of GeoSEA sub array 2 on the outer rise of the downbending oceanic Nazca plate seaward of the trench. The stations are deployed on both sides of an extensional normal fault originating from the plate's bending close to the trench. Scale at the top of the image is in km.

All stations lowered on the deep-sea cable were deployed within 20 m of their originally planned positions (Figure 6.1.4.3). The stations all drifted in a northwest direction, however, as the topography variations in the working area are trending N-S, this drift was not corrected during deployment by repositioning the vessel. Only a distinct E-W drift would have affected the array, as some stations may then not have been installed on the correct side of the fault zone. Station A204 slipped off the hook of the deep-sea cable and hence fell down to the seafloor uncontrolled. It is positioned approximately 60 m away from the planned site. It needs to be noticed, however, that the relative position shown here is based on the position of RV SONNE's GPS station (compare station A101 in 6.1.3.1), so the discrepancy likely is far less than indicated here.

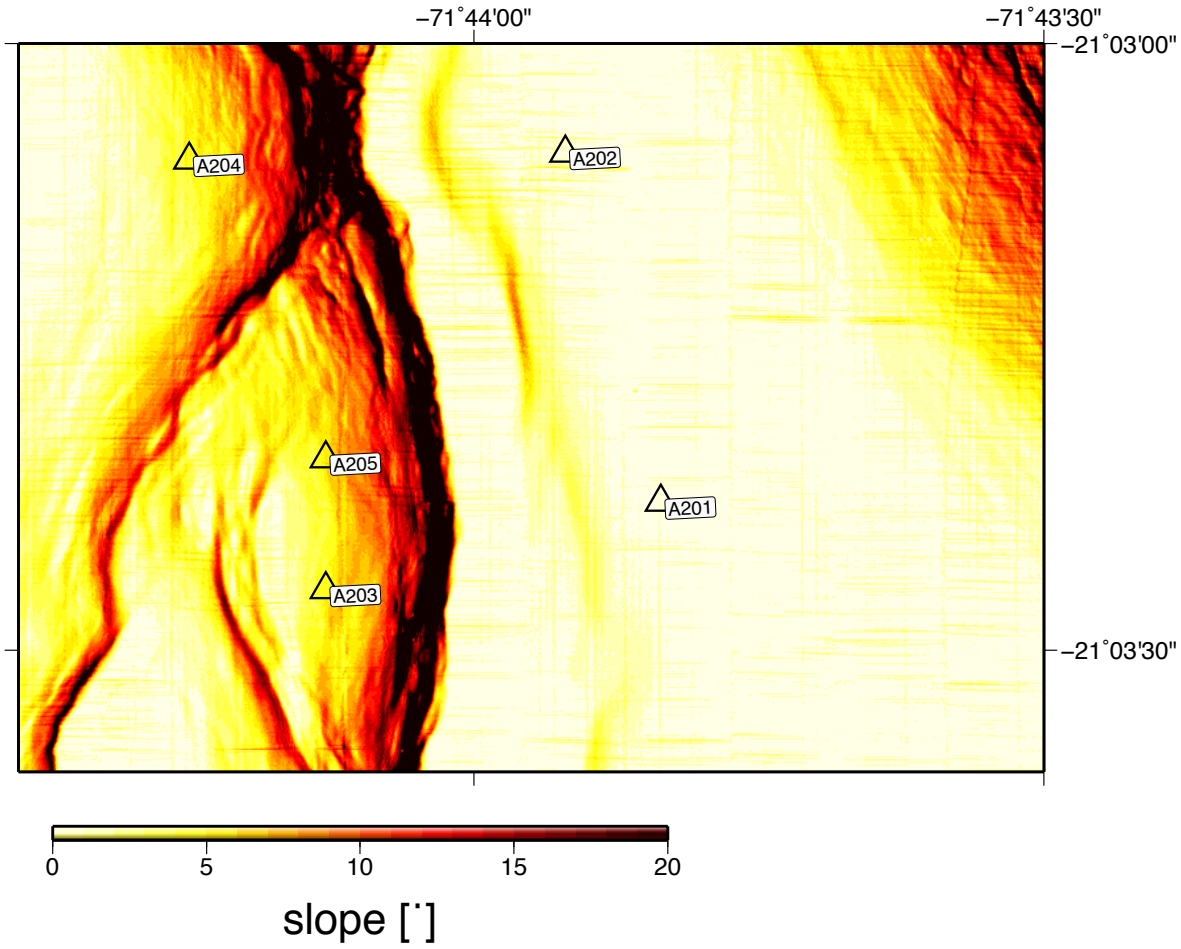

Figure 6.1.4.2: Slope map of GeoSEA sub array 2 showing the inclination of the study area. Slopes are evident on the western throw of a plate bending related normal fault, which runs in a N-S direction parallel to the deep-sea trench located to the east of the study area.

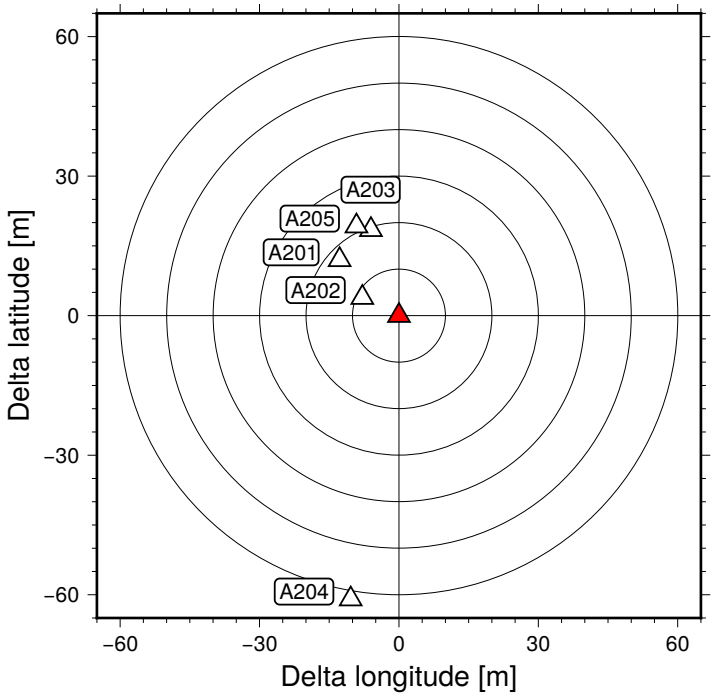

Figure 6.1.4.3: Deployment precision plot for GeoSEA array 2. The red triangle represents the planned location for each station, respectively. Circles are spaced at 10 m, indicating the discrepancy between the deployment site and the originally planned location. Station A204 was not lowered on the deep-sea cable, but was deployed in 'free-fall' mode.

Table 6.1.4.1 shows the measured baselines immediately after the deployment. As expected, modeled baselines (indicated by green numbers in Table 6.1.4.1) deviate highest from measured baselines (black numbers) for station A204.

From \ To	A201 2201	A202 2202	A203 2203	A204 2204	A205 2205	
A201 2201	0.0	550.6 531.9	527.5 514.0	888.1 816.3	514.8 505.2	4
A202 2202	550.6 531.9	0.0	757.8 743.5	575.3 522.1	591.2 579.5	4
A203 2203	527.5 514.0	757.8 743.5	0.0	685.6 642.0	199.1 201.0	4
A204 2204	888.1 816.3	575.3 522.1	685.6 642.0	0.0	499.8 448.5	4
A205 2205	514.8 505.2	591.2 579.5	199.1 201.0	499.8 448.5	0.0	4
	4	4	4	4	4	

Table 6.1.4.1: Overview of expected (green) and measured (black) baselines.

All stations log sound velocity, pressure, baselines and high-resolution temperature with a logging period of 90 minutes. Inclination is logged at a rate of 10; battery status is logged at a rate of 100.

Figure 6.1.4.4. shows examples of logged physical parameters from stations A201 (upper panels) and A204 (lower panel). Sound velocity in m/s, temperature in °C and pressure in dbar are shown for each stations, respectively. The expected close correlations between the sound velocity and the temperature loggings is documented, as is the tidal signal on the pressure data.

Baselines for stations A201, A202, A203 and A205 are presented in Figure 6.1.4.5. Based on these unprocessed and uncorrected data, a precision (repeatability) of <4 mm is documented.

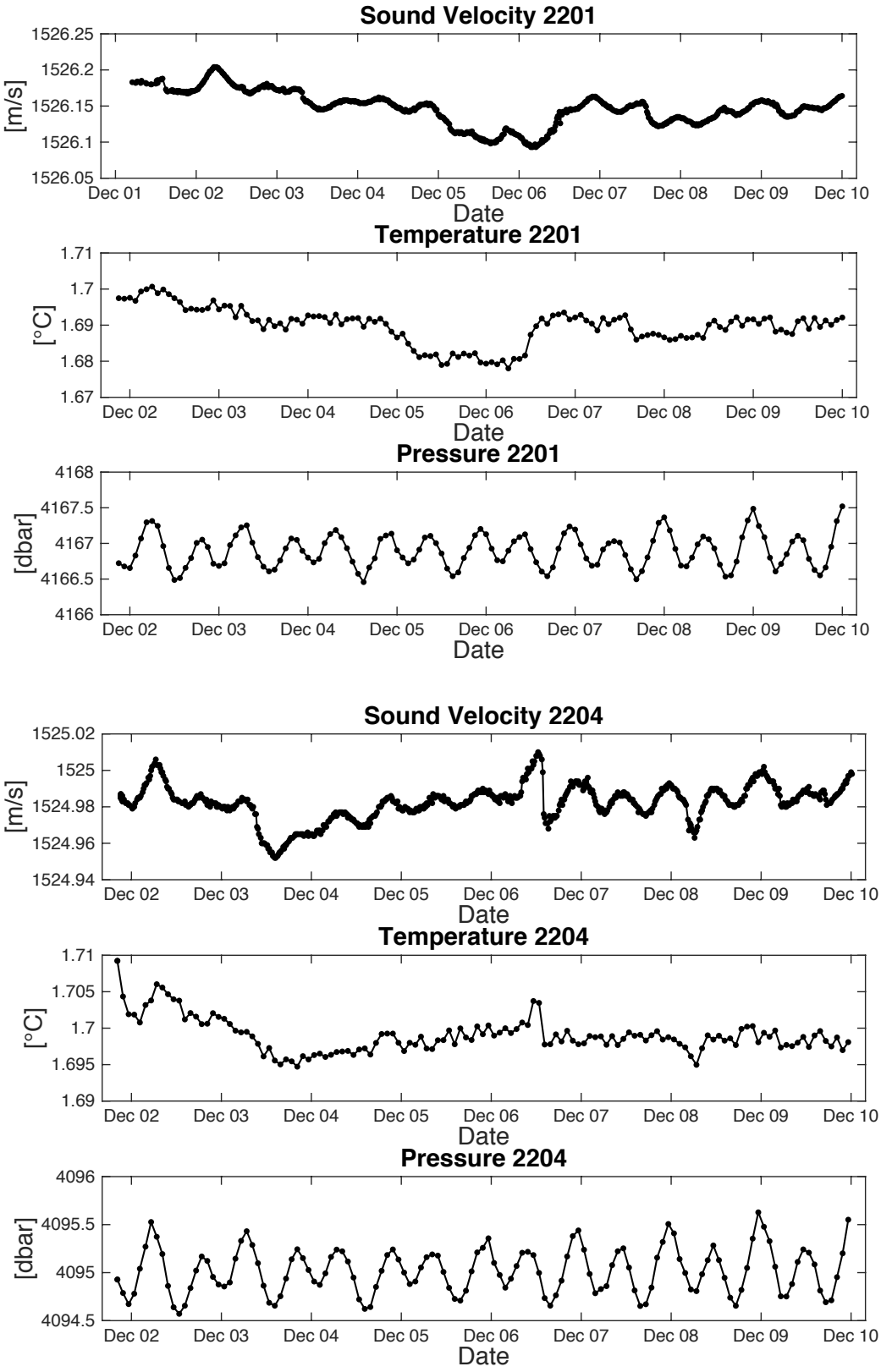

Figure 6.1.4.4: Logging data plotted against time for stations A201 (2201, upper panels) and A204 (2204, lower panels). Sound velocity is in m/s, temperature in °C and pressure data in dbar.

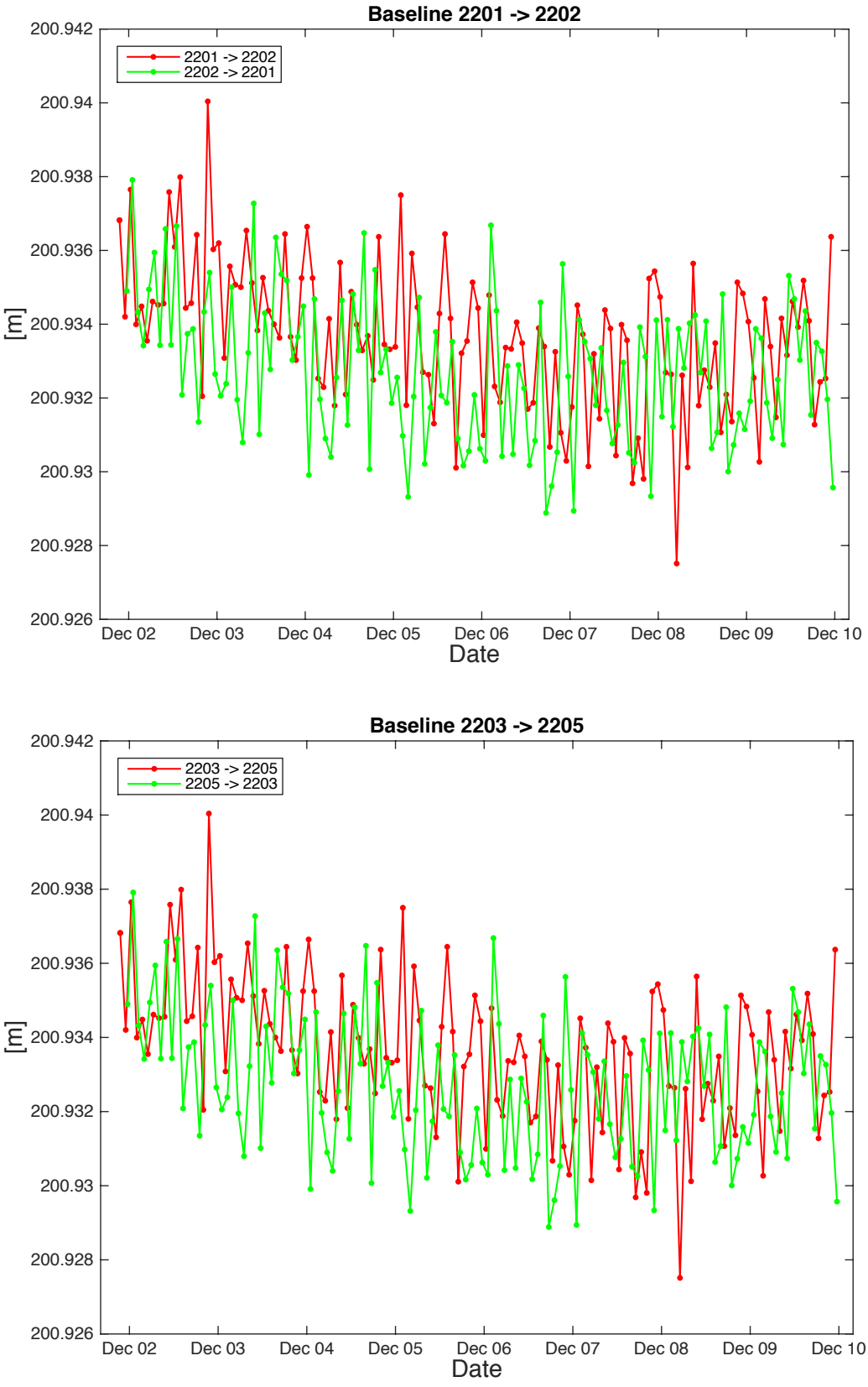

Figure 6.1.4.5: Baselines between stations A201 (2201) and A202 (2202) (upper panel) and between stations A203 (2203) and A205 (2205) (lower panel). See Figure 6.1.3.9 caption for additional display information.

6.1.5 Working Area 3: Lower continental slope

Working area 3 on the lower continental slope approximately 10 km east of the deformation front is located in water depth >5000 m and thus is the deepest location of any GeoSEA sub array. The region is characterized by complex tectonics, which pose a significant challenge to the deployment as ridges and troughs separated by steep slopes are ubiquitous throughout the area.

Prior to instrument deployment, we conducted a CTD measurement to a depth of 4500 m (Figure 6.1.5.1). The CTD rosette was lowered at 20°47.05S/71°04.00W. A comparison between the CTD in area 1 (Figure 6.1.3.1) and in area 3 is provided in the appendix (Appendix C).

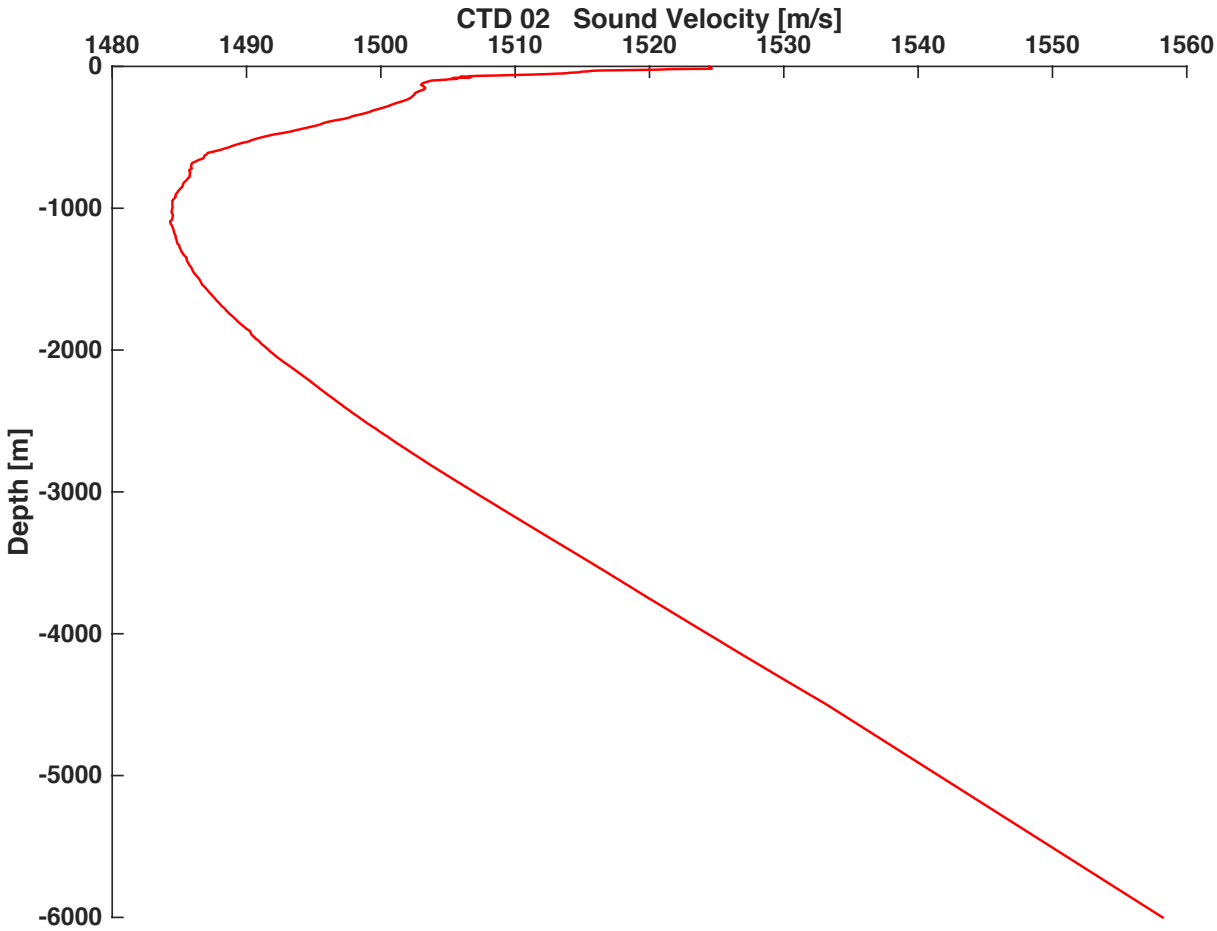

Figure 6.1.5.1: CTD sound velocity profile acquired in working area 3.

An array consisting of ten stations (A301-A310) was deployed in a configuration centered around two stations (A301 and A310), which are located on a topographic elevation in the center of the network (Figure 6.1.5.2).

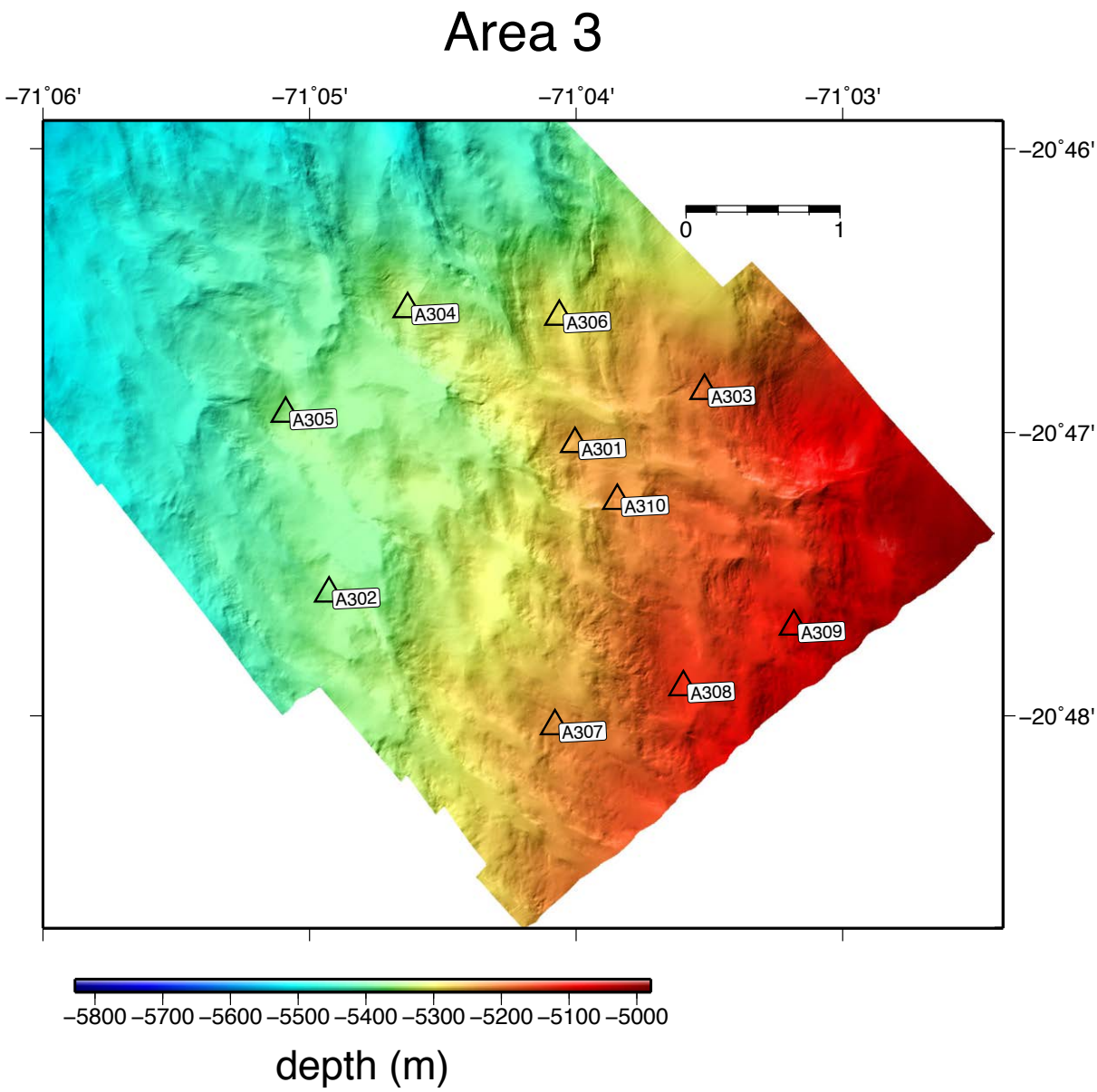

Figure 6.1.5.2: Location map of GeoSEA sub array 3 on the lower continental slope of northern Chile. The stations are deployed surrounding two central stations (A301 and A310). These two stations receive and send baseline interrogations to all surrounding stations as well as to each other. Scale at the top of the image is in km.

The steep slopes and a rough terrain required a precise positioning of the stations (Figure 6.1.5.3), which are located in water depths between 5098 m – 5368 m. All of the stations (except A302, A305, and A306) lie within 15 m of their planned original deployment sites (Figure 6.1.5.4). The remaining three stations are

all positioned on large plateaus with less than 5° inclination, requiring less precision during deployment compared to stations which are deployed close to a scarp or cliff,

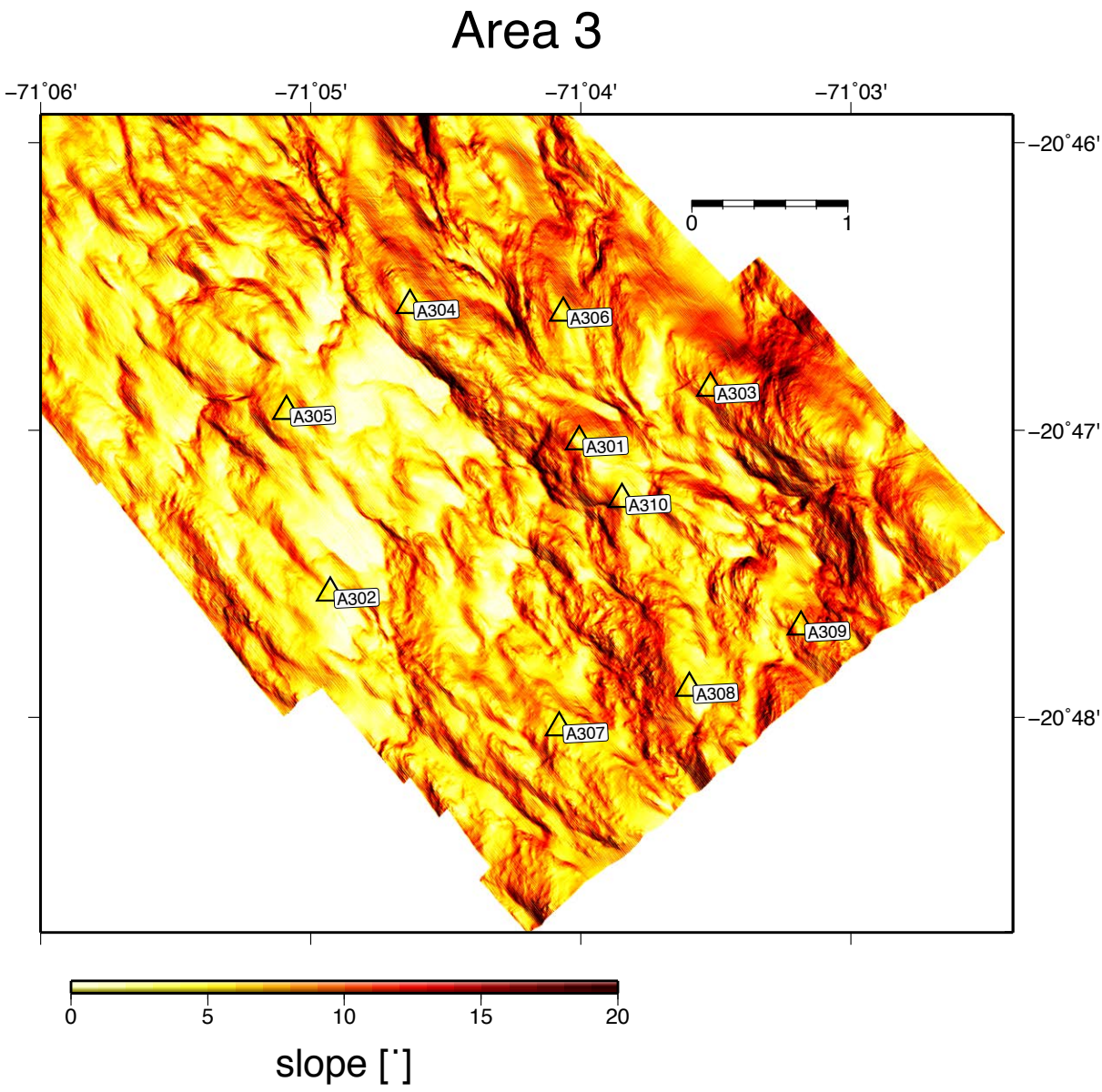

Figure 6.1.5.3: Slope map of GeoSEA sub array 3 showing the inclination of the study area. Steep slopes are present throughout the deployment area with inclinations commonly exceeding 10°.

such as A303 or A309, which needed to be deployed in close proximity to their planned sites (< 10 m) (Figure 6.1.5.4). All expected baselines, which were modeled beforehand, could be achieved (Table 6.1.5.1).

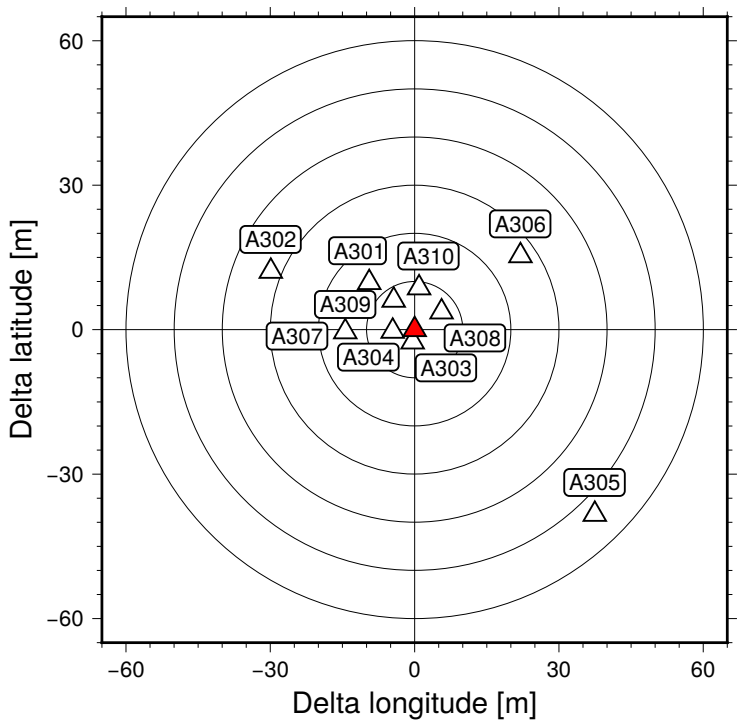

Figure 6.1.5.4: Deployment precision plot for GeoSEA array 3. The red triangle represents the planned location for each station, respectively. Circles are spaced at 10 m, indicating the discrepancy between the deployment site and the originally planned location. Discrepancy is lower than 15 m for 7 out of 10 stations. See text for further explanations on locations of stations A302, A305 and A306.

To

From	A301 2301	A302 2302	A303 2303	A304 2304	A305 2305	A306 2306	A307 2307	A308 2308	A309 2309	A310 2310	
A301 2301	0.0	1869.8 1873.0	909.9 920.0	1394.0 1381.0	1886.7 1834.0	836.5 824.0	1840.7 1869.0	1736.8 1753.0	1865.8 1876.0	470.0 475.0	9
A302 2302	1869.8 1873.0	0.0	2770.8	1916.8 1906.0	1205.9 1130.0	2345.5	1707.2 1730.0	2389.9 2421.0	3037.1	1970.9 1980.0	6
A303 2303	909.9 920.0	2770.8	0.0	1999.3 1999.0	2722.1	1057.0 1052.0	2384.5 2415.0	1932.6 1939.0	1650.4 1644.0	912.7 917.0	7
A304 2304	1394.0 1381.0	1916.8 1906.0	1999.3 1999.0	0.0	1039.7 1045.0	990.4 993.0	2876.5	3045.7	3259.6	1853.0 1845.0	6
A305 2305	1886.7 1834.0	1205.9 1130.0	2722.1	1039.7 1045.0	0.0	1888.7 1872.0	2686.0	3143.4	3590.1	2233.3 2178.0	5
A306 2306	836.5 824.0	2345.5	1057.0 1052.0	990.4 993.0	1888.7 1872.0	0.0	2667.1	2546.6	2538.8 2529.0	1264.8 1255.0	6
A307 2307	1840.7 1869.0	1707.2 1730.0	2384.5 2415.0	2876.5	2686.0	2667.1	0.0	876.0 902.0	1683.0	1515.7 1542.0	5
A308 2308	1736.8 1753.0	2389.9 2421.0	1932.6 1939.0	3045.7	3143.4	2546.6	876.0 902.0	0.0	816.3 824.0	1282.4 1293.0	6
A309 2309	1865.8 1876.0	3037.1	1650.4 1644.0	3259.6	3590.1	2538.8 2529.0	1683.0	816.3 824.0	0.0	1412.7 1419.0	5
A310 2310	470.0 475.0	1970.9 1980.0	912.7 917.0	1853.0 1845.0	2233.3 2178.0	1264.8 1255.0	1515.7 1542.0	1282.4 1293.0	1412.7 1419.0	0.0	9
	9	6	7	6	5	6	5	6	5	9	

Table 6.1.5.1: Overview of expected (green) and measured (black) baselines for area 3.

In addition, some long baselines exceeding 2000 m are also measured (e.g. A306-A309: 2538 m). The only baseline shorter than 2000 m that cannot successfully be logged is between stations A307 and A309. This is likely due to a steep slope at the site of A308, which limits the line-of-sight here.

Figure 6.1.5.5 shows the network layout on the seafloor bathymetry. The green lines represent all interrogated baselines between the stations.

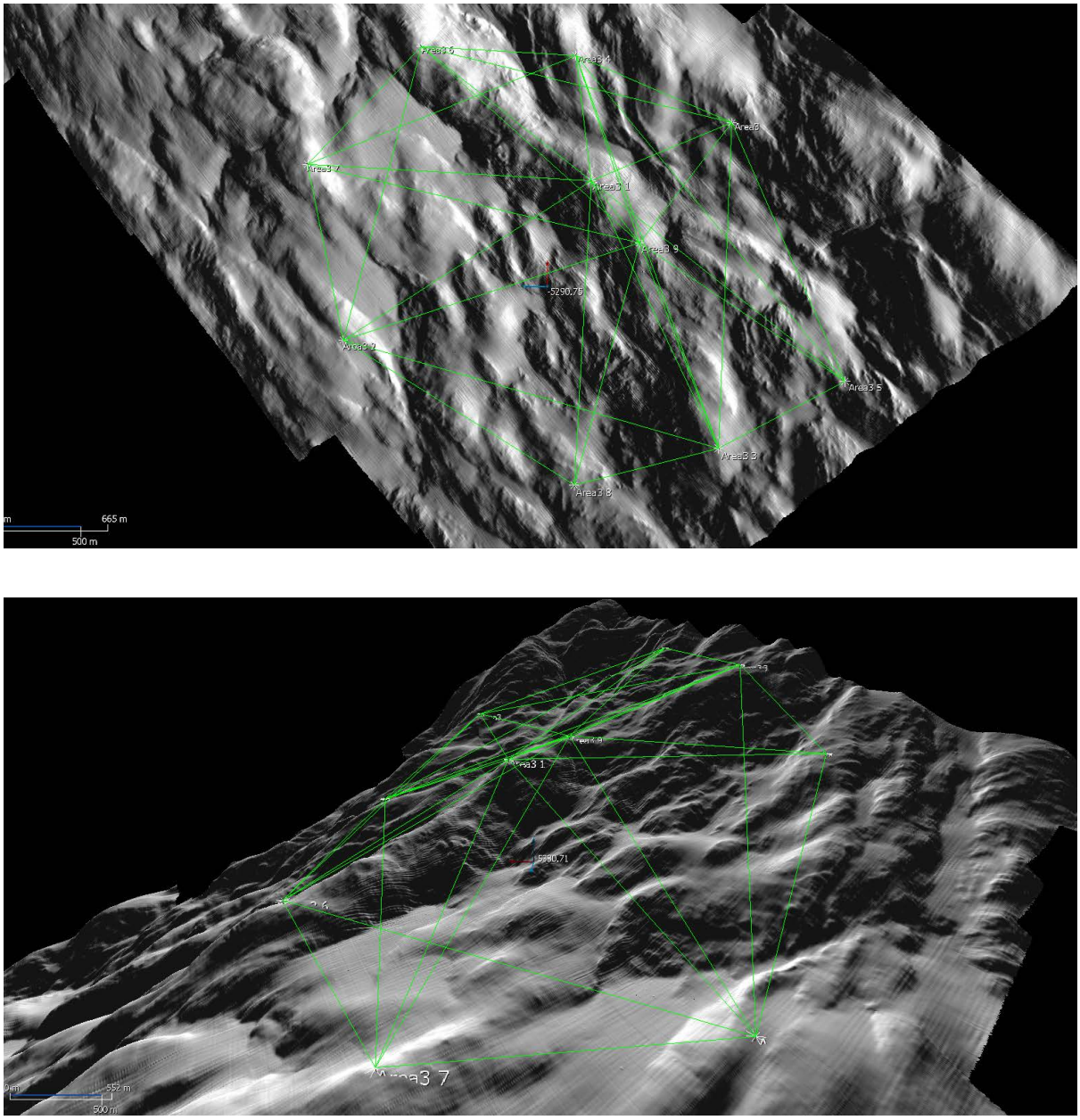

Figure 6.1.5.5: Seafloor view for GeoSEA sub array 3 on the lower continental slope. A total of 8 stations were placed surrounding 2 central stations. Green lines show all the measured baselines between the stations. Bottom image shows the array in a perspective view.

The two central stations A301 and A310 receive baselines from all surrounding stations and hence are characterized by the highest energy consumption. All stations have been assigned a logging period of 160 minutes, when they measure sound velocity, travel times between transponder stations, pressure and high-resolution temperature. Inclination values are logged at a rate of 100; battery status is logged at a rate of 101. The central stations A301 and A310 alternately log the sound velocity (i.e. baseline) at a rate of 2.

Figure 6.1.5.6 displays the measured physical parameters for station A304 and A308, respectively. Striking here is the correlation between the pressure variations and the sound velocity, which is less expected than a correlation between sound velocity and temperature (compare Figure 6.1.4.4). It must be noted, however, that the temperature variations are very small in comparison to the values measured in areas 1 and 2. In area 1, the temperature varies by 0.02-0.04°C, in area 2 by 0.02°C and in area 3 only by 0.005°C.

Computed baselines for between stations A305 → A306 and A302 → A307 are shown in Figure 6.1.5.7. Baseline variations of these yet unprocessed data are lower than 4 mm on average, documenting the high precision of the network. The shown baselines are between two pairs of transponders, which are 1870 m and 1728 m apart, respectively. Due to the fact that temperature variations and hence variations in the sound velocity are not as distinct as in areas located in shallower water, we expect that this deep-water network will render a higher resolution than e.g. the network in area 1, which is located in water depth of ~2500 m.

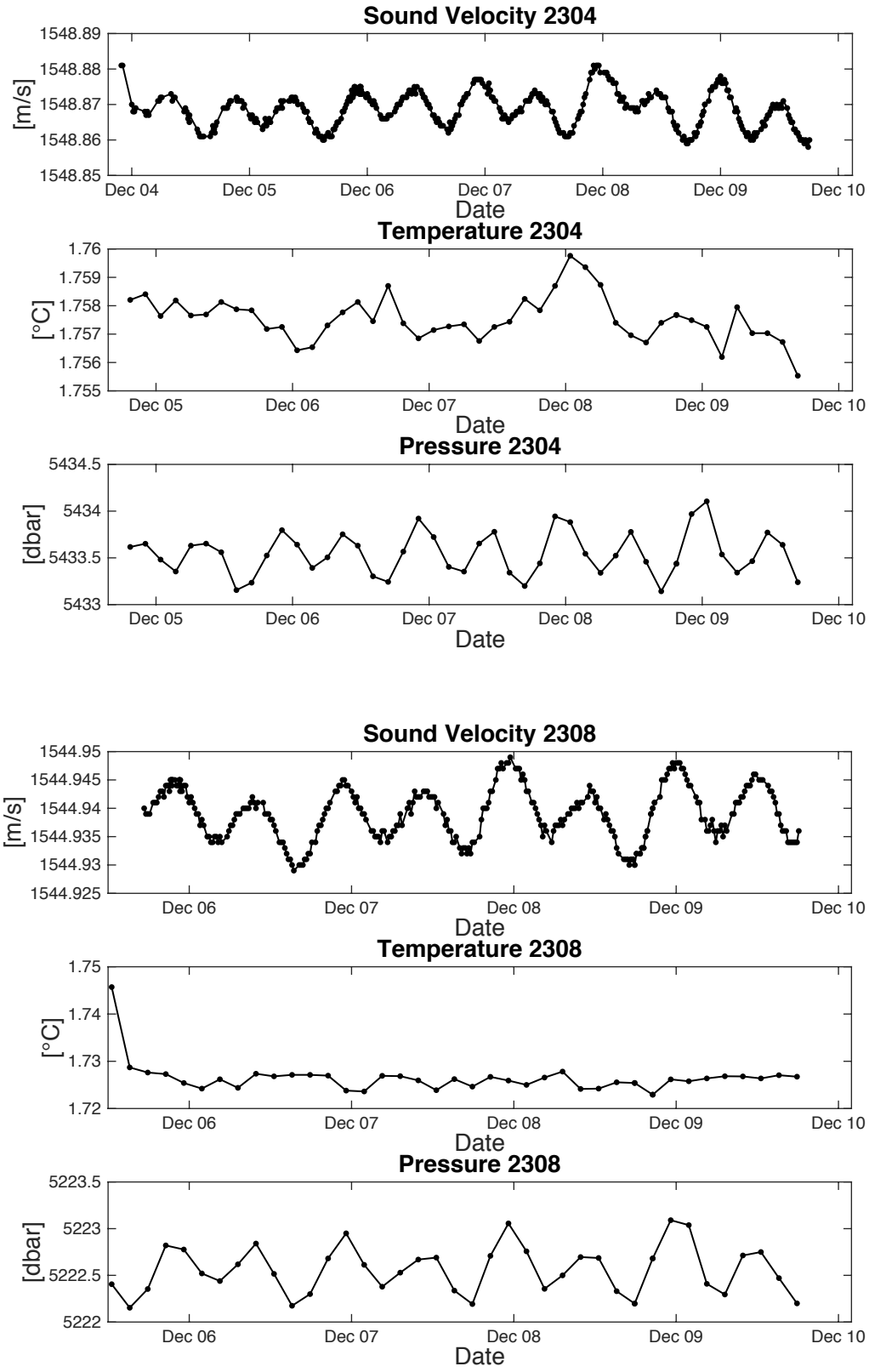

Figure 6.1.5.6: Logging data of area 2 plotted against time for stations A304 (2304, upper panels) and A308 (2308, lower panels). Sound velocity is in m/s, temperature in °C and pressure data in dbar.

Figure 6.1.5.7: Baselines between stations A305 (2305) and A306 (2306) (upper panel) and between stations A302 (2302) and A307 (2307) (lower panel). See Figure 6.1.3.9 caption for additional display information.

6.2 Seismology

6.2.1 Instrumentation

A total of 15 OBS instruments were recovered during Leg I of SO244 after a 12 months deployment on the Chilean forearc. All instruments are provided by the GEOMAR pool and were re-deployed during Leg II of SO244.

The GEOMAR OBS-2002

The GEOMAR Ocean Bottom Seismometer 2002 (OBS-2002) is a design based on experience gained with the GEOMAR Ocean Bottom Hydrophone (OBH; Flueh and Bialas 1996) and the GEOMAR Ocean Bottom Seismometer (OBS, Bialas and Flueh, 1999). The basic system is constructed to carry a hydrophone and a small seismometer for higher frequency active-seismic profiling. However, due to the modular design of the front end it can be adapted to different seismometers and hydrophones or pressure sensors. The sensors are OAS and *HTI-01-PCA* hydrophones from High Tech Inc. The sensitive seismometer is deployed between the anchor and the OBS frame (Figure 6.2.1.1), which allows for optimal coupling with the sea floor. The three-component seismometer (KUM), usually used for active seismic profiling, is housed in a titanium tube, modified from a package built by Tim Owen (Cambridge) earlier. Geophones of 4.5 Hz natural frequency were used during SO244-2. The recording device is a *MLS* recorder of *SEND GmbH*, which is contained in its own pressure tube and mounted next to the buoyant body opposite the release transponder (see Figure 6.2.1.1). The floatation is made of syntactic foam and is rated, as are all other components of the system, for a water depth of 6000 m.

While deployed to the seafloor the entire system rests horizontally on the anchor frame. The instrument is attached to the anchor with a release transponder. The release transponder is the *K/MT562* made by KUM GmbH. Communication with the instrument for release and range is possible through a transducer hydrophone, which is lowered ~20 m into the water. Over ranges of 4 to 5 miles release and range commands are successful. After releasing its anchor weight of approximately 60 kg the instrument turns 90° into the vertical and ascends to the surface with the floatation on top. This ensures a maximally reduced system height and water current sensibility at the ground (during measurement). On the other hand the sensors are

well protected against damage during recovery and the transponder is kept under water, allowing permanent ranging, while the instrument floats to the surface.

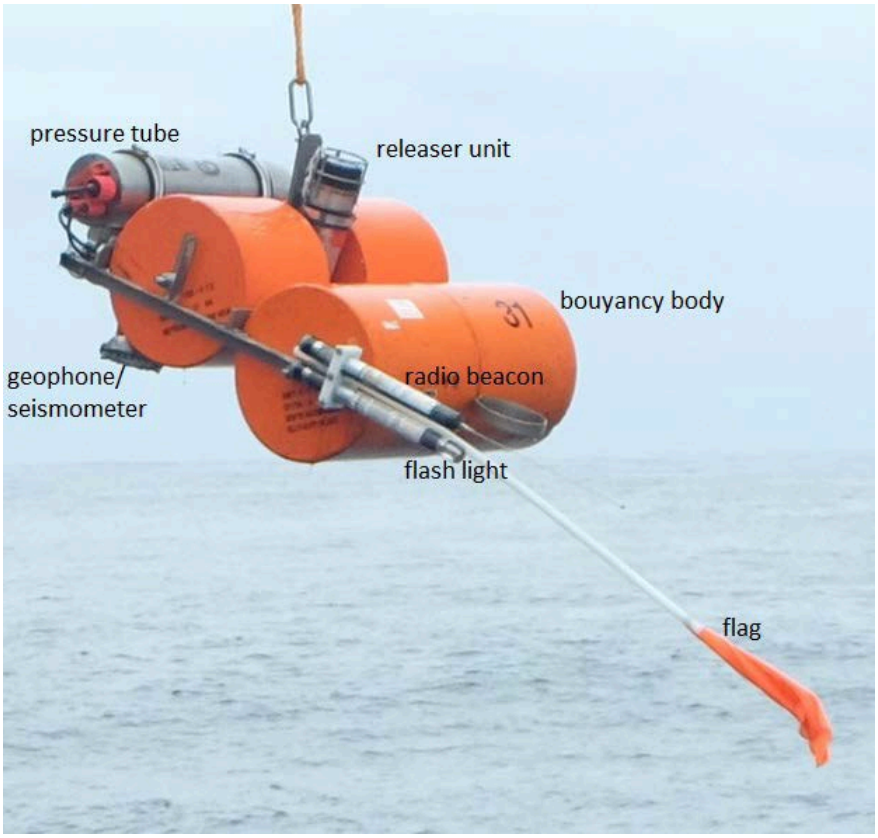

Figure 6.2.1.1: GEOMAR OBS (Design 2002).

6.2.2 Deployment

Fourteen instruments were re-deployed to cover the aftershock region of the April 1, 2014 Iquique/Pisagua earthquake (Figure 6.2.2.1). In addition, one instrument was deployed to the south of the rupture zone (Figures 6.2.2.1 and 6.2.2.2).

The deployment sites are slightly shifted from the locations of the previous deployment of November 2014 from OPV Comandante Toro (Figure 6.2.2.2). The reason for this is that the currently deployed stations shall be integrated into a 3D-seismic grid for an active seismic experiment using RV Langseth as platform in 2016. The previous and current layouts of OBS also serve as the offshore extension of the numerous networks installed onshore (Figure 6.2.2.2).

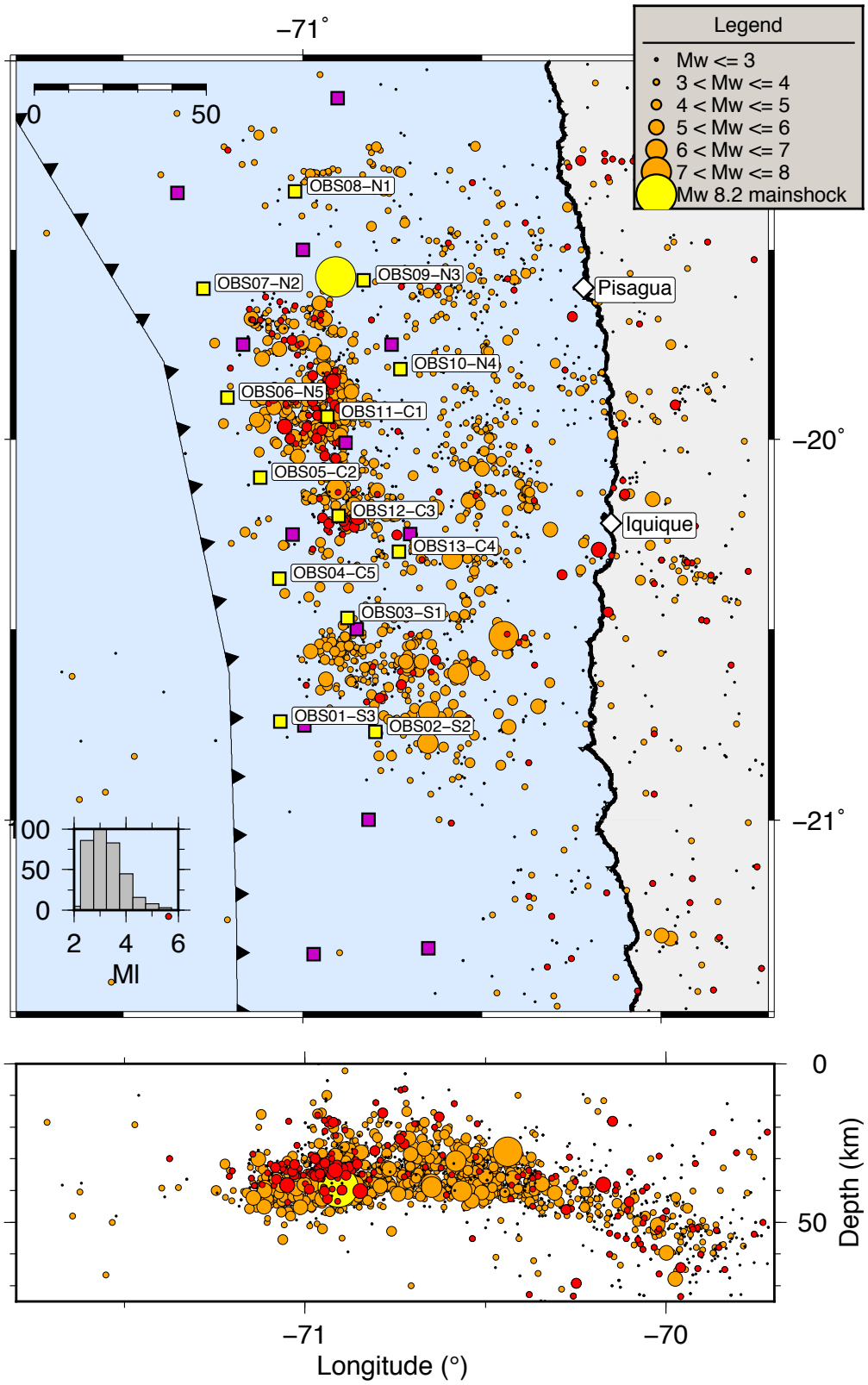

Figure 6.2.2.1: Distribution of OBS stations and aftershock seismicity (CSN catalogue, 1 April 2014 until 29 November 2015). The yellow squares indicate the 14 OBS stations installed during SO244, leg2 and are labelled with their station names. The purple squares show the location of the OBS installed during December 2014 with OVP Toro and de-installed during SO244, leg1. 389 events occurring since the deployment of the OBS stations (1 December 2014 until 29 November 2015 December) are shown in red.

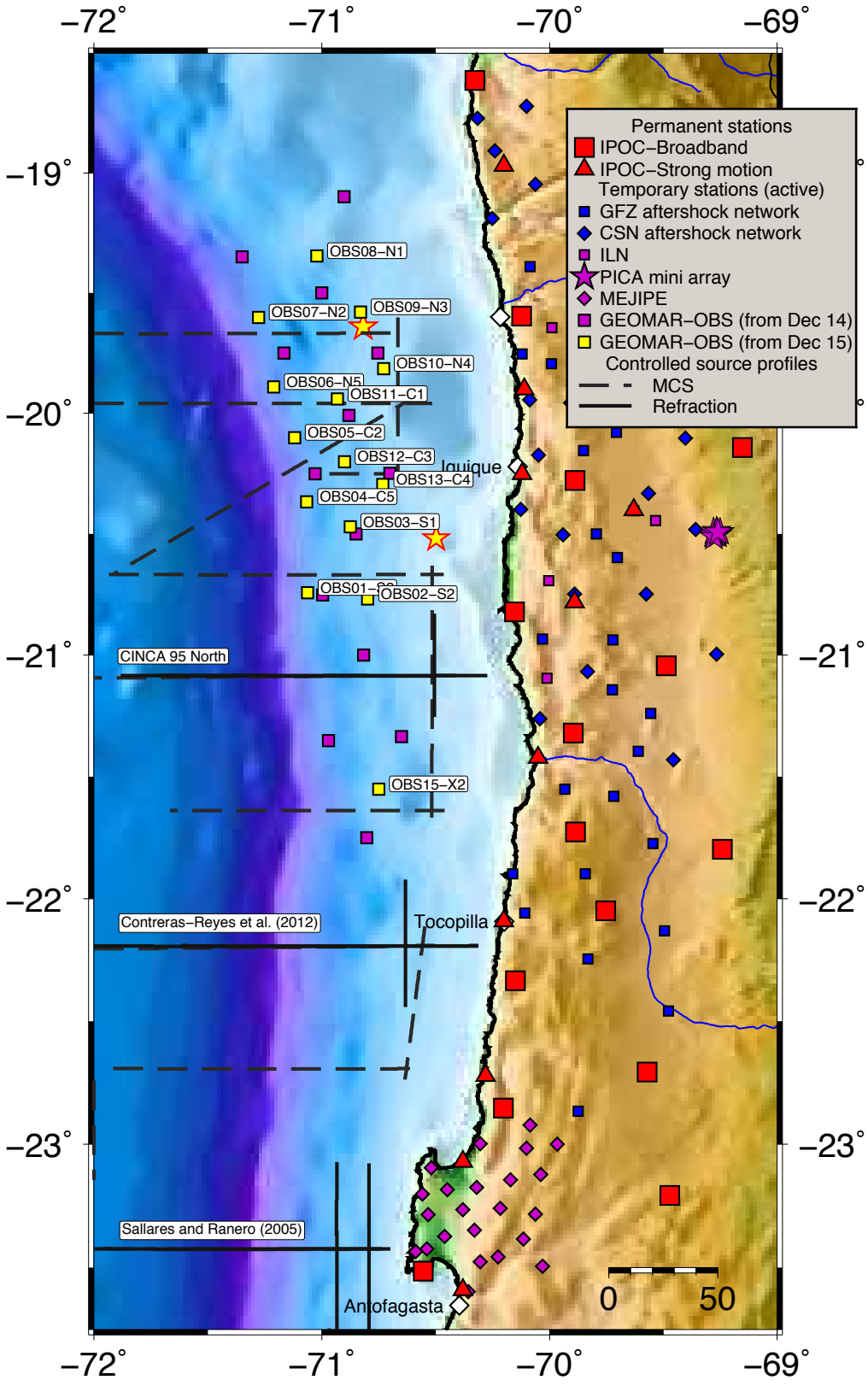

Figure 6.2.2.2: Location map of the seismological stations installed along the north Chilean forearc. The yellow squares indicate the 14 OBS stations installed during SO244, leg2 and are labelled with their station names. The purple squares show the location of the OBS installed during December 2014 with OVP Toro and de-installed during SO244, leg1. Black solid lines correspond to the seismic reflection profiles acquired by GEOMAR in 1995. Black dashed lines indicate MCS profiles acquired by BGR 1995.

Figure 6.2.2.3 shows the location map of OBS stations OBS01-OBS14 deployed during Leg II of SO244. The stations will be recovered by RV Langseth in 2016 and contain Li-batteries as well as alkali batteries as an energy source.

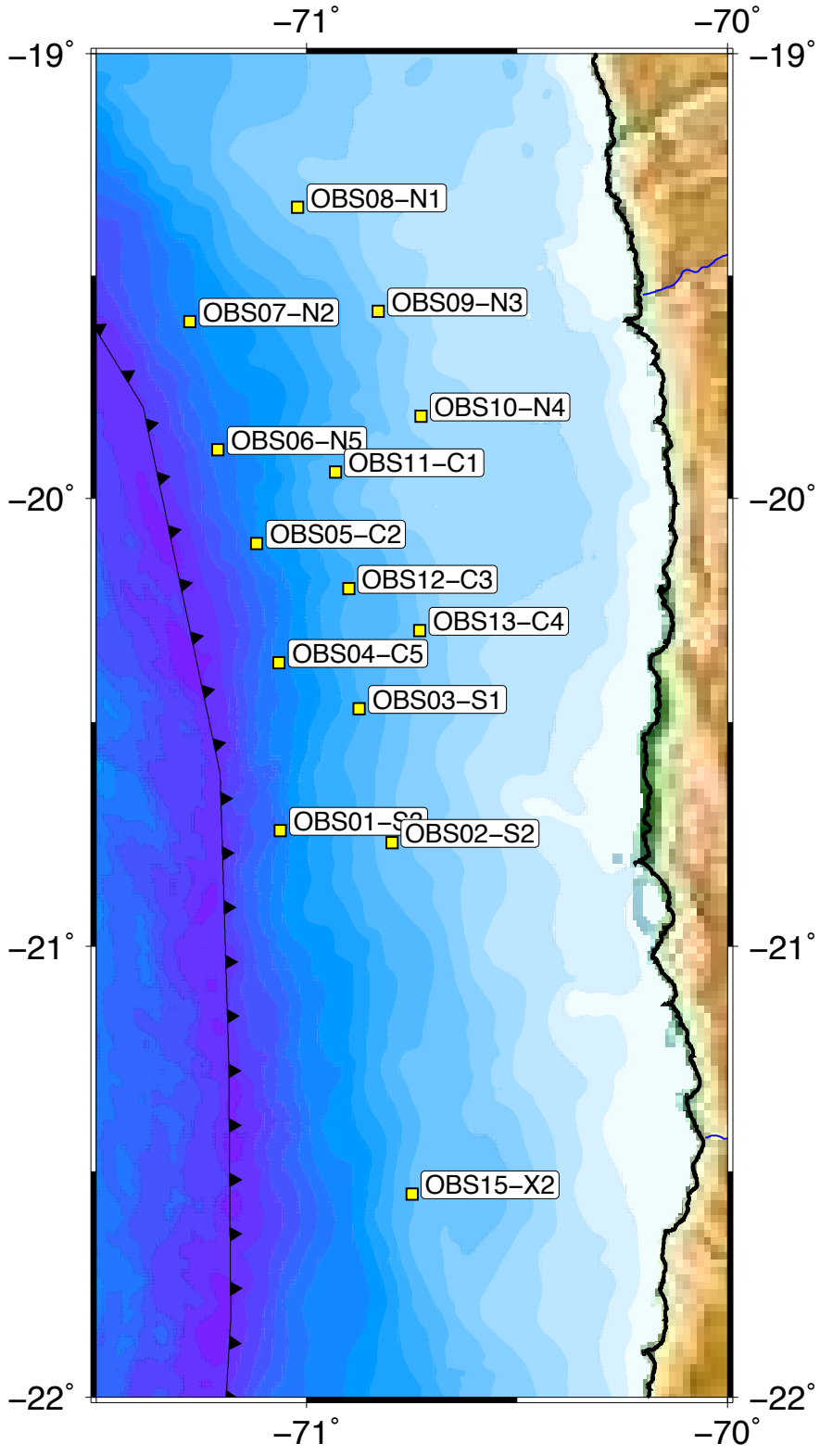

Figure 6.2.2.3: Location map of OBS stations deployed during SO244-2.

6.2.3 First Results of OBS Deployment Nov. 2014 – Nov. 2015

Of the 15 deployed instruments, four stations recorded data throughout the entire deployment. Unfortunately, two instruments died right at the beginning of the deployment and on nine stations recording stopped or is incomplete due to battery failure or leakage of geophone connections during the measurement.

Figure 6.2.3.1 shows the OBS distribution of the TORO network recovered during SO244-1 along with the seismicity recorded by the Centro Sismológico Nacional de la Universidad de Chile (CSN). Several clusters of earthquakes occur in this part of the Chilean Margin.

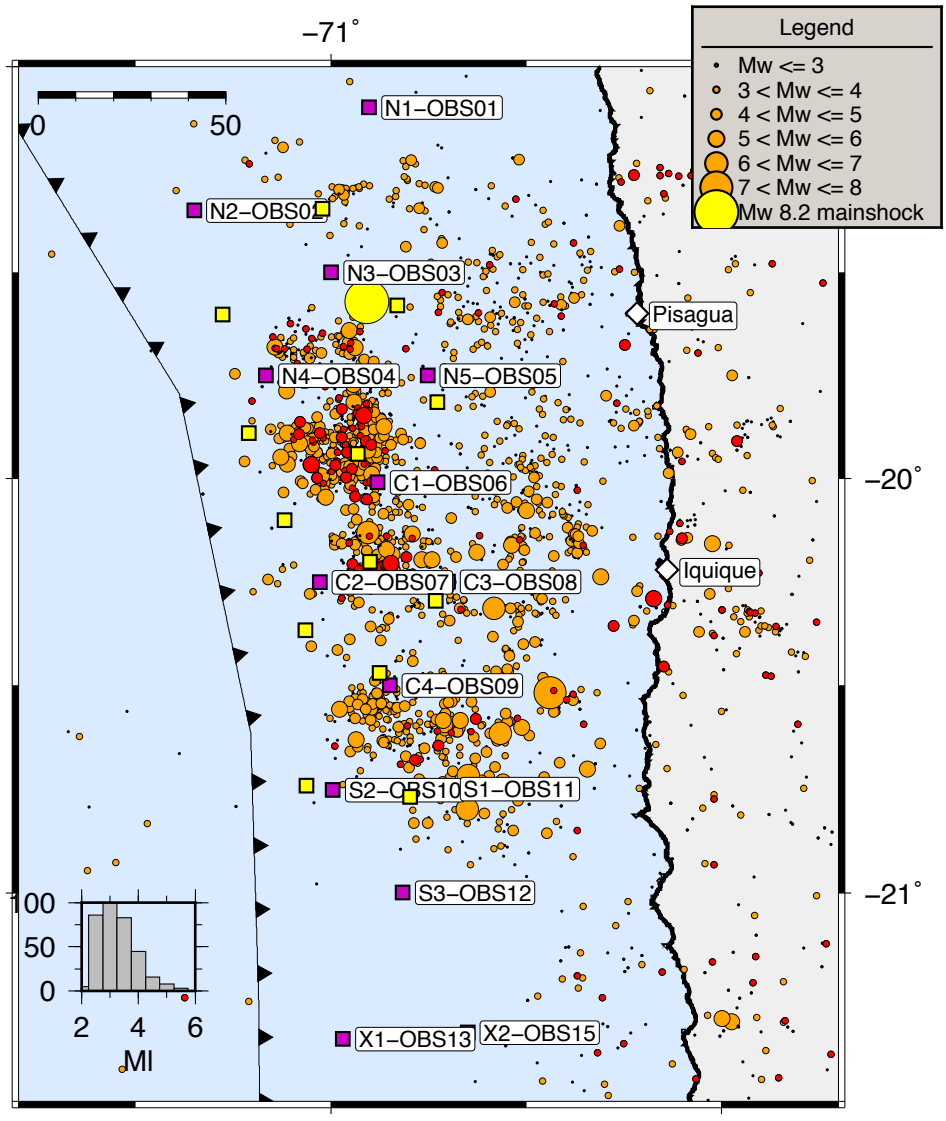

Figure 6.2.3.1: Distribution of the TORO OBS network (yellow squares) along with earthquakes, which are available from the CSN catalogue. See Figure 6.2.2.1 caption for display information.

The GEOMAR OBS recorded a large number of earthquakes. We chose one day of recording on January 9th 2015, where the CSN catalogue recorded five earthquakes of different magnitudes, ranging from 2.5 to 5.2 (Figure 6.2.3.2).

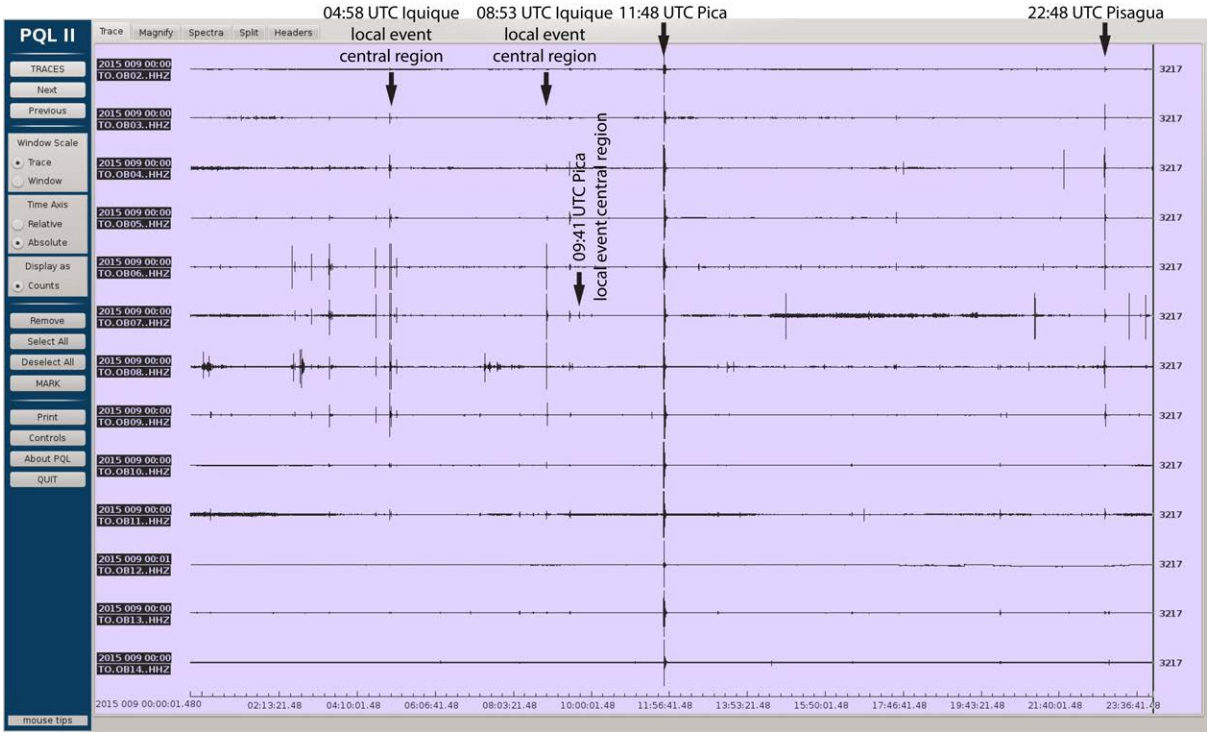

Figure 6.2.3.2: Vertical component of the 13 OBS geophones for January 9th 2015. The earthquakes, which are available from the CSN catalogue are indicated by arrows.

On January 9th 2015 our offshore OBS data show at least 100 earthquakes of which 52 occur in the central area of OBS stations OBS06-OBS08 (C1-C3 TORO network). Figure 6.2.3.4 shows three of these characteristic local earthquakes in the central area. Depending on their magnitude, these local earthquakes are partly only seen on stations OBS06-OBS08 (C1-C3 TORO network), whereas some of these local earthquakes are recorded on all 13 offshore stations, like the 04:58 UTC Iquique event in Figure 6.2.3.3. The difference in the onset of P and S waves of the local earthquakes gives us a depth estimate of 15 to 20 km for these events. Since the detection rate of the OBS network is more then tenfold above the landnetwork the whole number of detectable events is estimated with ~3500 and a magnitude of completeness unit below the CSN catalogue.

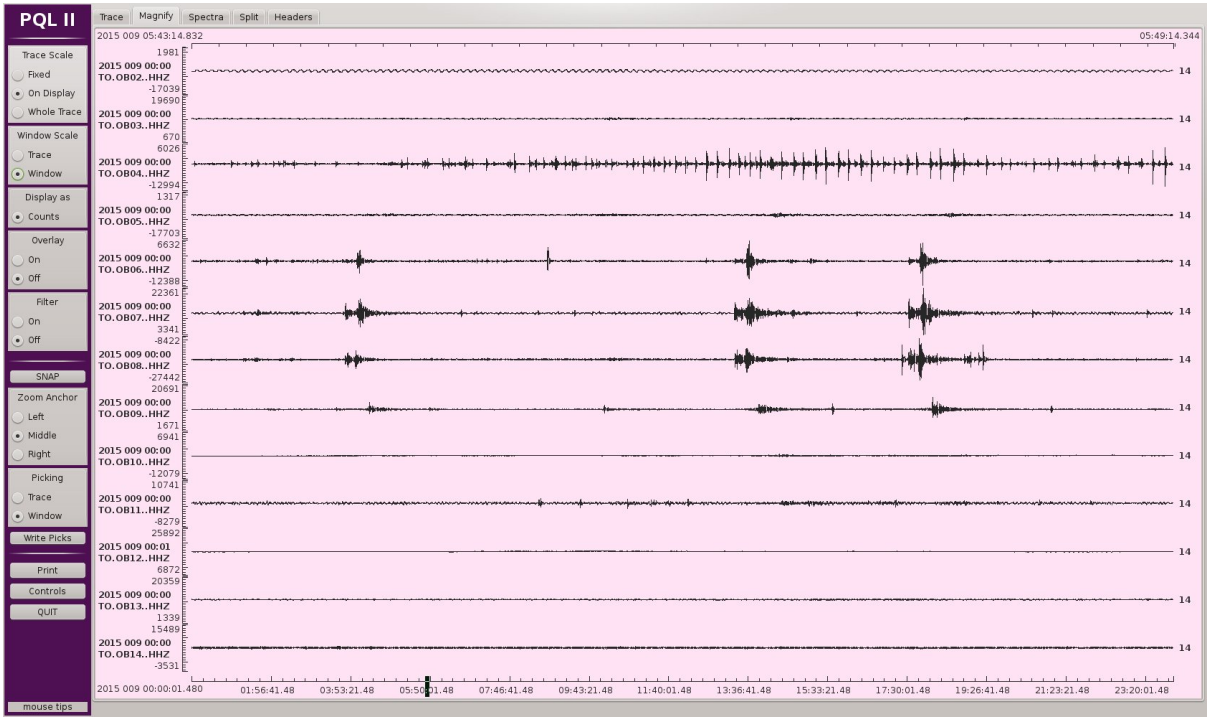

Figure 6.2.3.4: Detail of the vertical component of the 13 OBS geophones for January 9th 2015 showing six minutes. Three earthquakes occurred within ~4 minutes. They all arrive simultaneously at stations OBS06-OBS08 and are visible also at their neighboring stations. These local events locate in the central area between OBS stations OBS06-OBS08 (C1-C3).

6.3 Multibeam Bathymetry

6.3.1 The Kongsberg EM122 and EM710 systems

Two multibeam echosounder systems are available onboard RV SONNE for bathymetric mapping of the seafloor: A KONGSBERG EM122 for deep-water operations and a KONGSBERG EM710 for shallow water. Both systems were used during RV SONNE cruise 244-2. During stationary works, the Kongsberg multibeam system did not record data.

The Kongsberg Maritime EM122 multibeam echosounder operates at 12 kHz in water depths from 20 meters up to full ocean depth. The Kongsberg EM710 full performance version multibeam echosounder operates at frequency ranges of 70 to 100 kHz. The minimum operation depth is 3 m below its transducers, and the maximum acquisition depth is ~2000 m.

For both, the Kongsberg Maritime EM122 and EM710, two different transmission pulses can be selected: a CW (Continuous Wave) or FM (Frequency

Modulated) chirp. The sounding mode can be either equidistant or equiangle, depending on operation preferences and requirements. The systems can be operated in single-ping or dual-ping mode, where one beam is slightly tilted forward and the second ping slightly tilted towards the aft of the vessel. The whole beam can also be inclined towards the front or the back, and the pitch of the vessel can be compensated dynamically. The EM122 system produces 432 beams. The EM710 system generates 256 beams. Both systems produce a beam with a maximum width of 150° across the ship and 0.5° along and 1° across the ship.

Considering that the outermost beams are noisy when using the maximum transmit width of 150°, this was reduced to a fixed value of 140° for the whole cruise for both, the EM122 and EM710 systems. This means that in general the swath covered was a function of depth only: $w=2´d´\tan(140°/2)$ or roughly $5.5´d$, where w is the swath width and d is the water depth. The number of soundings acquired in every ping cycle is 432. This implies that the spacing between soundings for one swath is equal to $5.5d$ / (432-1) = $0.01275d$. As an example at 1,000m water depth spacing between adjacent soundings is 12,7m and at 6,000m water depth spacing is 76.5m. This is the resolution *across* the track. On the other hand, the ping rate depends on the water depth and is greater or equal to $TWT=2´d/C$, where C is the sound speed in the water column. The distance between one ping and the next one depends on the ping rate and on the ship's speed (V), and is equal to $TWT´V$. This is the resolution *along* the track.

The echo signals detected from the seafloor go through a transceiver unit (Kongsberg Seapath) into the data acquisition computer or operator station. In turn, the software that handles the whole data acquisition procedure is called Seafloor Information System (SIS). In order to correctly determine the point on the seafloor, where the acoustic echo is coming from, information abouth the ship's position, movement and heading, as well as the sound velocity profile in the water column are required.

Positioning is implemented onboard RV SONNE with conventional GPS/GLONASS plus differential GPS (DGPS) by using either DGPS satellites or DGPS land stations, resulting in quasi-permanent DGPS positioning of the vessel.

These signals also go through the transceiver unit (Seapath) to the operator station. Ship's motion and heading are compensated within the Seapath and SIS by using a Kongsberg MRU 5+ motion sensor. Beamforming also requires sound speed data at the transducer head, which is available from a Valeport MODUS SVS sound velocity probe. This signal goes directly into the SIS operator station. Finally, the sound velocity profiles for the entire water column were used from the CTD measurements described in chapters 6.1.3 and 6.1.5.

6.3.2 Multibeam bathymetry data

Throughout most of RV SONNE cruise 244-2 the Kongsberg EM122 system was used, mapping the seafloor in water depths >2000 m. The map in Figure 3.1 shows the data coverage achieved during cruise SO244 Leg I and II.

One shallow-water region was mapped with the Kongsberg EM710 system. The data, as well as a comparison of bathymetric data acquired with the EM122 in the same area, are displayed in Figure 6.3.2.2. The higher resolution of the EM710 data enhances small-scale bathymetric structures in the shallow-water area. This is even more evident when comparing detailed sub-sets of the data. Figure 6.3.2.3 compares two regions of the survey. The ~10 m resolution data of the EM710 system returns far more structural detail than the ~75 m resolution grid of the EM122 system. Scarps that are vainly visible in the EM122 stand out clear and crisp in the higher resolution data. Even though the EM710 data still has about 5 times less resolution than AUV-based bathymetry, it poses a reliable alternative to deep-water instruments when working in water depth <2000 m. The data set acquired here will be used as a priori information by Dr. Jeff McGuire, Woods Hole Oceanographic Institution, USA for deployment of their seafloor geodesy instruments.

The deep water mapping using the EM122 system focused on the outer rise area south of GeoSEA working area 2, as this region was previously uncharted (Figure 6.3.2.4). The negligible sediment cover of the outer rise is insufficient to drape the distinct original spreading-related seafloor fabric trending NW-SE. Numerous volcanic edifices of different sizes overprint these structures. Towards the trench, plate-

bending related normal faults dominate the seafloor morphology.

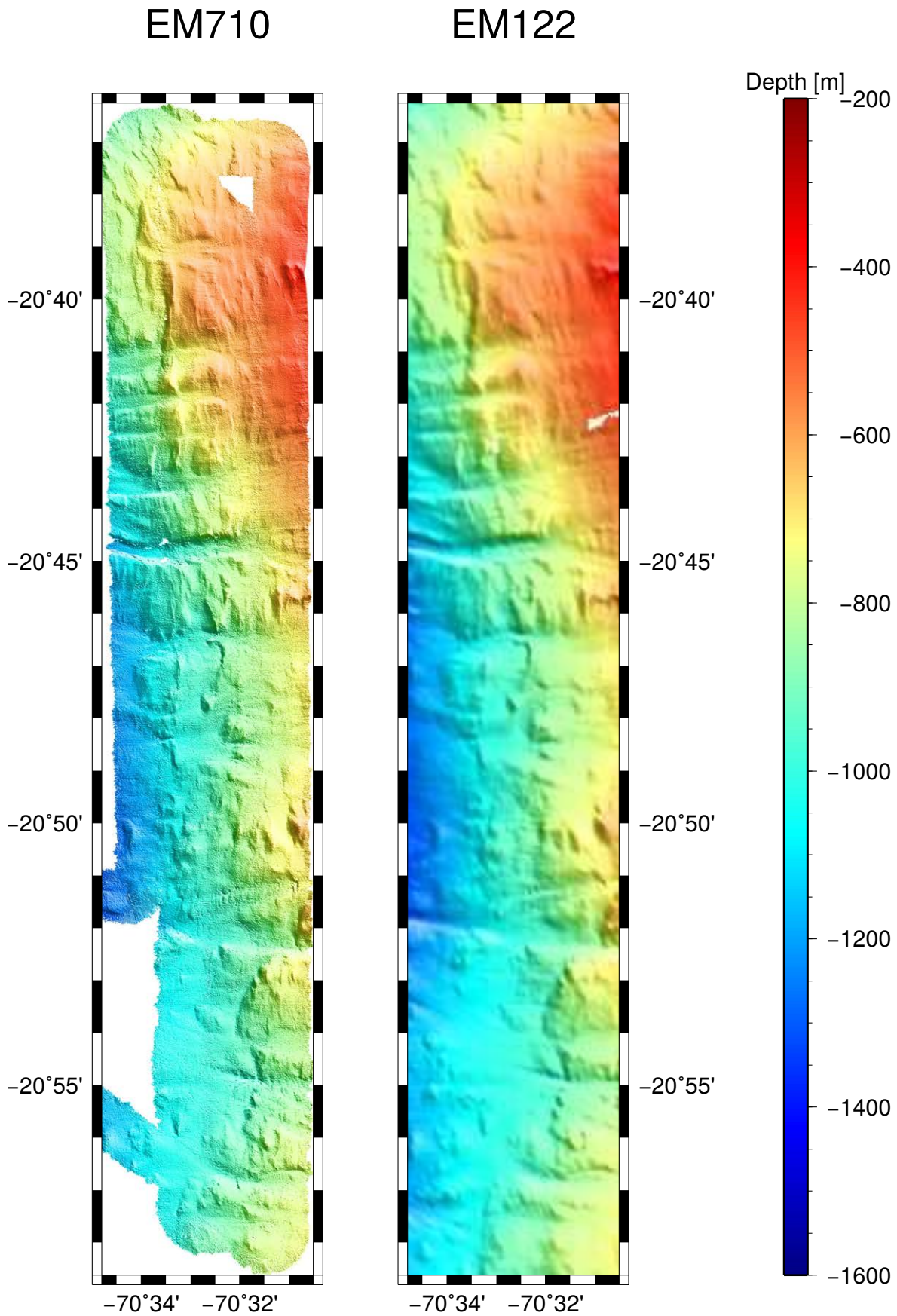

Figure 6.3.2.2: Bathymetric map recorded with the EM710 (left). Note the very high resolution compared with the data recorded with the EM122 (right) in the shallow-water area.

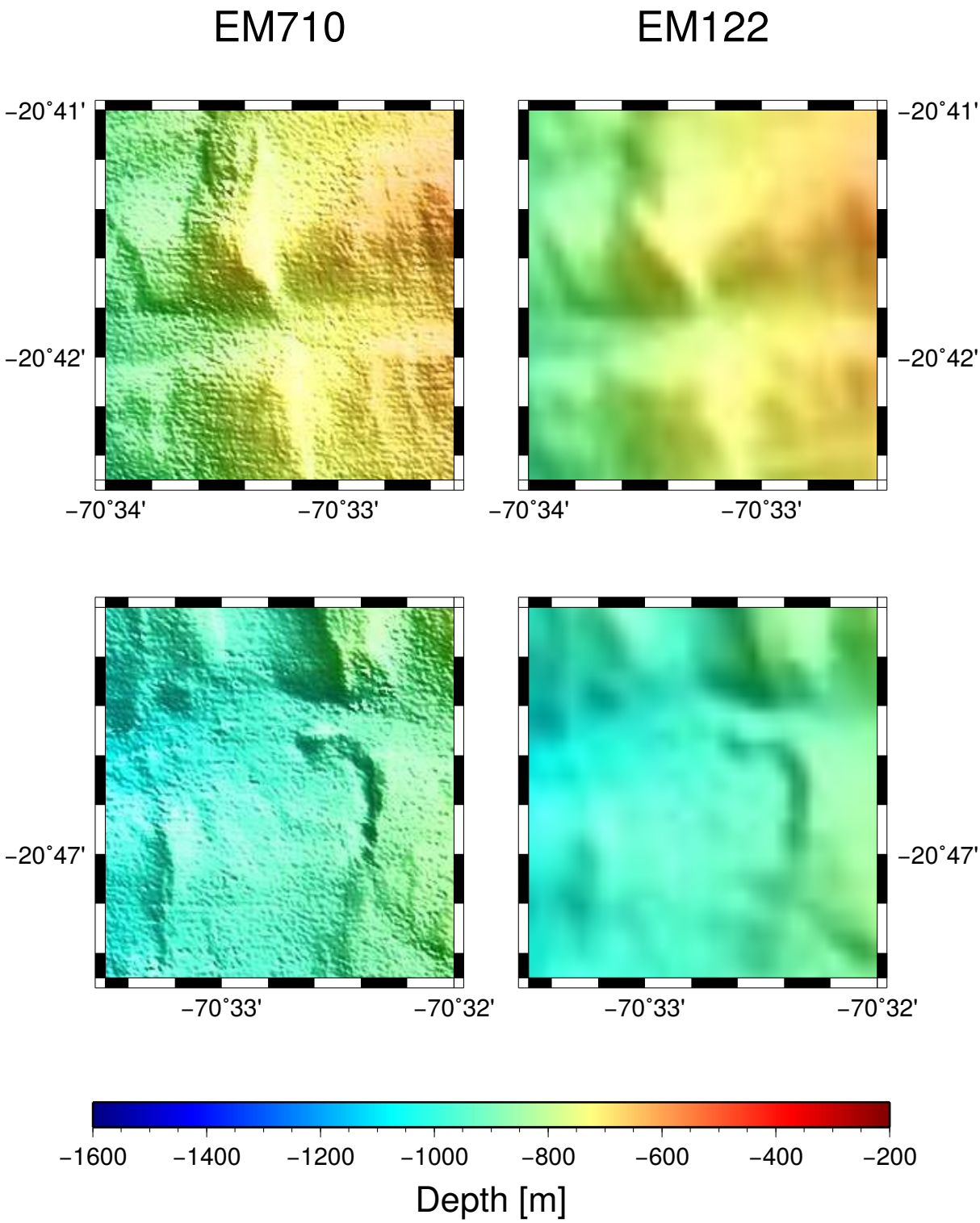

Figure 6.3.2.3: Detailed comparison between data acquired by the EM710 and EM122 systems. EM710 is rated for water depth shallower than ~2000 m, where it returns data with a resolution of ~10 m. EM122 has a resolution of ~75 m.

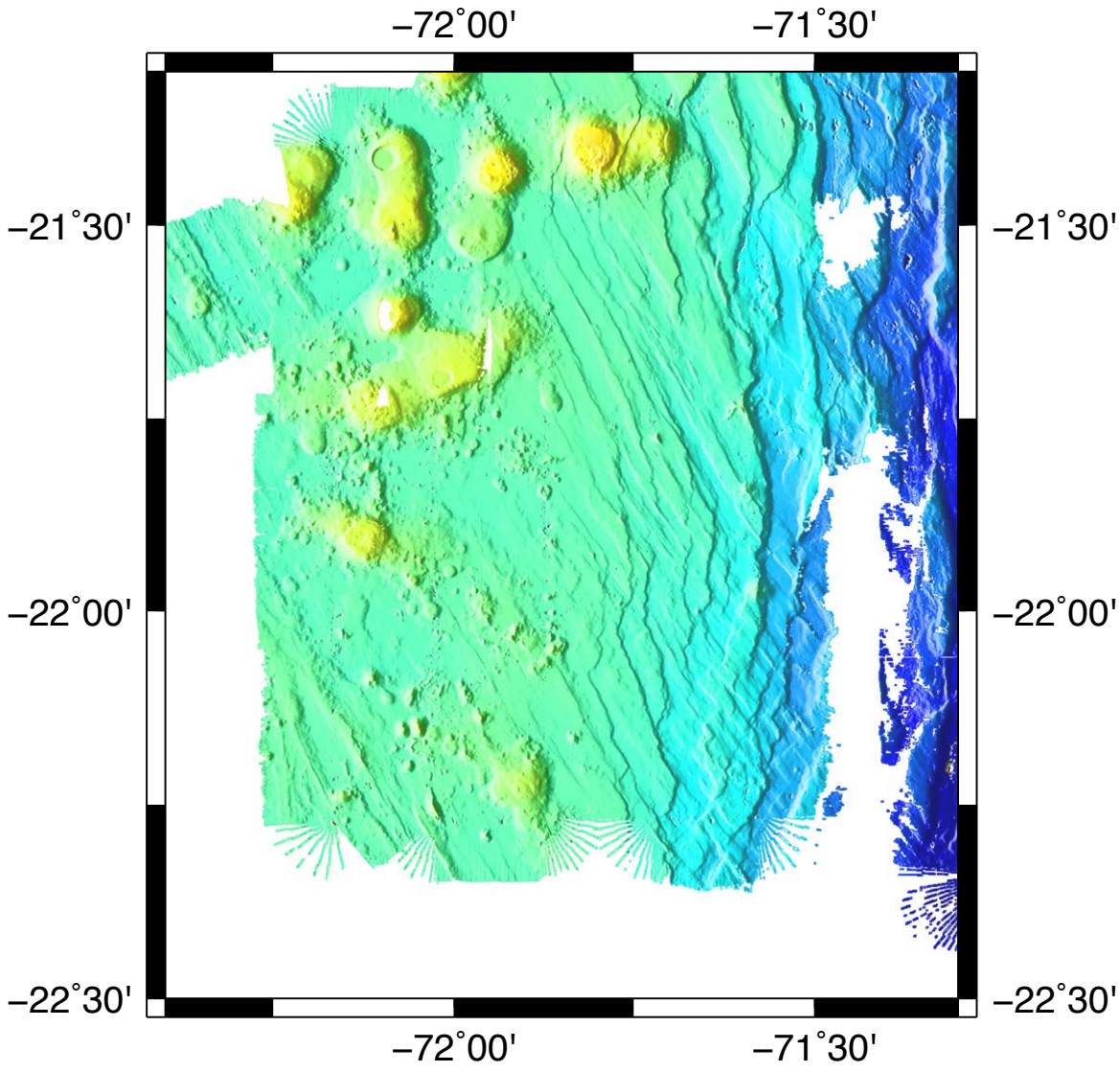

Figure 6.3.2.4: Swath bathymetric survey of the outer rise region mapped with EM122 during SO244 Leg II. These data will be merged with previously acquired data from Leg I to achieve full coverage of the trench.

7. Acknowledgements / Danksagung

The cruise SO244-2 was financed in the scope of the project GEOSEA by the German Federal Ministry for Education and Research (Bundesministerium für Bildung und Forschung / BMBF) under grant No. 03G0244A. The GeoSEA array and the GeoSURF wave glider were financed by the BMBF under grant 03F0658I. We are grateful for the continuous support of marine sciences with an outstanding platform such as RV SONNE. The authors wish to express their gratitude to the various colleagues who have supported the work prior and during the cruise. Particular thanks are directed to the director of the Centro Sismológico Nacional de la Universidad de Chile (CSN) S. Barrientos, Univ. de Chile, Santiago. The Leitstelle Deutsche Forschungsschiffe in Hamburg, Germany and Briese Schiffahrts GmBH & Co. KG are acknowledged for their support and assistance. The installation of the GeoSEA array was only made possible by the scientists' and the crew's experience; without the excellent support of the ship's master, Captain Lutz Mallon and the entire crew of RV SONNE throughout the cruise this project could not have been realized. Their highly professional work and high motivation proved a prerequisite for the success of SO244.

8. References / Literaturverzeichnis

Ballu V, Ammann J, Pot O, de Viron O, Sasagawa GS, Reverdin G, Bouin MN, Cannat M, Deplus C, Deroussi S et al. (2009a) A seafloor experiment to monitor vertical deformation at the Lucky Strike volcano, Mid-Altantic Ridge. Journal of Geodesy 10.1007/s00190–008-0248-3.

Ballu V, Bouin MN, Calmant S, Folcher E, Bore JM, Ammann J, Pot O, Diament M, Pelletier B (2009b) Absolute seafloor vertical positioning using combined pressure gauge and kinematic GPS data. Journal of Geodesy doi: 10.1007/s00190–009-0345-y.

Béjar-Pizarro, M. et al., Asperities and barriers on the seismogenic zone in North Chile: state-of-the-art after the 2007 *M*w 7.7 Tocopilla earthquake inferred by GPS and InSAR data, Geophys. J. Int., 183, 390-406, 2010.

Bialas, J., and Flueh, E. R., Ocean Bottom Seismometers, Sea Technology, 40, 4, 41-46, 1999.

Boebel, O, Busack, M., Flueh, E., Gouretski, V., Rohr, H., Macrander, A., Krabbenhoeft, A., Motz, M., Radtke, T., The GITEWS ocean bottom sensor packages, Nat. Haz. Earth Syst. Sciences, 10, 1750-1780, 2010.

Briggs, R. W., Sieh, K., Meltzner, A. J., Natawidjaja, D., Galetzka, J., Suwargadi, B., Hsu, Y.-j., Simons, M., Hananto, N., Suprihanto, I., Prayudi, D., Avouac, J.-P., Prawirodirdjo, L., Bock, Y., Deformation and Slip Along the Sunda Megathrust in the Great 2005 Nias-Simeulue Earthquake, Science, 311, doi: 10.1126/science.1122602.

Chadwell, C.D., F.N. Spiess Plate motion at the ridge-transition boundary of the south Cleft Segment of the Juan de Fuca ridge from GPS-data, Journal of Geophysical Research, Vol. 113, B04415, 15 pp., 2008.

Chadwell, C, Sweeney, A. D., Acoustic Ray-Trace Equations for Seafloor Geodesy, Marine Geodesy, 33, 164-186, 2010.

Chadwick. W., Nooner, S., Butterfield, D., Lilley, M., Seafloor deformation and forecasts of the April 2011 eruption at Axial Seamount, Nature Geosc., DOI: 10.1038/NGEO1464, 2012.

Contreras-Reyes, E, J. Jara, I. Grevemeyer, S. Ruiz, D. Carrizo, Abrupt change in the dip of the subducting plate beneath north Chile. Nature Geoscience, 5, 342-345, 2012.

Delacourt, C., Raucoules, D., Le Mouélic, S., Carnec, C., Feurer, D., Allemand P., and Cruchet, C., (2009), Observation of a Large Landslide on La Reunion Island Using Differential Sar Interferometry (JERS and Radarsat) and Correlation of Optical (Spot5 and Aerial) Images, Sensors , 9(1), 616-630

Dzurisin, D., 2003, A comprehensive approach to monitoring volcano deformation as a window on the eruption cycle, Reviews of Geophysics, 41(1), 1.1-1.29, doi:10.1029/2001RG000107.

Flueh, E.R., and Bialas, J., A digital, high data capacity ocean bottom recorder for seismic investigations, Int. Underwater Systems Design, 18, 3, 18-20, 1996.

Heki, K., A tale of two earthquakes, Science, 332, 1390-1391, 2011.

Hsu, Y., Simons, M., Avouac, J. P., Galetzka, J., Sieh, K., Chlieh, M., Natawidjaja, D., Prawirodirdjo, L., Bock, Y., Frictional afterslip following the Mw 8.7, 2005 Nias-Simeulue earthquake, Sumatra, Science, 312, doi: 10.1126/science.1126960, 2006.

Kanamori, H., Brodsky, E., The Physics of Earthquakes, Reports on Progress in Physics, 67, 1429-1496, 2004.

Kopp,H., Invited Review Paper: The control of subduction zone structural complexity and geometry on margin segmentation and seismicity, Tectonophysics, doi: 10.1016/j.tecto.2012.12.037, 2013.

Lay, T., Yue, H., Brodsky, E.E., An, C. (2014), The 1 April 2014 Iquique, Chile, Mw 8.1 earthquake rupture sequence. Geophys. Res. Lett., 41, 2014GL060238. doi: 10.1002/2014GL060238.

Liu, Z., Owen, S., Dong, D., Lundgren, P., Webb, F., Hetland, E., Simons, M., Estimation of interplate coupling in the Nankai trough, Japan using GPS data from 1996 to 2006, Geophys. J. Int., 181, doi: 10.1111/j.1365-246X.2010.04600.x, 2010.

Michel, R. and J.P. Avouac, Deformation due to the 17 August Izmit, Turkey, earthquake measured from SPOT images, J. Geophys. Res, 107, 2002

Newman, A. V., Hidden depths, Nature, 474, 441-443, 2011.

Osada, Y., Kido, M., Fujimoto, H., and Kaneda, Y., Development of a seafloor acoustic ranging system toward the seafloor cable network system, Ocean Eng., 35, 1401-1405, 2008.

Phillips, K., Chadwell, C, Hildebrand, J., Vertical deformation measurements on the submerged south flank of Kılauea volcano reveal seafloor motion associated with volcanic collapse, J. Geophys. Res., 113, 2008.

Ruiz, S., Metois, M., Fuenzalida, A., Ruiz, J., Leyton, F., Grandin, R., Vigny, C., Madariaga, R., Campos, J. (2014), Intense foreshocks and a slow slip event preceded the 2014 Iquique Mw 8.1 earthquake. Science 1256074. doi:10.1126/science.1256074

Schurr, B., et al., (2014), Gradual unlocking of plate boundary controlled initiation of the 2014 Iquique earthquake. Nature 512, doi: 10.1038/nature13681

Wang, K., Hu, Y., He, J., Deformation cycles of subduction earthquakes in a viscoelastic Earth, Nature, 484, 327-332, 2012.

9. Abbreviations / Abkürzungen

AMT	--	Autonomous Monitoring Transponder
AUV	--	Autonomous Underwater Vehicle
CNS	--	Centro Sismológico Nacional de la Universidad de Chile
GeoSEA	--	Geodetic Earthquake Observatory on the Seafloor
GeoSURF	--	Geodetic Earthquake Observatory Surface Vehicle
IPOC	--	Integrated Plate Boundary Observatory Chile
OBS	--	Ocean Bottom Seismometer

10. Appendices / Anhänge

Appendix A: Participating Institutions / Liste der teilnehmenden Institutionen

GEOMAR
Helmholtz-Zentrum für Ozeanforschung Kiel
Wischhofstr .1-3
24148 Kiel, Germany
www.geomar.de

Universidad de Chile
Departamento de Geofísica
Santiago de Chile, Chile
www.uchile.cl

Servicio Hidrográfico y Oceanográfico de la Armada de Chile (SHOA)
Errázuriz 254, Playa Ancha
Valparaíso, Chile
www.shoa.mil.cl

Sonardyne International Ltd.
Blackbushe Business Park
Yateley, Hampshire
GU46 6GD United Kingdom
www.sonardyne.com

Christian-Albrechts-Universität zu Kiel (CAU)
Christian-Albrechts-Platz 4
24188 Kiel, Germany
www.uni-kiel.de

Appendix B: CTD Profiles CTD01 (Area 1) and CTD02 (Area 3)

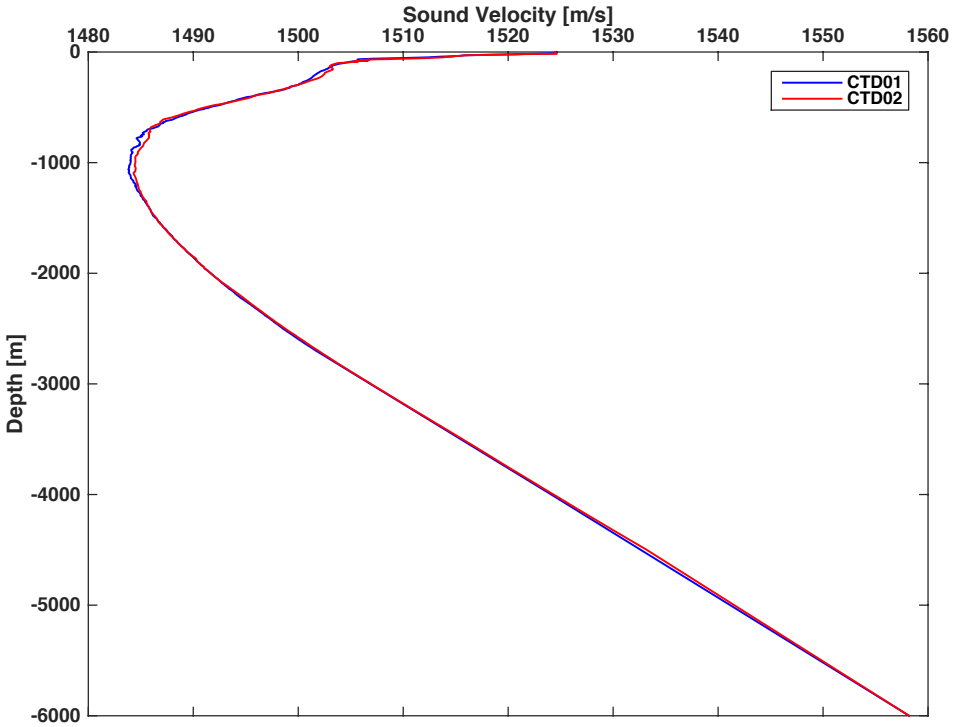

Appendix E: OBS Deployment

	INST.	LAT (S)	LON (W)	DEPTH	RELEASE	RELEASE ENABLE	REC.	SYNC	CYLIND.	ANT.	SENSORS	REMARKS
		D:M	D:M	(m)	CODE	DISABLE	NO.	TIME	NO.	CH.		
SO244-2	OBS 01	20° 44.49'	71° 03.75'	5350	133664	120015/120036	MLS 000709	5.12.15/21:42	65	D	OAS 44 (negative) + Owen 0205-027	
	OBS 02	20° 46.11'	70° 47.87'	2501	427524	410310/410333	MLS 000712	6.12.15/21:33	66	A	Owen 0708-101	no hydrophone
	OBS 03	20° 28.18'	70° 52.57'	2898	143272	141117/141134	MLS 061202	6.12.15/19:33	3	D	OAS 27 (negative) + Owen 1205-125	
	OBS 04	20° 22.01'	71° 03.96'	5071	444674	461737/461754	MLS 040807	6.12.15/20:19	58	D	HTI 80 (negative) + Owen 1001-114	
	OBS 05	20° 06.03'	71° 07.13'	4819	427430	410051/410072	MLS 100901	7.12.15/12:30	75	B	OAS 03 (positive) + Owen 1205-129	
	OBS 06	19° 53.40'	71° 12.65'	5346	427737	411005/411026	MLS 991249	7.12.15/15:45	74	C	HTI 91 (positive) + Owen 0807-098	
	OBS 07	19° 36.14'	71° 16.65'	4887	430424	412470/412501	MLS 991240	7.12.15/16:22	59	A	OAS 26 (negative) + Owen 0509-075	
	OBS 08	19° 20.75'	71° 01.30'	1735	131415	113424/113441	MLS 991248	7.12.15/19:05	60	C	HTI 39 (negative)	no geophone
	OBS 09	19° 34.79'	70° 49.81'	1729	133525	117432/117457	MLS 040304	7.12.15/20:33	62		HTI 108 (negative) + Owen 0403-055	no sender
	OBS 10	19° 48.93'	70° 43.65'	1432	134037	120410/120433	MLS 081002	7.12.15/22:07	71	C	HTI 109 (negative) + Owen 0205-031	
	OBS 11	19° 56.43'	70° 55.91'	2736	435610	440126/440143	MLS 020601	8.12.15/04:03	61	B	HTI 12 (negative) + Owen 0807-094	
	OBS 12	20° 12.09'	70° 54.02'	2998	430135	411537/411552	MLS 991255	8.12.15/05:49	73	D	HTI 73 (negative) + Owen 1001-121	
	OBS 13	20° 17.72'	70° 43.85'	2100	430274	412104/412127	MLS 991247	8.12.15/07:37	72	A	HTI 67 (positive) + Owen 0509-072	
	OBS 15	21° 32.991'	70° 45.003'	2787	646673	663540/663565	MLS 010409	11.12.15/19:40	64	B	HTI 113 (positive) + Owen 0310-048	

Appendix D: GeoSEA Transponder Station List

	Station	Transponder adress	Unit ID	Transponder S/N	Deployment at seafloor				REMARKS
					Date / UTC Time (dd.mm.yy / hh:mm)	LAT (S) D:M	LON (W) D:M	DEPTH (m)	
SO244-2 Area 1	A101	2701	00372A	284790-002	28.11.15 / 15:48	20°47,943 S	70°48,910 W	2733	Freefall; from Posidonia release position ~1200m
	A102	2702	0043D4	284790-003	28.11.15 / 23:16	20°47,677 S	70°48,460 W	2603	
	A103	2703	0037A7	284790-004	29.11.15 / __:__	20°47,577 S	70°48,995 W	2744,7	
	A104	2615	003905	284790-005	29.11.15 / 13:19	20°47,373 S	70°48,521 W	2615	
	A105	2705	0030B6	284790-008	29.11.15 / 21:41	20°48,118 S	70°49,381 W	2863	
	A106	2706	003A56	284792-009	06.12.15 / 16:44	20°47,792 S	70°49,444 W	2836	
	A107	2707	002FAF	284792-010	06.12.15 / 20:03	20°47,884 S	70°49,825 W	2860	
	A108	2708	00374B	284790-001	07.12.15 / 12:46	20°47,611 S	70°49,994 W	2852,3	set offset from start time to 55min to avoid time clash with A104
SO244-2 Area 2	A201	2201	0036DB	284791-006	30.11.15 / 11:41	21°03,370 S	71°43,846 W	4105,7	
	A202	2202	003732	284791-008	30.11.15 / 17:21	21°03,089 S	71°43,923 W	4104,9	
	A203	2203	003793	284791-009	01.12.15 / 13:20	21°03,439 S	71°44,135 W	4065,9	
	A204	2204	003111	284792-006	01.12.15 / 17:01	21°03,127 S	71°44,256 W	4034	
	A205	2205	003328	284791-005	01.12.15 / 20:19	21°03,330 S	71°44,134 W	4059,3	approx. 22m more northern than planned; release 20:20
SO244-2 Area 3	A301	2301	003787	284790-006	02.12.15 / 12:35	20°47,035 S	71°4,011 W	5243	
	A302	2302	0036FE	284790-007	02.12.15 / 18:48	20°47,561 S	71°4,945W	5367,8	
	A303	2303	003584	284790-008	03.12.15 / 13:38	20°46,853 S	71°3,520 W	5200,1	
	A304	2304	00353F	284789-005	03.12.15 / __:__	20°46,565 S	71°4635 W	____	planned depth: 5336,1m; time tripod in wather: 16:17
	A305	2305	00377F	284790-010	04.12.15 / 12:40	20°46,955 S	71°5,068 W	5357	
	A306	2306	00311D	284789-001	04.12.15 / 17:20	20°46,584 S	71°4,051 W	5295	Turned off "log when woken" for SV sensor for testing the battery consumption of SV
	A307	2307	003911	284789-002	04.12.15 / 21:46	20°48,037 S	71°4,088 W	5233,6	Receiver wait increased from 3600ms to 4400ms on 8th.december 2015 in order to get 2305
	A308	2308	003739	284789-003	05.12.15 / 11:15	20°47,897 S	71°3,595 W	5133	
	A309	2309	003723	284789-004	05.12.15 / 16:07	20°47,682 S	71°3,186 W	5098	Turned the baseline 2709-2707 on 2709 off; upload the new configuration
	A310	2310	0036FB	284791-002	05.12.15 / 20:44	20°47,237 S	71°3,846 W	5223	

Appendix C: Station List / Stationsliste

SO244-2			Station list											
			Time (UTC)					Begin / on seafloor		End / off seafloor				
Start Date	St. No.			Start Sci.	End Sci.		Duration	Latitude	Longitude	Latitude	Longitude	Water	Recovery	Supervisor
2015	SO244-2	Instrument	Begin	Program	Program	End	hh:mm	S	W	S	W	depth (m)	Remarks	
28.11.15	244/2_1-1	CTD	09:13:08	09:16:18	11:24:27	11:25:09	02:12	20° 47,938' S	70° 48,932' W	20° 47,977' S	70° 48,936' W	2738,9	maxSL: 2723m	WTD
28.11.15	244/2_2-1	Acoustic Geodetic Seafloor Station	12:00:42	15:48:11	16:50:34	17:36:05	05:35	20° 47,977' S	70° 48,931' W	20° 47,862' S	70° 48,722' W	2738	A101	H.Kopp
28.11.15	244/2_2-2	Acoustic Geodetic Seafloor Station	19:37:32	19:48:24	22:52:02	00:51:04	05:13	20° 47,682' S	70° 48,461' W	20° 47,717' S	70° 48,466' W	2602,9	A102	H.Kopp
29.11.15	244/2_2-3	Acoustic Geodetic Seafloor Station	09:12:02	09:49:40	13:12:19	14:38:31	05:26	20° 47,403' S	70° 48,544' W	20° 47,416' S	70° 48,535' W	2626,3	A104	H.Kopp
29.11.15	244/2_2-4	Acoustic Geodetic Seafloor Station	15:15:45	15:18:04	17:31:18	19:05:31	03:49	20° 47,608' S	70° 49,001' W	20° 47,618' S	70° 49,019' W		A103	H.Kopp
29.11.15	244/2_2-5	Acoustic Geodetic Seafloor Station	19:25:12	19:30:25	21:25:53	23:45:42	04:20	20° 48,132' S	70° 49,388' W	20° 48,152' S	70° 49,402' W	2873,2	A105	H.Kopp
29.11.15	244/2_3-1	KONGSBERG EM122	23:52:53	23:54:31	08:35:43	08:36:00	08:43	20° 48,192' S	70° 49,568' W	21° 4,019' S	71° 44,080' W	2910,8		F.Petersen
30.11.15	244/2_4-1	Acoustic Geodetic Seafloor Station	09:00:42	09:22:32	12:54:13	14:27:24	05:26	21° 3,349' S	71° 43,830' W	21° 3,417' S	71° 43,848' W	4117,2	A201	H.Kopp
30.11.15	244/2_4-2	Acoustic Geodetic Seafloor Station	15:00:18	15:04:16	17:22:47	20:37:28	05:37	21° 3,122' S	71° 43,932' W	21° 3,133' S	71° 43,934' W	4111,7	A202	H.Kopp
30.11.15	244/2_4-3	Acoustic Geodetic Seafloor Station	20:56:02	21:09:21	12:36:49	15:19:27	18:23	21° 3,480' S	71° 44,141' W	21° 3,485' S	71° 44,133' W		A203	H.Kopp
01.12.15	244/2_4-4	Wave Glider	10:43:55	10:45:10	22:54:02	23:00:00	12:16	21° 3,484' S	71° 44,138' W	21° 3,065' S	71° 43,831' W			D.Lange
01.12.15	244/2_4-5	Acoustic Geodetic Seafloor Station	15:42:01	16:11:56	16:42:29	17:53:57	02:11	21° 3,128' S	71° 44,238' W	21° 3,123' S	71° 44,261' W		A204	H.Kopp
01.12.15	244/2_4-6	Acoustic Geodetic Seafloor Station	18:12:03	18:17:38	20:20:07	22:03:56	03:51	21° 3,365' S	71° 44,145' W	21° 3,376' S	71° 44,136' W		A205	H.Kopp
02.12.15	244/2_5-1	CTD	03:50:23	03:53:09	07:17:33	07:18:23	03:28	20° 47,052' S	71° 4,001' W	20° 47,048' S	71° 4,006' W	5246,6	SLmax: 4500m	WTD
02.12.15	244/2_6-1	Acoustic Geodetic Seafloor Station	09:00:23	09:57:12	12:35:35	14:35:01	05:34	20° 47,052' S	71° 3,998' W	20° 47,083' S	71° 4,017' W		A301	H.Kopp
02.12.15	244/2_6-2	Acoustic Geodetic Seafloor Station	16:12:05	16:14:00	18:47:12	20:55:24	04:43	20° 47,597' S	71° 4,934' W	20° 47,597' S	71° 4,936' W		A302	H.Kopp
03.12.15	244/2_6-3	Acoustic Geodetic Seafloor Station	11:00:09	11:11:51	13:25:55	15:37:29	04:37	20° 46,887' S	71° 3,522' W	20° 46,887' S	71° 3,524' W		A303	H.Kopp
03.12.15	244/2_6-4	Acoustic Geodetic Seafloor Station	16:10:26	16:11:55	18:52:22	21:00:21	04:49	20° 46,577' S	71° 4,636' W	20° 46,597' S	71° 4,646' W	5339,2	A304	H.Kopp
03.12.15	244/2_7-1	KONGSBERG EM122	21:05:27	21:06:26	08:47:50	08:48:09	11:42	20° 46,625' S	71° 4,687' W	20° 46,819' S	71° 5,093' W	5367,5		F.Petersen
04.12.15	244/2_6-5	Acoustic Geodetic Seafloor Station	09:00:29	09:11:51	11:40:47	13:43:05	04:42	20° 46,955' S	71° 5,082' W	20° 46,988' S	71° 5,070' W	5357	A305	H.Kopp
04.12.15	244/2_6-6	Acoustic Geodetic Seafloor Station	14:20:58	14:27:16	16:41:43	19:10:01	04:49	20° 46,649' S	71° 4,054' W	20° 46,625' S	71° 4,066' W		A306	H.Kopp
04.12.15	244/2_6-7	Acoustic Geodetic Seafloor Station	19:32:17	19:34:47	21:40:28	23:46:38	04:14	20° 48,069' S	71° 4,063' W	20° 48,074' S	71° 4,089' W		A307	H.Kopp
05.12.15	244/2_6-8	Acoustic Geodetic Seafloor Station	09:00:03	09:09:24	11:15:38	13:19:29	04:19	20° 47,929' S	71° 3,605' W	20° 47,930' S	71° 3,608' W		A308	H.Kopp
05.12.15	244/2_6-9	Acoustic Geodetic Seafloor Station	13:45:00	13:51:05	16:05:06	18:07:24	04:22	20° 47,716' S	71° 3,197' W	20° 47,716' S	71° 3,194' W		A309	H.Kopp
05.12.15	244/2_6-10	Acoustic Geodetic Seafloor Station	18:37:29	18:39:06	20:50:53	01:42:06	07:04	20° 47,269' S	71° 3,858' W	20° 47,254' S	71° 3,383' W		A310	H.Kopp
06.12.15	244/2_2-6	Acoustic Geodetic Seafloor Station	15:12:17	15:14:01	16:45:44	17:57:26	02:45	20° 47,817' S	70° 49,441' W	20° 47,824' S	70° 49,464' W		A106	H.Kopp
06.12.15	244/2_2-7	Acoustic Geodetic Seafloor Station	18:19:41	18:24:22	19:57:56	21:09:36	02:49	20° 47,916' S	70° 49,832' W	20° 47,921' S	70° 49,831' W		A107	H.Kopp
06.12.15	244/2_8-1	KONGSBERG EM710	23:24:21	23:27:12	09:22:12	09:23:01	09:58	20° 58,004' S	70° 31,249' W	20° 51,223' S	70° 34,043' W	762,1		F.Petersen
07.12.15	244/2_2-8	Acoustic Geodetic Seafloor Station	11:00:01	11:16:54	12:51:56	16:58:47	05:58	20° 47,627' S	70° 49,986' W	20° 47,670' S	70° 49,014' W		A108	H.Kopp
07.12.15	244/2_9-1	Seismic Ocean Bottom Receiver	17:50:42			14:21:19	20:30	20° 46,114' S	70° 47,871' W	21° 33,006' S	70° 45,009' W	2596,3		A.Krabbenhoeft
07.12.15	244/2_9-1	Seismic Ocean Bottom Receiver		17:51:17				20° 46,108' S	70° 47,871' W			2501,4	OBS02	A.Krabbenhoeft
07.12.15	244/2_9-1	Seismic Ocean Bottom Receiver		19:39:57				20° 28,192' S	70° 52,567' W			2898,5	OBS03	A.Krabbenhoeft
07.12.15	244/2_9-1	Seismic Ocean Bottom Receiver		20:52:58				20° 22,010' S	71° 3,961' W			5011,9	OBS04	A.Krabbenhoeft
07.12.15	244/2_9-1	Seismic Ocean Bottom Receiver		22:28:20				20° 6,026' S	71° 7,133' W			4819,3	OBS05	A.Krabbenhoeft
07.12.15	244/2_9-1	Seismic Ocean Bottom Receiver		23:50:38				19° 53,399' S	71° 12,653' W			5345,9	OBS06	A.Krabbenhoeft
08.12.15	244/2_9-1	Seismic Ocean Bottom Receiver		01:37:55				19° 36,126' S	71° 16,650' W			4881,2	OBS07	A.Krabbenhoeft
08.12.15	244/2_9-1	Seismic Ocean Bottom Receiver		03:40:22				19° 20,743' S	71° 1,293' W			1736,1	OBS08	A.Krabbenhoeft
08.12.15	244/2_9-1	Seismic Ocean Bottom Receiver		05:35:45				19° 34,789' S	70° 49,802' W			1728,9	OBS09	A.Krabbenhoeft
08.12.15	244/2_9-1	Seismic Ocean Bottom Receiver		07:19:02				19° 48,932' S	70° 43,646' W			1432,8	OBS10	A.Krabbenhoeft
08.12.15	244/2_9-1	Seismic Ocean Bottom Receiver		08:49:37				19° 56,435' S	70° 55,912' W			2735,6	OBS11	A.Krabbenhoeft
08.12.15	244/2_9-1	Seismic Ocean Bottom Receiver		10:30:00				20° 12,095' S	70° 54,017' W			2999,2	OBS12	A.Krabbenhoeft
08.12.15	244/2_9-1	Seismic Ocean Bottom Receiver		11:44:36				20° 17,717' S	70° 43,848' W			2100,4	OBS13	A.Krabbenhoeft

Appendix C: Station List / Stationsliste

SO244-2			Station list										
			Time (UTC)					Begin / on seafloor		End / off seafloor			
Start Date	St. No.			Start Sci.	End Sci.		Duration	Latitude	Longitude	Latitude	Longitude	Water	Recovery	Supervisor
2015	SO244-2	Instrument	Begin	Program	Program	End	hh:mm	S	W	S	W	depth (m)	Remarks	
08.12.15	244/2_9-1	Seismic Ocean Bottom Receiver		18:17:29				20° 44,494' S	70° 3,756' W			5349,6	OBS01	A.Krabbenhoeft
12.12.15	244/2_9-1	Seismic Ocean Bottom Receiver		14:19:54				21° 32,993' S	70° 45,003' W			2787,4	OBS14	A.Krabbenhoeft
08.12.15	244/2_10-1	Wave Glider	14:52:33	15:06:44	11:25:00	11:45:00	20:52	20° 47,838' S	70° 49,022' W	20° 47,296' S	70° 48,492' W	2764,8		D.Lange
08.12.15	244/2_11-1	Acoustic Geodetic Seafloor Station	18:52:05	18:53:05	23:58:23	00:00:07	05:08	20° 47,275' S	71° 3,867' W	20° 47,279' S	71° 3,862' W	5233,4	Modem	H.Kopp
09.12.15	244/2_12-1	Acoustic Geodetic Seafloor Station	12:00:00	18:53:05	15:57:17	15:58:12	03:58	20° 47,302' S	70° 48,478' W	20° 47,624' S	70° 49,993' W		Modem	H.Kopp
09.12.15	244/2_13-1	Acoustic Geodetic Seafloor Station	17:33:18	17:35:28	19:41:52	19:43:36	02:10	20° 47,114' S	71° 3,948' W	20° 47,110' S	71° 3,962' W		Modem	H.Kopp
09.12.15	244/2_14-1	Wave Glider	23:43:26	23:49:13	42:17,0	11:53:58	12:10	21° 3,272' S	71° 44,084' W	21° 3,351' S	71° 44,043' W			D.Lange
10.12.15	244/2_15-1	KONGSBERG EM122	01:07:22	01:08:54	10:56:35	10:57:48	09:50	21° 2,194' S	71° 44,410' W	21° 2,805' S	71° 44,530' W	4085,6		F.Petersen
10.12.15	244/2_16-1	Wave Glider	11:20:50	11:22:12	11:42:17	11:53:58	00:33	21° 3,040' S	71° 43,952' W	21° 3,351' S	71° 44,043' W		WG recovery	D.Lange
10.12.15	244/2_17-1	KONGSBERG EM122	14:30:48	14:33:20	02:09:32	02:10:10	11:39	21° 25,148' S	71° 34,760' W	22° 16,215' S	72° 10,046' W	4600		F.Petersen
End of SO244-2														

Appendix F: Logging Data / Daten

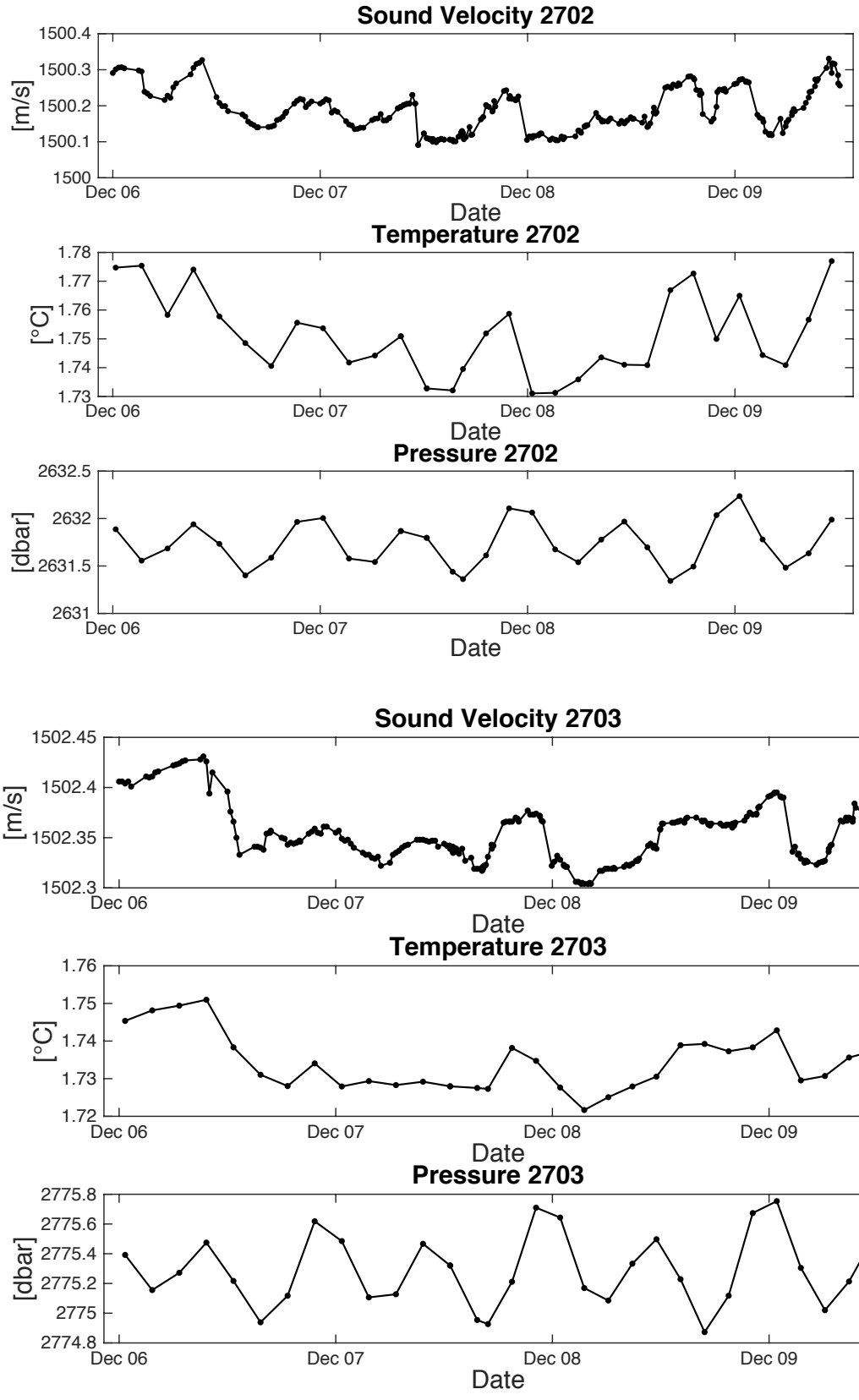

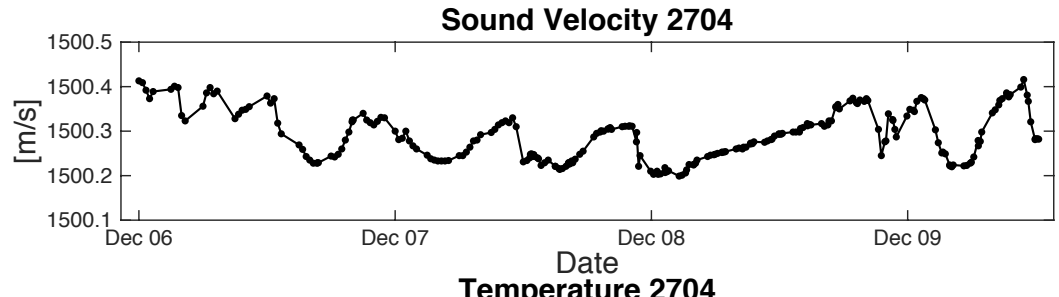
Sound Velocity 2704
[m/s]
1500.5
1500.4
1500.3
1500.2
1500.1
Dec 06
Dec 07
Dec 08
Dec 09
Date

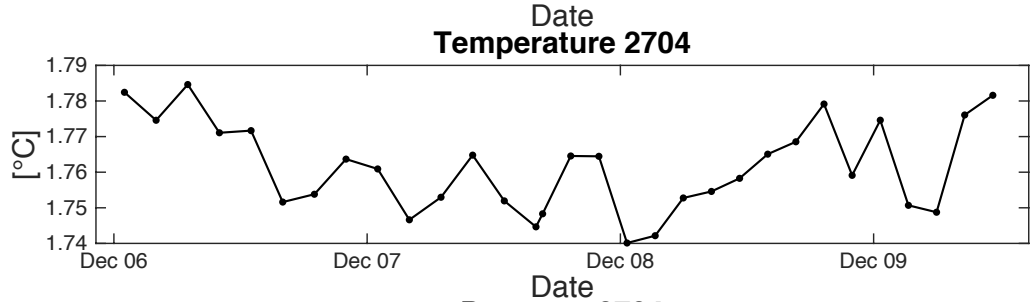
Temperature 2704
[°C]
1.79
1.78
1.77
1.76
1.75
1.74
Dec 06
Dec 07
Dec 08
Dec 09
Date

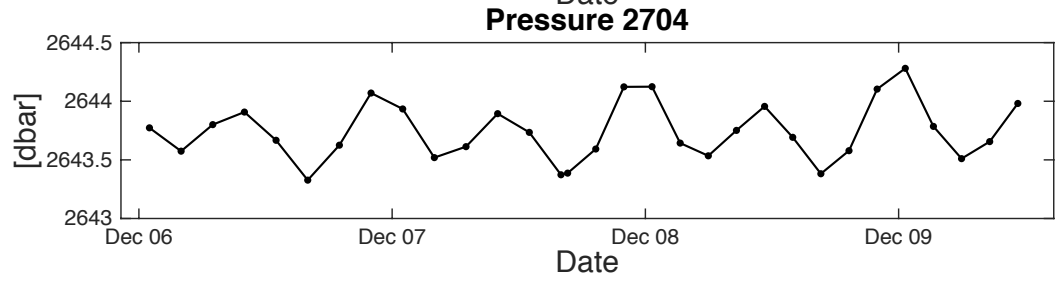
Pressure 2704
[dbar]
2644.5
2644
2643.5
2643
Dec 06
Dec 07
Dec 08
Dec 09
Date

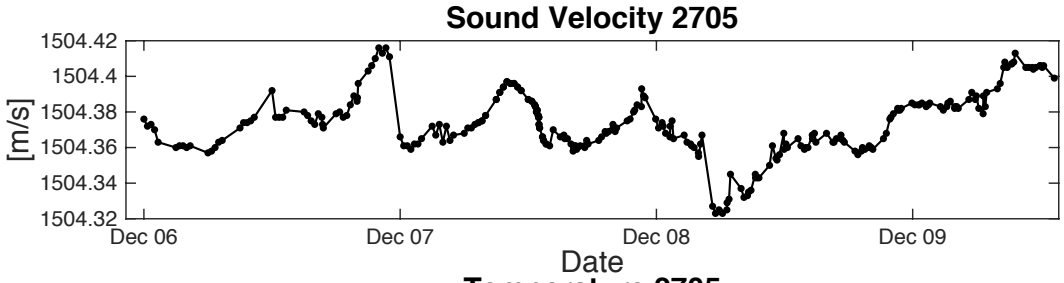
Sound Velocity 2705
[m/s]
1504.42
1504.4
1504.38
1504.36
1504.34
1504.32
Dec 06
Dec 07
Dec 08
Dec 09
Date

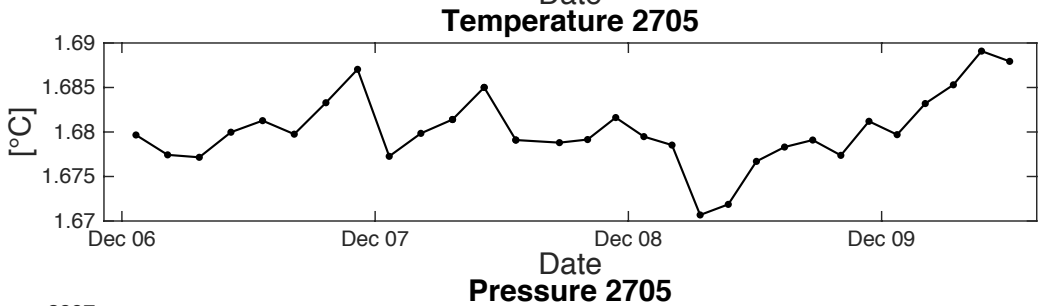
Temperature 2705
[°C]
1.69
1.685
1.68
1.675
1.67
Dec 06
Dec 07
Dec 08
Dec 09
Date

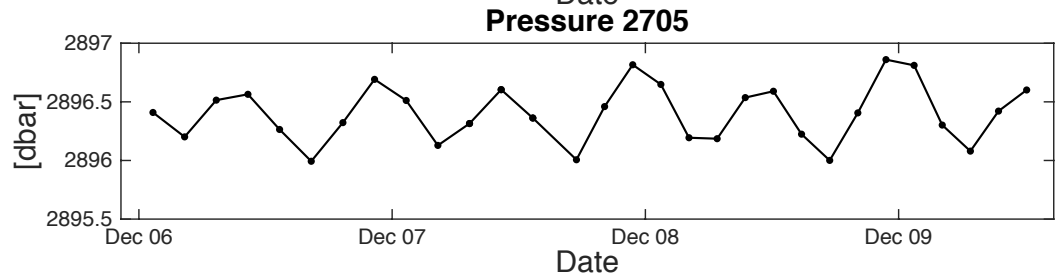
Pressure 2705
[dbar]
2897
2896.5
2896
2895.5
Dec 06
Dec 07
Dec 08
Dec 09
Date

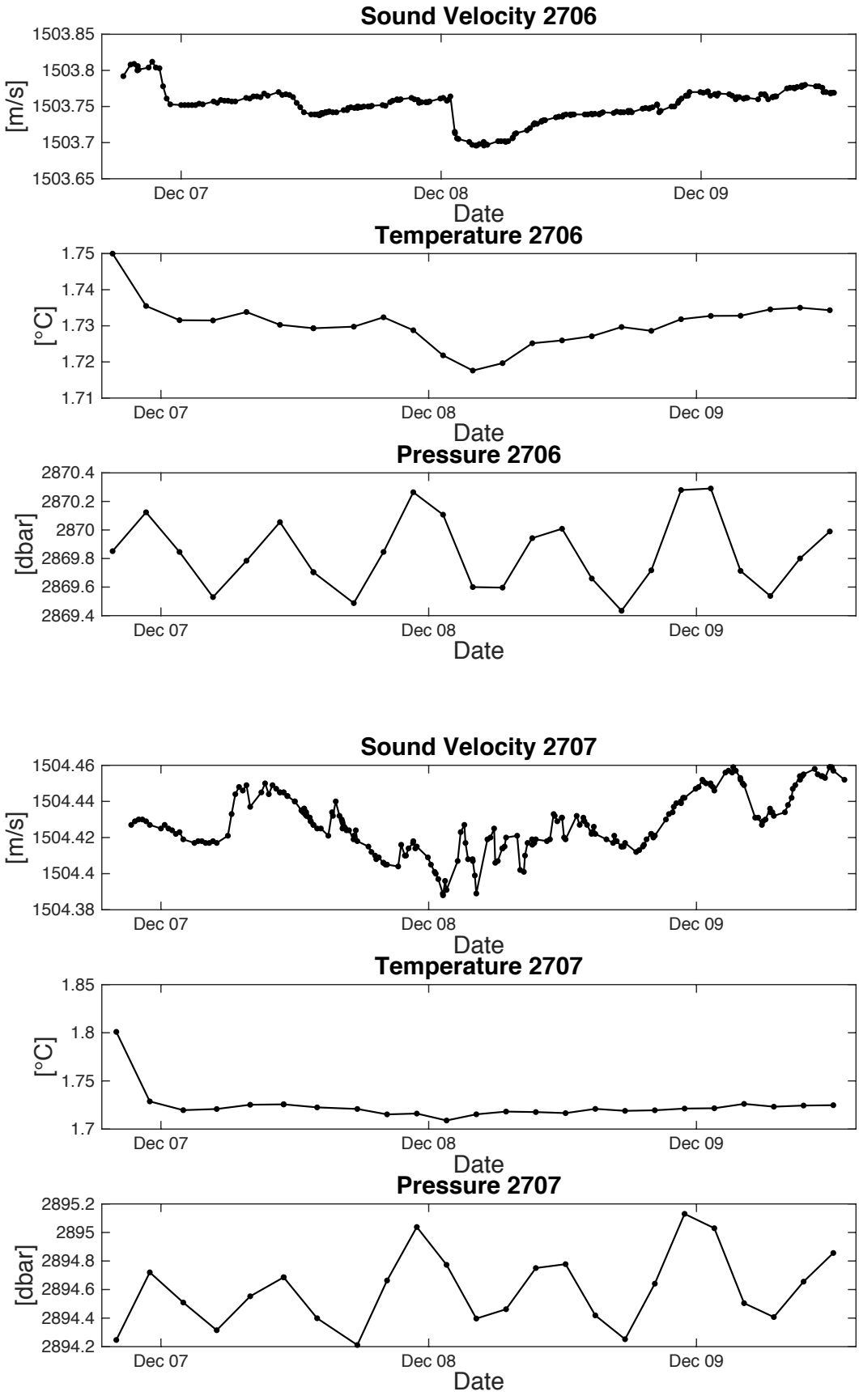
Sound Velocity 2706
[m/s]
1503.85
1503.8
1503.75
1503.7
1503.65
Dec 07
Dec 08
Dec 09
Date
Temperature 2706
[°C]
1.75
1.74
1.73
1.72
1.71
Dec 07
Dec 08
Dec 09
Date
Pressure 2706
[dbar]
2870.4
2870.2
2870
2869.8
2869.6
2869.4
Dec 07
Dec 08
Dec 09
Date
Sound Velocity 2707
[m/s]
1504.46
1504.44
1504.42
1504.4
1504.38
Dec 07
Dec 08
Dec 09
Date
Temperature 2707
[°C]
1.85
1.8
1.75
1.7
Dec 07
Dec 08
Dec 09
Date
Pressure 2707
[dbar]
2895.2
2895
2894.8
2894.6
2894.4
2894.2
Dec 07
Dec 08
Dec 09
Date

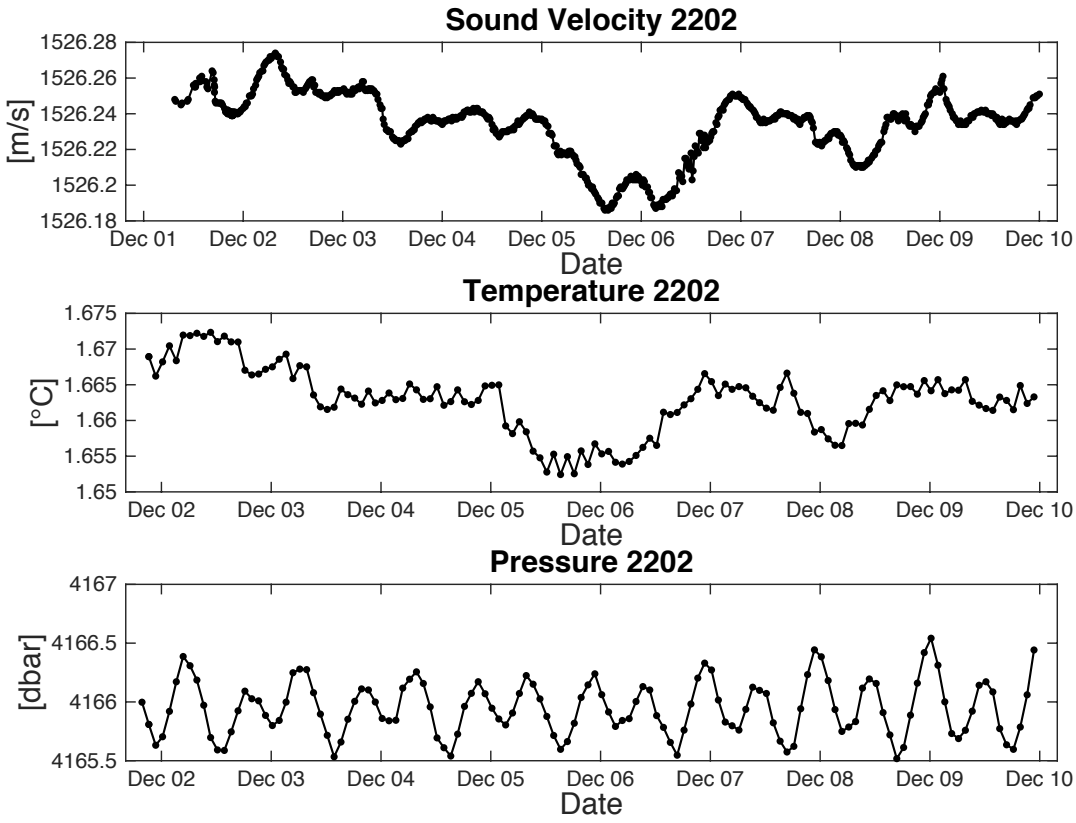
Sound Velocity 2202
[m/s]
1526.28
1526.26
1526.24
1526.22
1526.2
1526.18
Dec 01 Dec 02 Dec 03 Dec 04 Dec 05 Dec 06 Dec 07 Dec 08 Dec 09 Dec 10
Date
Temperature 2202
[°C]
1.675
1.67
1.665
1.66
1.655
1.65
Dec 02 Dec 03 Dec 04 Dec 05 Dec 06 Dec 07 Dec 08 Dec 09 Dec 10
Date
Pressure 2202
[dbar]
4167
4166.5
4166
4165.5
Dec 02 Dec 03 Dec 04 Dec 05 Dec 06 Dec 07 Dec 08 Dec 09 Dec 10
Date

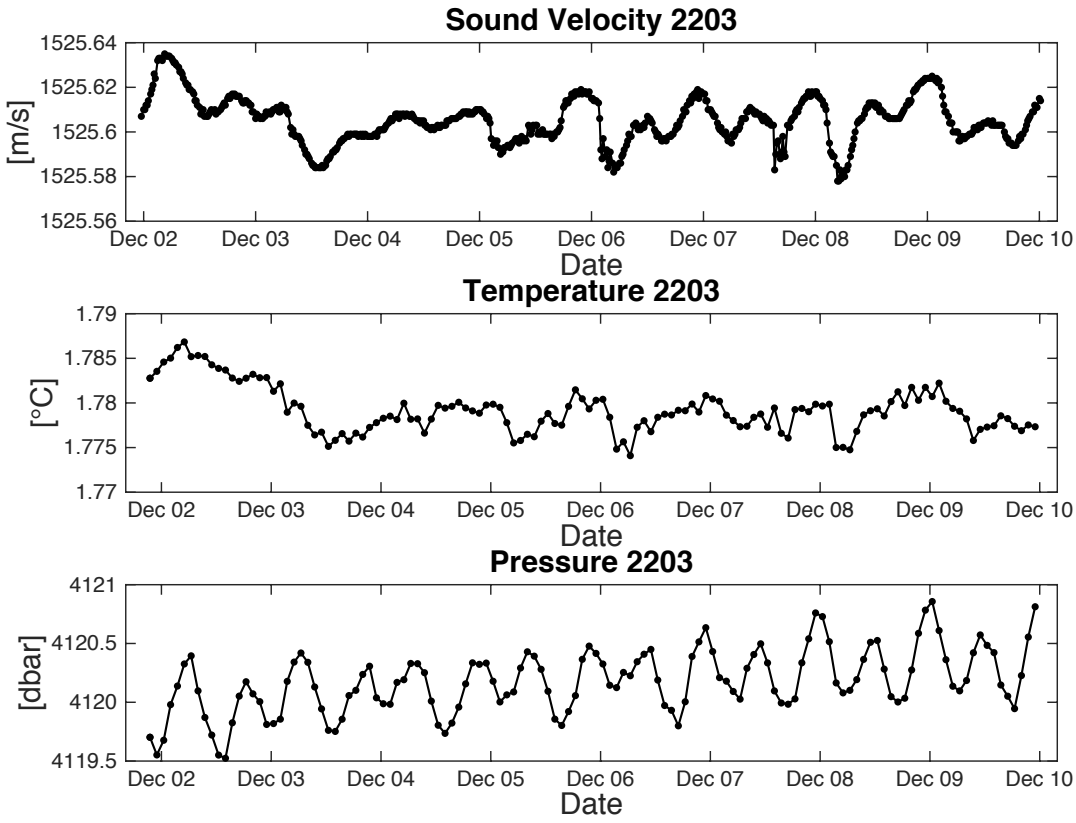
Sound Velocity 2203
[m/s]
1525.64
1525.62
1525.6
1525.58
1525.56
Dec 02 Dec 03 Dec 04 Dec 05 Dec 06 Dec 07 Dec 08 Dec 09 Dec 10
Date
Temperature 2203
[°C]
1.79
1.785
1.78
1.775
1.77
Dec 02 Dec 03 Dec 04 Dec 05 Dec 06 Dec 07 Dec 08 Dec 09 Dec 10
Date
Pressure 2203
[dbar]
4121
4120.5
4120
4119.5
Dec 02 Dec 03 Dec 04 Dec 05 Dec 06 Dec 07 Dec 08 Dec 09 Dec 10
Date

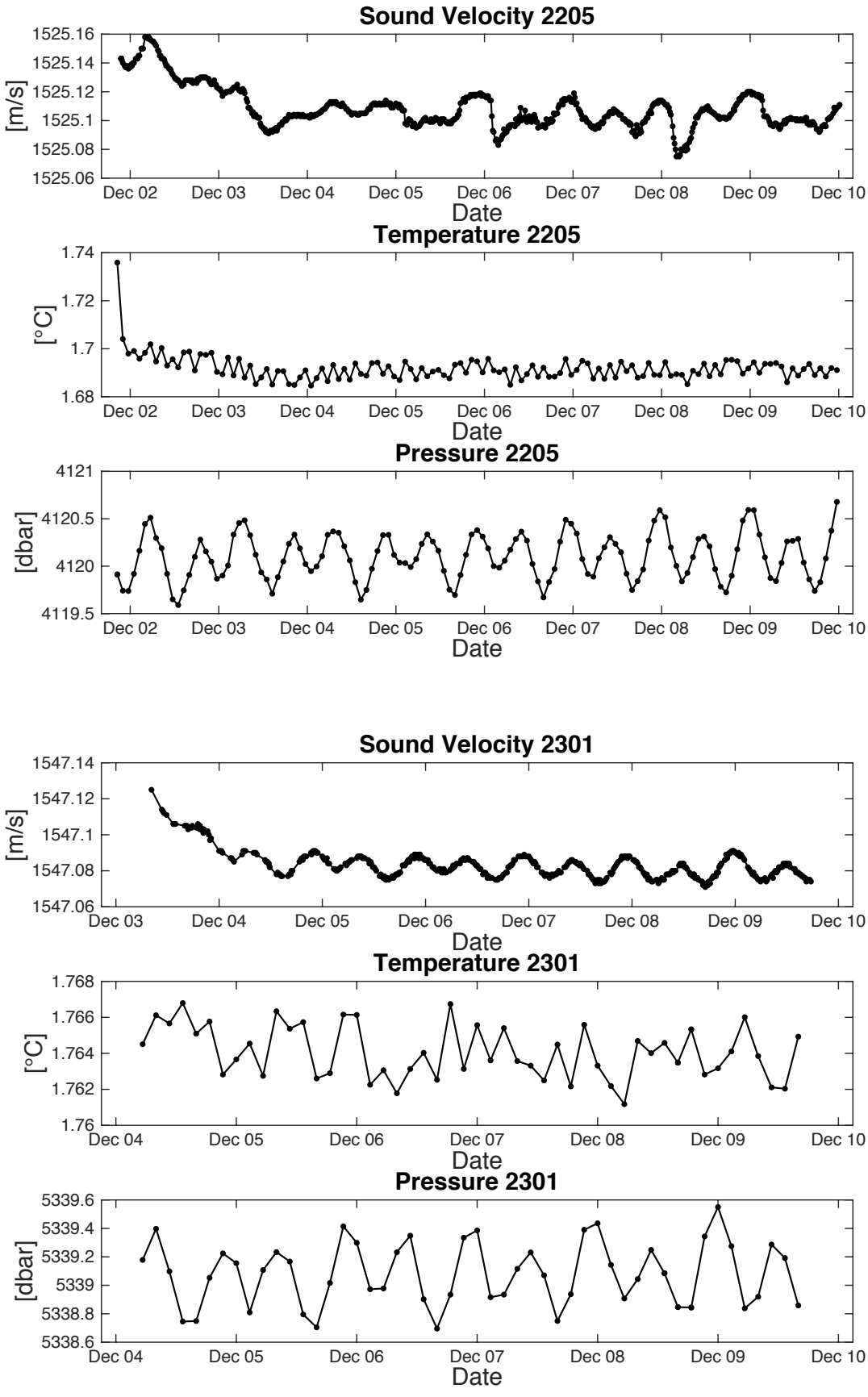
Sound Velocity 2205
[m/s]
1525.16
1525.14
1525.12
1525.1
1525.08
1525.06
Dec 02 Dec 03 Dec 04 Dec 05 Dec 06 Dec 07 Dec 08 Dec 09 Dec 10
Date
Temperature 2205
[°C]
1.74
1.72
1.7
1.68
Dec 02 Dec 03 Dec 04 Dec 05 Dec 06 Dec 07 Dec 08 Dec 09 Dec 10
Date
Pressure 2205
[dbar]
4121
4120.5
4120
4119.5
Dec 02 Dec 03 Dec 04 Dec 05 Dec 06 Dec 07 Dec 08 Dec 09 Dec 10
Date
Sound Velocity 2301
[m/s]
1547.14
1547.12
1547.1
1547.08
1547.06
Dec 03 Dec 04 Dec 05 Dec 06 Dec 07 Dec 08 Dec 09 Dec 10
Date
Temperature 2301
[°C]
1.768
1.766
1.764
1.762
1.76
Dec 04 Dec 05 Dec 06 Dec 07 Dec 08 Dec 09 Dec 10
Date
Pressure 2301
[dbar]
5339.6
5339.4
5339.2
5339
5338.8
5338.6
Dec 04 Dec 05 Dec 06 Dec 07 Dec 08 Dec 09 Dec 10
Date

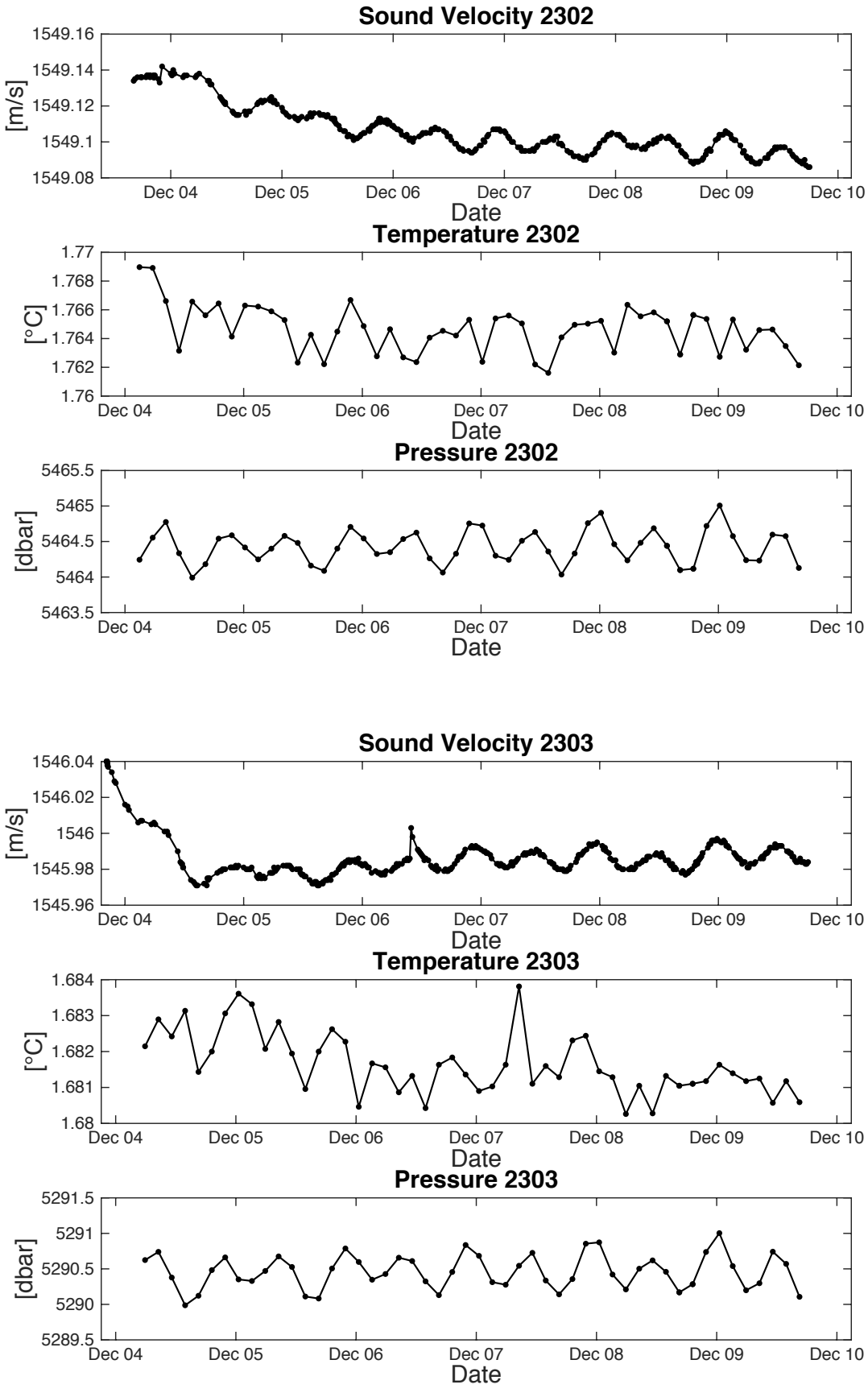
Sound Velocity 2302
[m/s]
1549.16
1549.14
1549.12
1549.1
1549.08
Dec 04
Dec 05
Dec 06
Dec 07
Dec 08
Dec 09
Dec 10
Date
Temperature 2302
[°C]
1.77
1.768
1.766
1.764
1.762
1.76
Dec 04
Dec 05
Dec 06
Dec 07
Dec 08
Dec 09
Dec 10
Date
Pressure 2302
[dbar]
5465.5
5465
5464.5
5464
5463.5
Dec 04
Dec 05
Dec 06
Dec 07
Dec 08
Dec 09
Dec 10
Date
Sound Velocity 2303
[m/s]
1546.04
1546.02
1546
1545.98
1545.96
Dec 04
Dec 05
Dec 06
Dec 07
Dec 08
Dec 09
Dec 10
Date
Temperature 2303
[°C]
1.684
1.683
1.682
1.681
1.68
Dec 04
Dec 05
Dec 06
Dec 07
Dec 08
Dec 09
Dec 10
Date
Pressure 2303
[dbar]
5291.5
5291
5290.5
5290
5289.5
Dec 04
Dec 05
Dec 06
Dec 07
Dec 08
Dec 09
Dec 10
Date

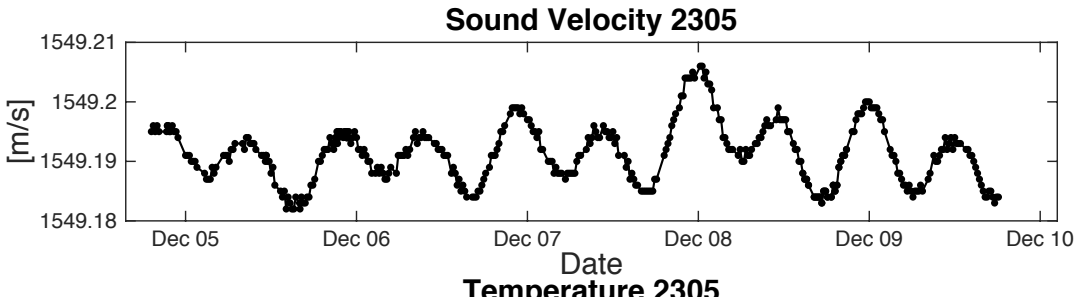
Sound Velocity 2305
[m/s]
1549.21
1549.2
1549.19
1549.18
Dec 05
Dec 06
Dec 07
Dec 08
Dec 09
Dec 10
Date

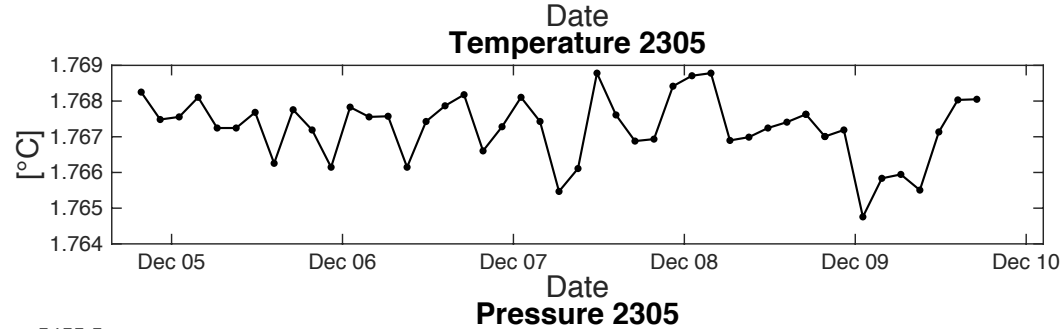
Temperature 2305
[°C]
1.769
1.768
1.767
1.766
1.765
1.764
Dec 05
Dec 06
Dec 07
Dec 08
Dec 09
Dec 10
Date

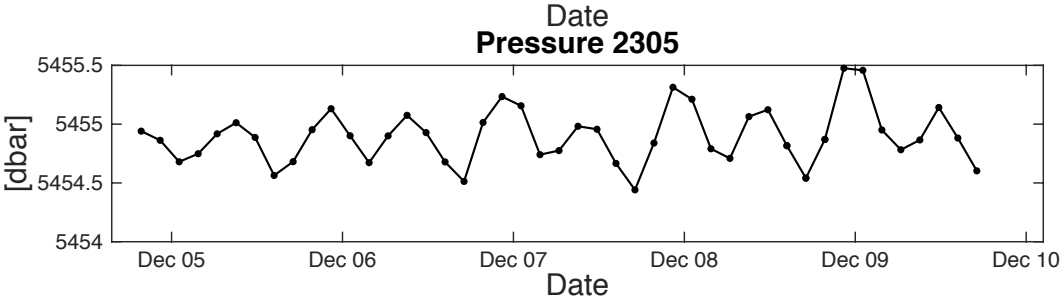
Pressure 2305
[dbar]
5455.5
5455
5454.5
5454
Dec 05
Dec 06
Dec 07
Dec 08
Dec 09
Dec 10
Date

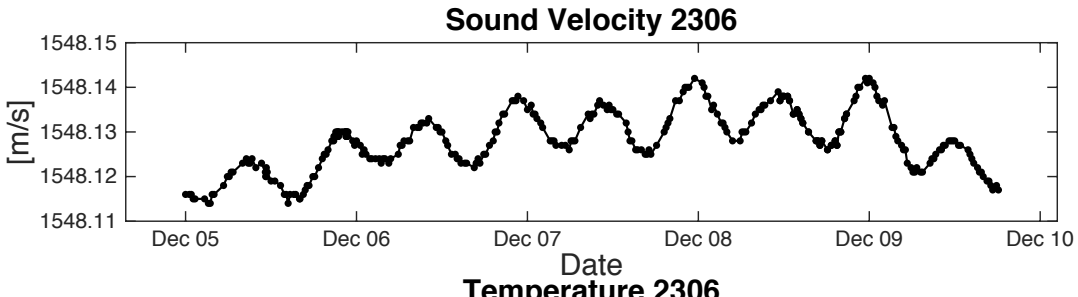
Sound Velocity 2306
[m/s]
1548.15
1548.14
1548.13
1548.12
1548.11
Dec 05
Dec 06
Dec 07
Dec 08
Dec 09
Dec 10
Date

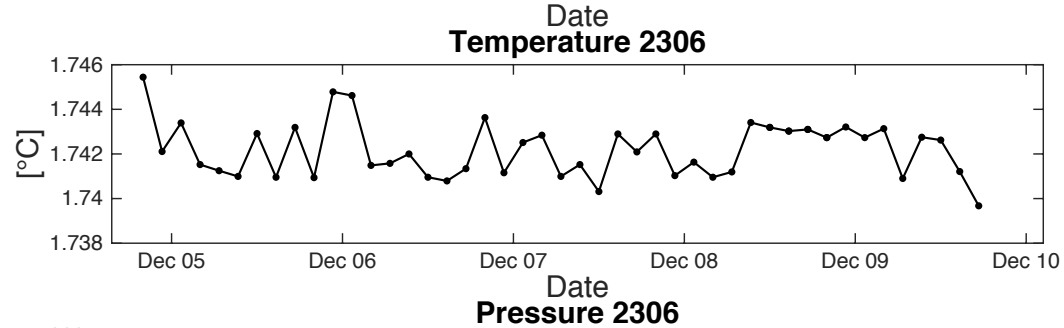
Temperature 2306
[°C]
1.746
1.744
1.742
1.74
1.738
Dec 05
Dec 06
Dec 07
Dec 08
Dec 09
Dec 10
Date

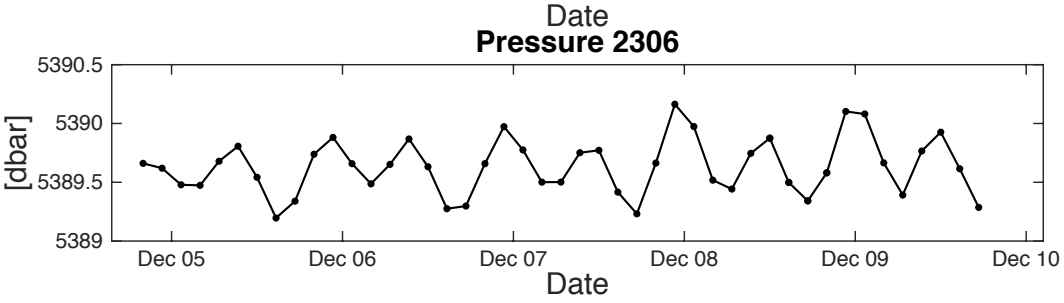
Pressure 2306
[dbar]
5390.5
5390
5389.5
5389
Dec 05
Dec 06
Dec 07
Dec 08
Dec 09
Dec 10
Date

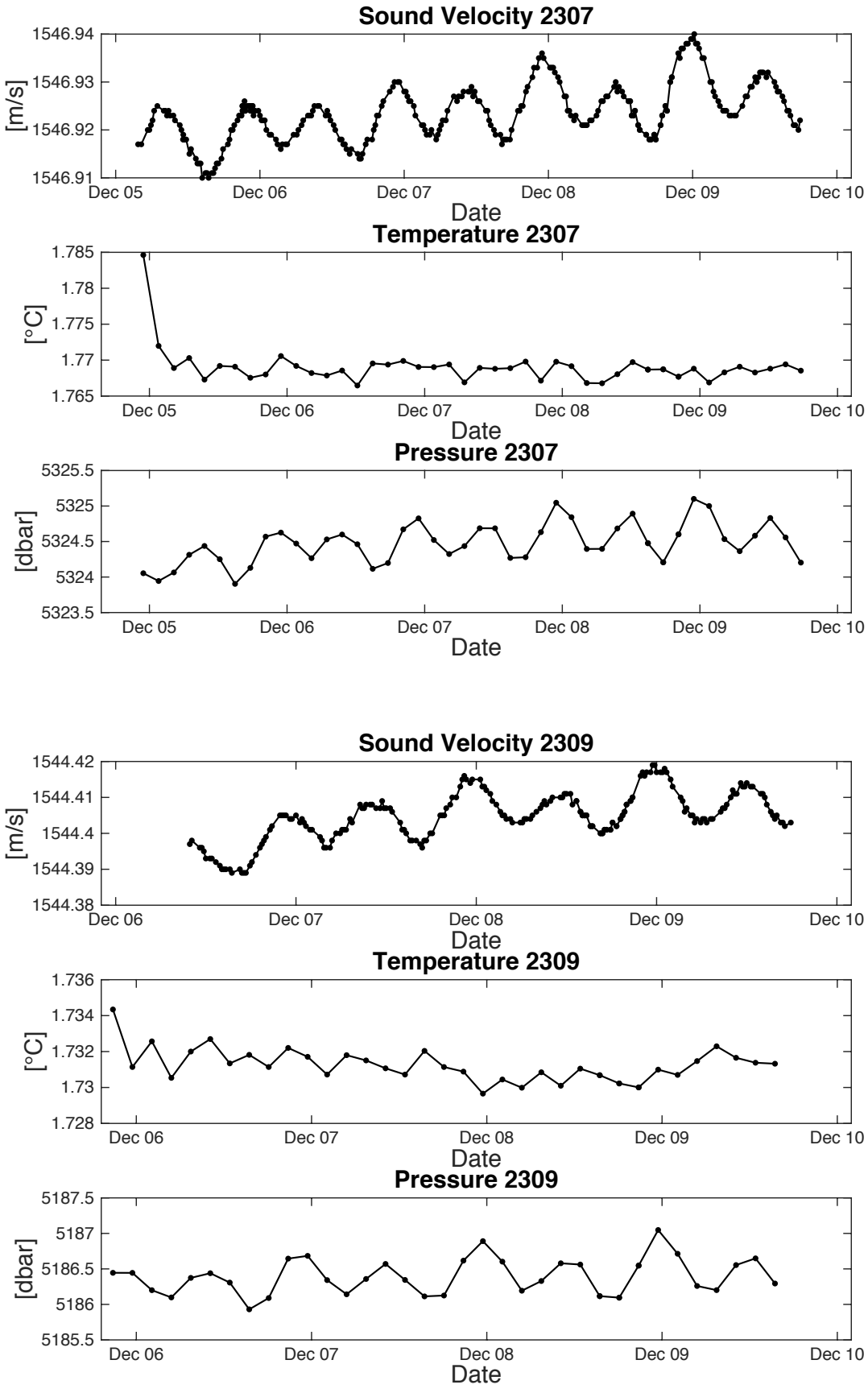
Sound Velocity 2307
[m/s]
1546.94
1546.93
1546.92
1546.91
Dec 05
Dec 06
Dec 07
Dec 08
Dec 09
Dec 10
Date
Temperature 2307
[°C]
1.785
1.78
1.775
1.77
1.765
Dec 05
Dec 06
Dec 07
Dec 08
Dec 09
Dec 10
Date
Pressure 2307
[dbar]
5325.5
5325
5324.5
5324
5323.5
Dec 05
Dec 06
Dec 07
Dec 08
Dec 09
Dec 10
Date
Sound Velocity 2309
[m/s]
1544.42
1544.41
1544.4
1544.39
1544.38
Dec 06
Dec 07
Dec 08
Dec 09
Dec 10
Date
Temperature 2309
[°C]
1.736
1.734
1.732
1.73
1.728
Dec 06
Dec 07
Dec 08
Dec 09
Dec 10
Date
Pressure 2309
[dbar]
5187.5
5187
5186.5
5186
5185.5
Dec 06
Dec 07
Dec 08
Dec 09
Dec 10
Date

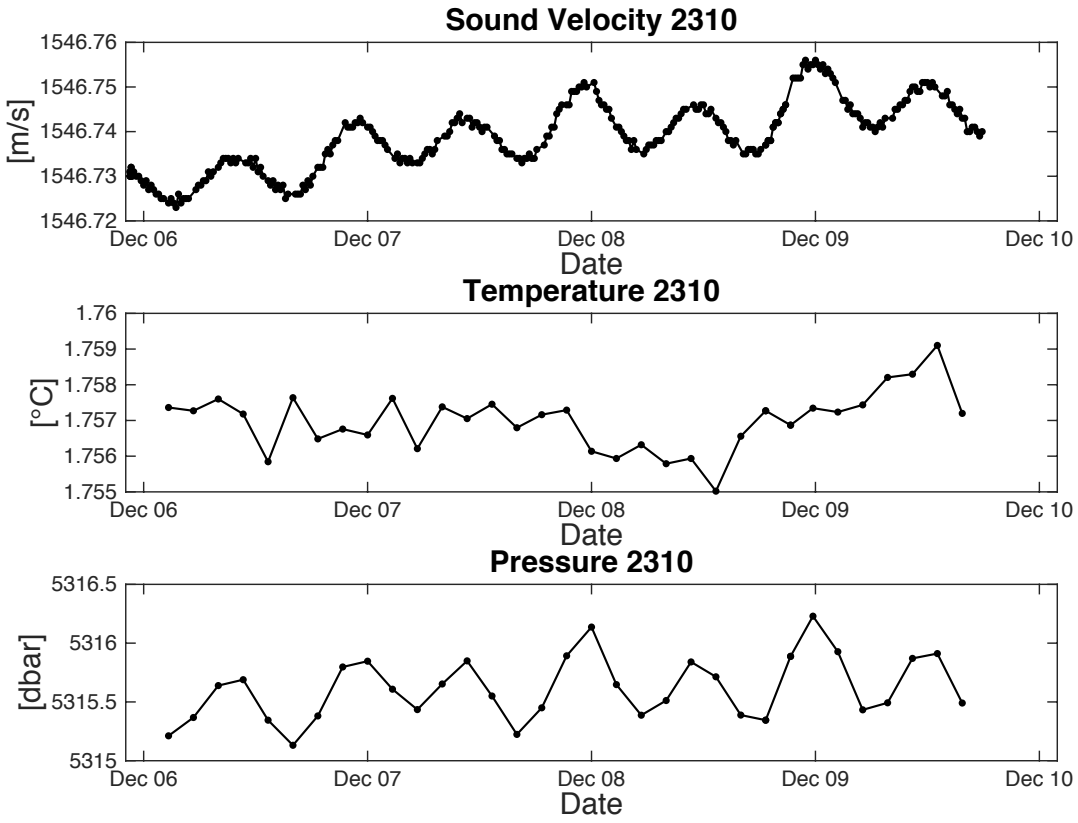

Note: Logging data for stations A101, A108, A201, A204, A304, and A308 are shown in Chapters 6.1.3-6.1.5.

Appendix G: Baselines / Baselines

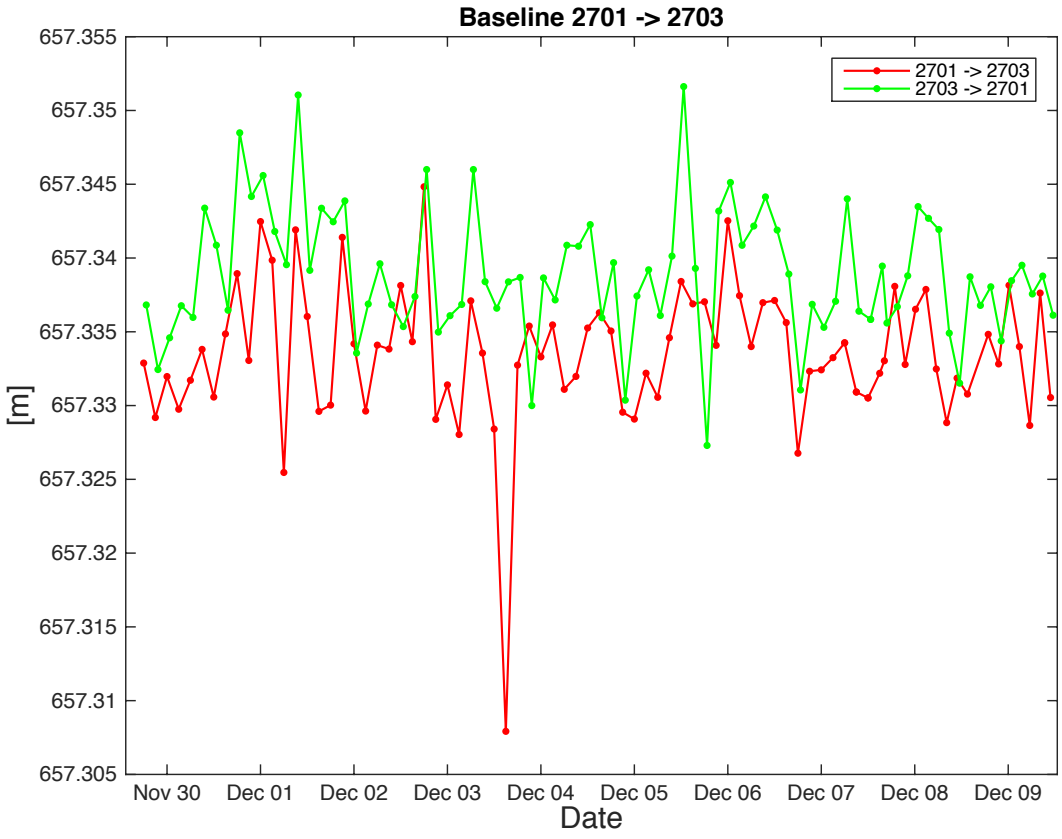

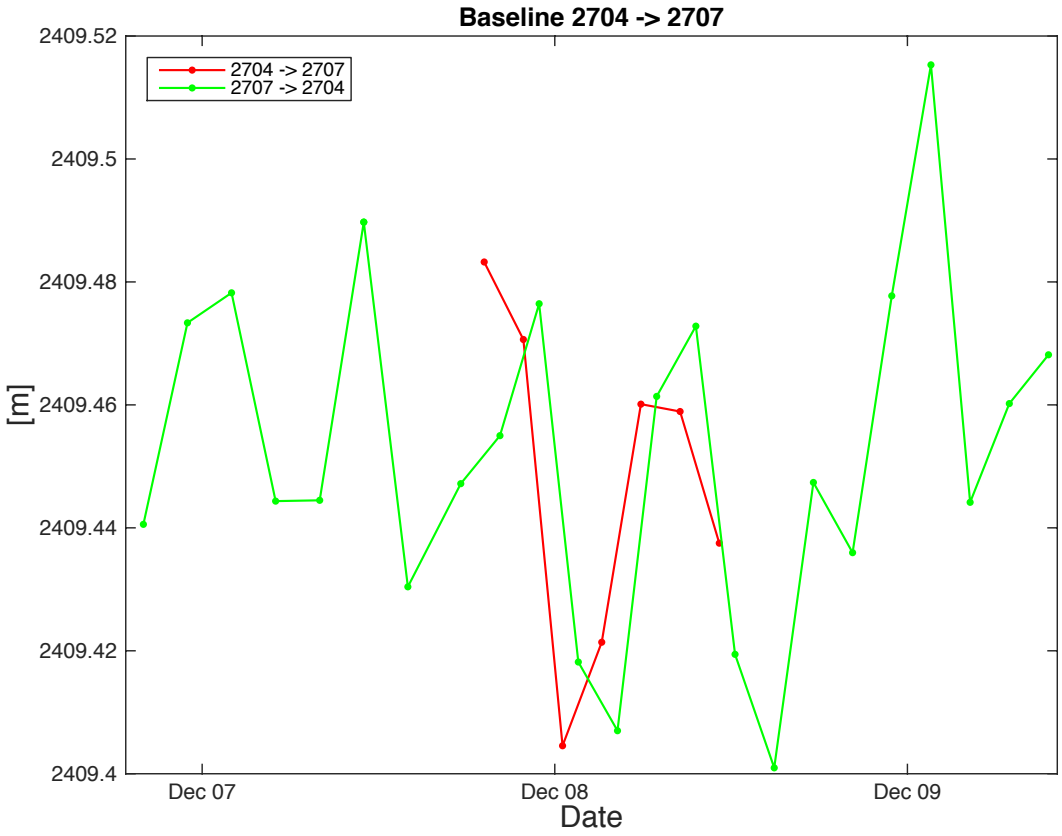

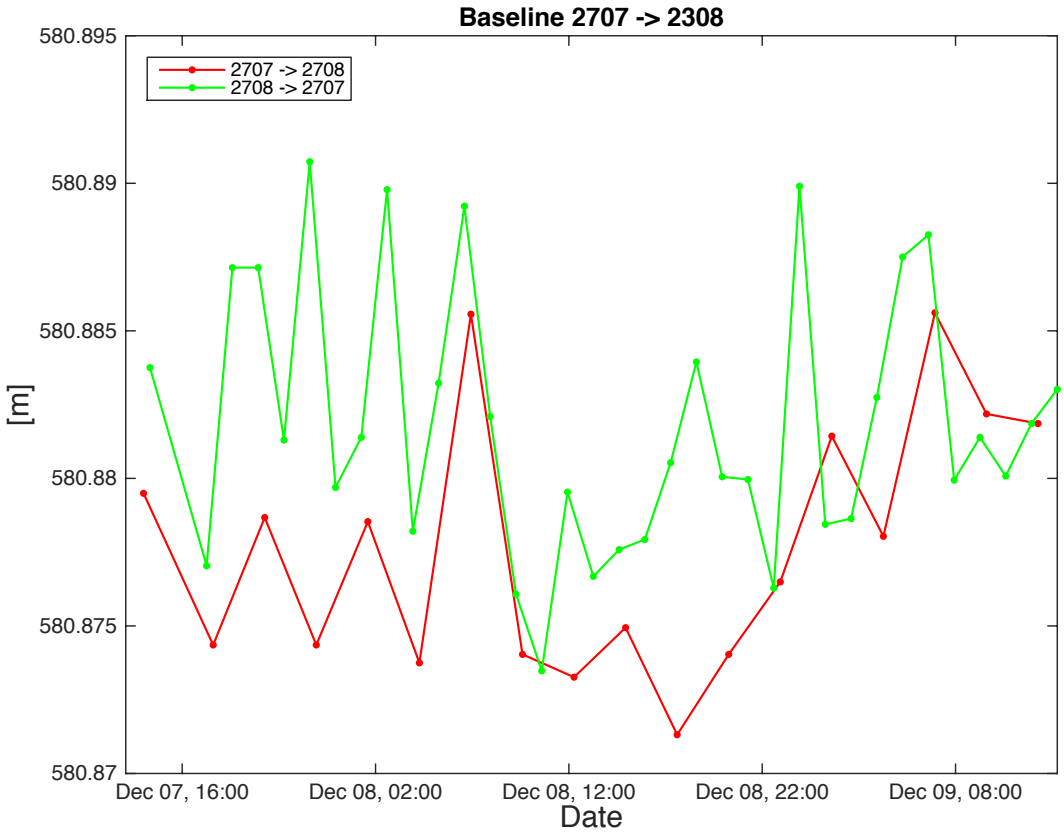
Baseline 2707 -> 2308
2707 -> 2708
2708 -> 2707
580.895
580.89
580.885
580.88
580.875
580.87
[m]
Dec 07, 16:00
Dec 08, 02:00
Dec 08, 12:00
Dec 08, 22:00
Dec 09, 08:00
Date

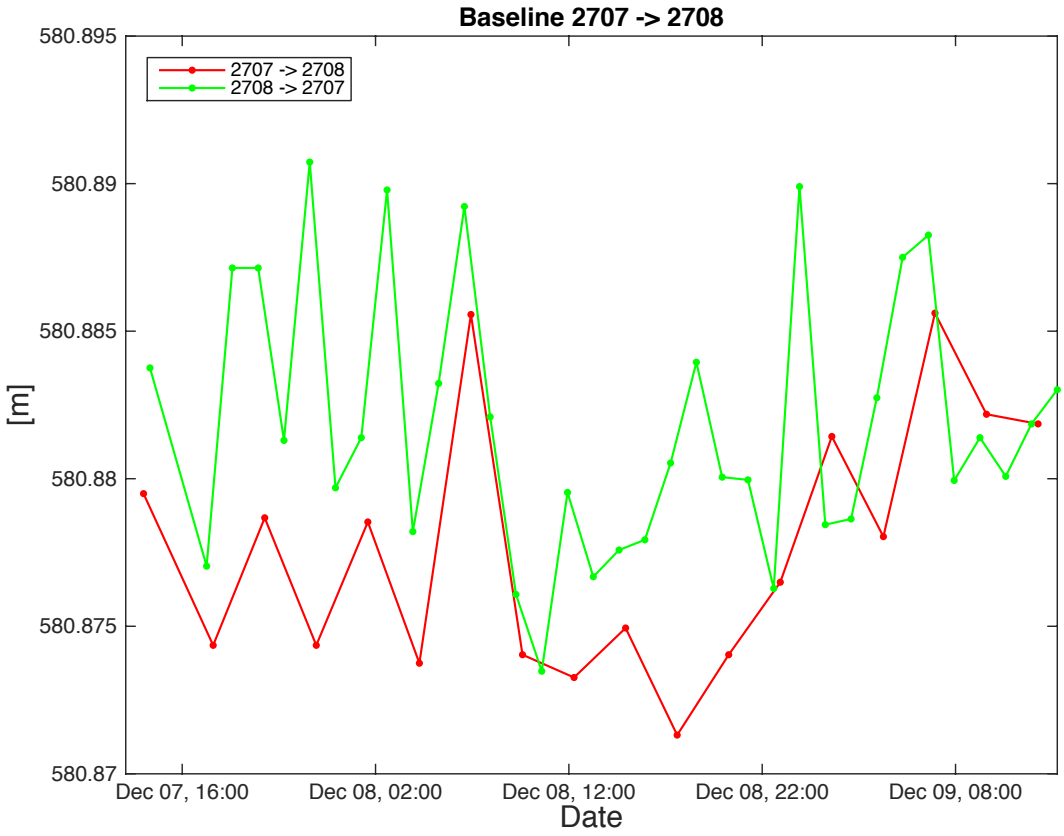
Baseline 2707 -> 2708
2707 -> 2708
2708 -> 2707
580.895
580.89
580.885
580.88
580.875
580.87
[m]
Dec 07, 16:00
Dec 08, 02:00
Dec 08, 12:00
Dec 08, 22:00
Dec 09, 08:00
Date

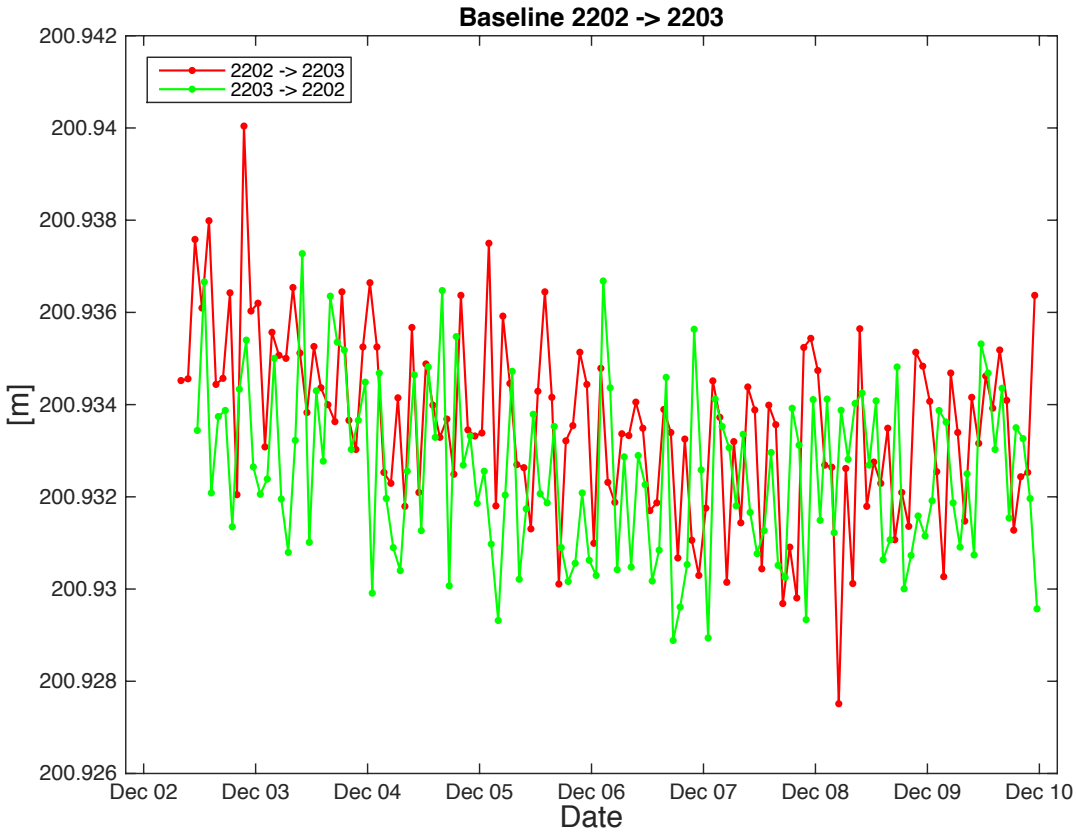
Baseline 2202 -> 2203
2202 -> 2203
2203 -> 2202
200.942
200.94
200.938
200.936
200.934
200.932
200.93
200.928
200.926
[m]
Dec 02
Dec 03
Dec 04
Dec 05
Dec 06
Dec 07
Dec 08
Dec 09
Dec 10
Date

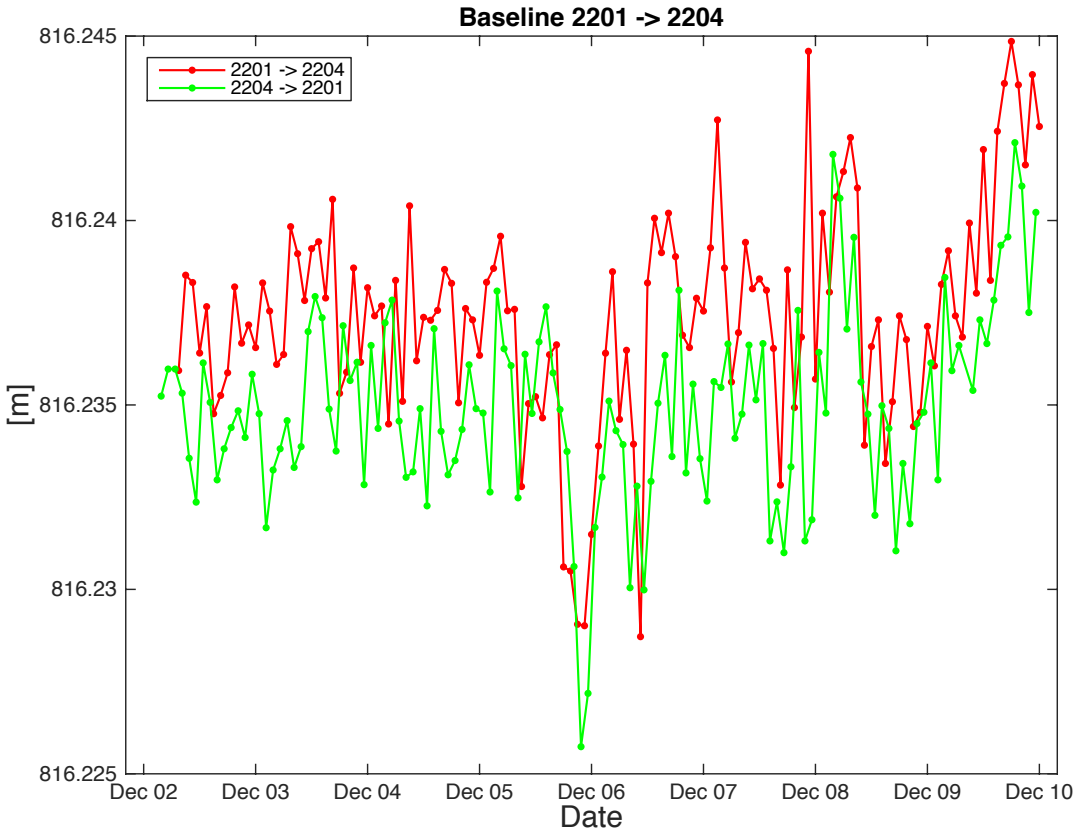
Baseline 2201 -> 2204
2201 -> 2204
2204 -> 2201
816.245
816.24
816.235
816.23
816.225
[m]
Dec 02
Dec 03
Dec 04
Dec 05
Dec 06
Dec 07
Dec 08
Dec 09
Dec 10
Date

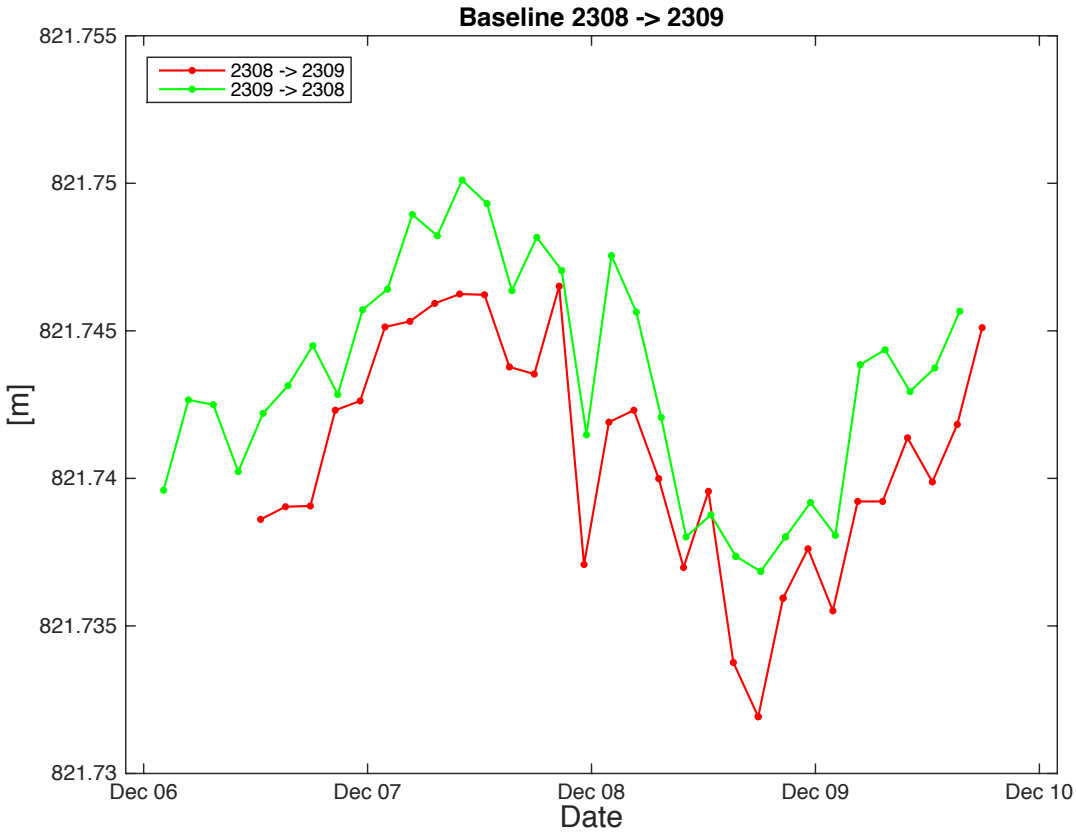
Baseline 2308 -> 2309
2308 -> 2309
2309 -> 2308
821.755
821.75
821.745
821.74
821.735
821.73
[m]
Dec 06
Dec 07
Dec 08
Dec 09
Dec 10
Date

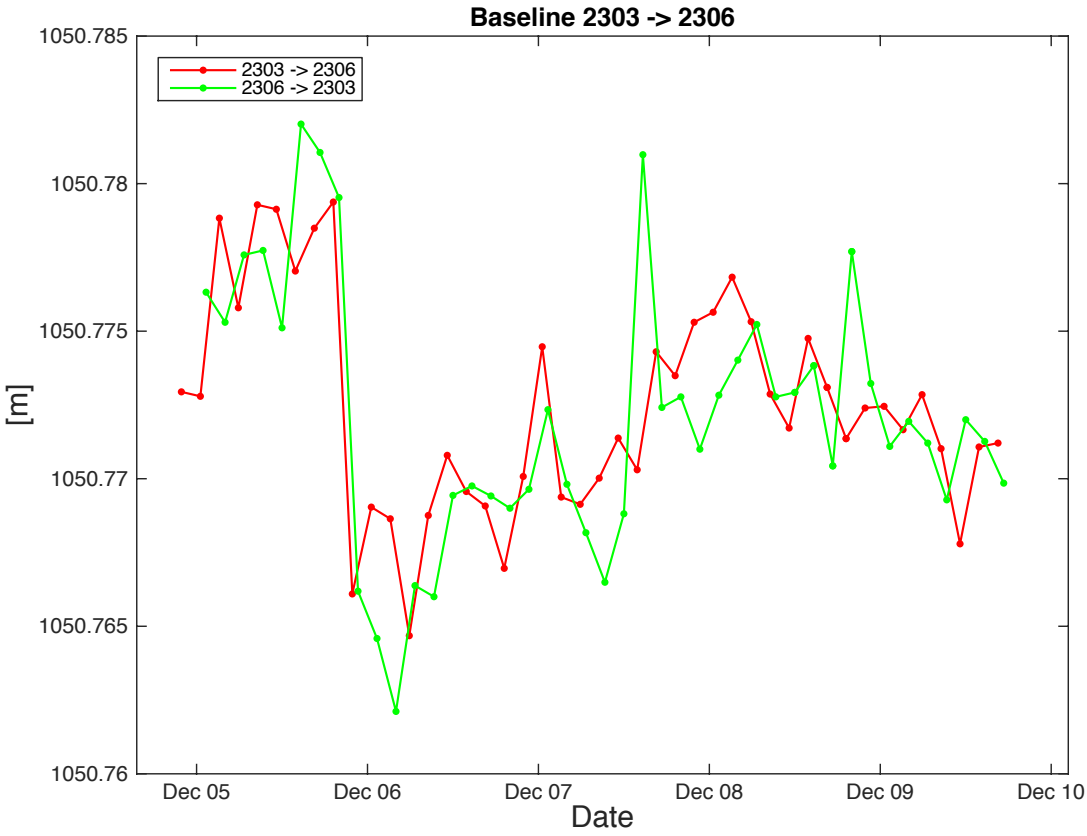
Baseline 2303 -> 2306
2303 -> 2306
2306 -> 2303
1050.785
1050.78
1050.775
1050.77
1050.765
1050.76
[m]
Dec 05
Dec 06
Dec 07
Dec 08
Dec 09
Dec 10
Date

GEOMAR
Helmholtz-Zentrum für Ozeanforschung Kiel

GEOMAR Reports

No.	Title
1	FS POSEIDON Fahrtbericht / Cruise Report POS421, 08. – 18.11.2011, Kiel - Las Palmas, Ed.: T.J. Müller, 26 pp, DOI: 10.3289/GEOMAR_REP_NS_1_2012
2	Nitrous Oxide Time Series Measurements off Peru – A Collaboration between SFB 754 and IMARPE –, Annual Report 2011, Eds.: Baustian, T., M. Graco, H.W. Bange, G. Flores, J. Ledesma, M. Sarmiento, V. Leon, C. Robles, O. Moron, 20 pp, DOI: 10.3289/GEOMAR_REP_NS_2_2012
3	FS POSEIDON Fahrtbericht / Cruise Report POS427 – Fluid emissions from mud volcanoes, cold seeps and fluid circulation at the Don-_Kuban deep sea fan (Kerch peninsula, Crimea, Black Sea) – 23.02. – 19.03.2012, Burgas, Bulgaria - Heraklion, Greece, Ed.: J. Bialas, 32 pp, DOI: 10.3289/GEOMAR_REP_NS_3_2012
4	RV CELTIC EXPLORER EUROFLEETS Cruise Report, CE12010 – ECO2@NorthSea, 20.07. – 06.08.2012, Bremerhaven – Hamburg, Eds.: P. Linke et al., 65 pp, DOI: 10.3289/GEOMAR_REP_NS_4_2012
5	RV PELAGIA Fahrtbericht / Cruise Report 64PE350/64PE351 – JEDDAH-TRANSECT -, 08.03. – 05.04.2012, Jeddah – Jeddah, 06.04 - 22.04.2012, Jeddah – Duba, Eds.: M. Schmidt, R. Al-Farawati, A. Al-Aidaroos, B. Kürten and the shipboard scientific party, 154 pp, DOI: 10.3289/GEOMAR_REP_NS_5_2013
6	RV SONNE Fahrtbericht / Cruise Report SO225 - MANIHIKI II Leg 2 The Manihiki Plateau - Origin, Structure and Effects of Oceanic Plateaus and Pleistocene Dynamic of the West Pacific Warm Water Pool, 19.11.2012 - 06.01.2013 Suva / Fiji – Auckland / New Zealand, Eds.: R. Werner, D. Nürnberg, and F. Hauff and the shipboard scientific party, 176 pp, DOI: 10.3289/GEOMAR_REP_NS_6_2013
7	RV SONNE Fahrtbericht / Cruise Report SO226 – CHRIMP CHatham RIse Methane Pockmarks, 07.01. - 06.02.2013 / Auckland – Lyttleton & 07.02. – 01.03.2013 / Lyttleton – Wellington, Eds.: Jörg Bialas / Ingo Klaucke / Jasmin Mögeltönder, 126 pp, DOI: 10.3289/GEOMAR_REP_NS_7_2013
8	The SUGAR Toolbox - A library of numerical algorithms and data for modelling of gas hydrate systems and marine environments, Eds.: Elke Kossel, Nikolaus Bigalke, Elena Piñero, Matthias Haeckel, 168 pp, DOI: 10.3289/GEOMAR_REP_NS_8_2013
9	RV ALKOR Fahrtbericht / Cruise Report AL412, 22.03.-08.04.2013, Kiel – Kiel. Eds: Peter Linke and the shipboard scientific party, 38 pp, DOI: 10.3289/GEOMAR_REP_NS_9_2013
10	Literaturrecherche, Aus- und Bewertung der Datenbasis zur Meerforelle (Salmo trutta trutta L.) Grundlage für ein Projekt zur Optimierung des Meerforellenmanagements in Schleswig-Holstein. Eds.: Christoph Petereit, Thorsten Reusch, Jan Dierking, Albrecht Hahn, 158 pp, DOI: 10.3289/GEOMAR_REP_NS_10_2013
11	RV SONNE Fahrtbericht / Cruise Report SO227 TAIFLUX, 02.04. – 02.05.2013, Kaohsiung – Kaohsiung (Taiwan), Christian Berndt, 105 pp, DOI: 10.3289/GEOMAR_REP_NS_11_2013
12	RV SONNE Fahrtbericht / Cruise Report SO218 SHIVA (Stratospheric Ozone: Halogens in a Varying Atmosphere), 15.-29.11.2011, Singapore - Manila, Philippines, Part 1: SO218- SHIVA Summary Report (in German), Part 2: SO218- SHIVA English reports of participating groups, Eds.: Birgit Quack & Kirstin Krüger, 119 pp, DOI: 10.3289/GEOMAR_REP_NS_12_2013
13	KIEL276 Time Series Data from Moored Current Meters. Madeira Abyssal Plain, 33°N, 22°W, 5285 m water depth, March 1980 – April 2011. Background Information and Data Compilation. Eds.: Thomas J. Müller and Joanna J. Waniek, 239 pp, DOI: 10.3289/GEOMAR_REP_NS_13_2013

GEOMAR
Helmholtz-Zentrum für Ozeanforschung Kiel

GEOMAR Reports

No.	Title
14	RV POSEIDON Fahrtbericht / Cruise Report POS457: ICELAND HAZARDS Volcanic Risks from Iceland and Climate Change:The Late Quaternary to Anthropogene Development Reykjavík / Iceland – Galway / Ireland, 7.-22. August 2013. Eds.: Reinhard Werner, Dirk Nürnberg and the shipboard scientific party, 88 pp, DOI: 10.3289/GEOMAR_REP_NS_14_2014
15	RV MARIA S. MERIAN Fahrtbericht / Cruise Report MSM-34 / 1 & 2, SUGAR Site, Varna – Varna, 06.12.13 – 16.01.14. Eds: Jörg Bialas, Ingo Klaucke, Matthias Haeckel, 111 pp, DOI: 10.3289/GEOMAR_REP_NS_15_2014
16	RV POSEIDON Fahrtbericht / Cruise Report POS 442, "AUVinTYS" High-resolution geological investigations of hydrothermal sites in the Tyrrhenian Sea using the AUV "Abyss", 31.10. – 09.11.12, Messina – Messina, Ed.: Sven Petersen, 32 pp, DOI: 10.3289/GEOMAR_REP_NS_16_2014
17	RV SONNE, Fahrtbericht / Cruise Report, SO 234/1, "SPACES": Science or the Assessment of Complex Earth System Processes, 22.06. – 06.07.2014, Walvis Bay / Namibia - Durban / South Africa, Eds.: Reinhard Werner and Hans-Joachim Wagner and the shipbord scientific party, 44 pp, DOI: 10.3289/GEOMAR_REP_NS_17_2014
18	RV POSEIDON Fahrtbericht / Cruise Report POS 453 & 458, "COMM3D", Crustal Structure and Ocean Mixing observed with 3D Seismic Measurements, 20.05. – 12.06.2013 (POS453), Galway, Ireland – Vigo, Portugal, 24.09. – 17.10.2013 (POS458), Vigo, Portugal – Vigo, Portugal, Eds.: Cord Papenberg and Dirk Klaeschen, 66 pp, DOI: 10.3289/GEOMAR_REP_NS_18_2014
19	RV POSEIDON, Fahrtbericht / Cruise Report, POS469, "PANAREA", 02. – 22.05.2014, (Bari, Italy – Malaga, Spain) & Panarea shallow-water diving campaign, 10. – 19.05.2014, Ed.: Peter Linke, 55 pp, DOI: 10.3289/GEOMAR_REP_NS_19_2014
20	RV SONNE Fahrtbericht / Cruise Report SO234-2, 08.-20.07.2014, Durban, -South Africa - Port Louis, Mauritius, Eds.: Kirstin Krüger, Birgit Quack and Christa Marandino, 95 pp, DOI: 10.3289/GEOMAR_REP_NS_20_2014
21	RV SONNE Fahrtbericht / Cruise Report SO235, 23.07.-07.08.2014, Port Louis, Mauritius to Malé, Maldives, Eds.: Kirstin Krüger, Birgit Quack and Christa Marandino, 76 pp, DOI: 10.3289/GEOMAR_REP_NS_21_2014
22	RV SONNE Fahrtbericht / Cruise Report SO233 WALVIS II, 14.05-21.06.2014, Cape Town, South Africa - Walvis Bay, Namibia, Eds.: Kaj Hoernle, Reinhard Werner, and Carsten Lüter, 153 pp, DOI: 10.3289/GEOMAR_REP_NS_22_2014
23	RV SONNE Fahrtbericht / Cruise Report SO237 Vema-TRANSIT Bathymetry of the Vema-Fracture Zone and Puerto Rico TRench and Abyssal AtlaNtic BiodiverSITy Study, Las Palmas (Spain) - Santo Domingo (Dom. Rep.) 14.12.14 - 26.01.15, Ed.: Colin W. Devey, 130 pp, DOI: 10.3289/GEOMAR_REP_NS_23_2015
24	RV POSEIDON Fahrtbericht / Cruise Report POS430, POS440, POS460 & POS467 Seismic Hazards to the Southwest of Portugal; POS430 - La-Seyne-sur-Mer - Portimao (7.4. - 14.4.2012), POS440 - Lisbon - Faro (12.10. - 19.10.2012), POS460 - Funchal - Portimao (5.10. - 14.10.2013), POS467 - Funchal - Portimao (21.3. - 27.3.2014), Ed.: Ingo Grevemeyer, 43 pp, DOI: 10.3289/GEOMAR_REP_NS_24_2015
25	RV SONNE Fahrtbericht / Cruise Report SO239, EcoResponse Assessing the Ecology, Connectivity and Resilience of Polymetallic Nodule Field Systems, Balboa (Panama) – Manzanillo (Mexico), 11.03. -30.04.2015, Eds.: Pedro Martínez Arbizu and Matthias Haeckel, 204 pp, DOI: 10.3289/GEOMAR_REP_NS_25_2015

GEOMAR
Helmholtz-Zentrum für Ozeanforschung Kiel

GEOMAR Reports

No.	Title
26	RV SONNE Fahrtbericht / Cruise Report SO242-1, JPI OCEANS Ecological Aspects of Deep-Sea Mining, DISCOL Revisited, Guayaquil - Guayaquil (Equador), 29.07.-25.08.2015, Ed.: Jens Greinert, 290 pp, DOI: 10.3289/GEOMAR_REP_NS_26_2015
27	RV SONNE Fahrtbericht / Cruise Report SO242-2, JPI OCEANS Ecological Aspects of Deep-Sea Mining DISCOL Revisited, Guayaquil - Guayaquil (Equador), 28.08.-01.10.2015, Ed.: Antje Boetius, 552 pp, DOI: 10.3289/GEOMAR_REP_NS_27_2015
28	RV POSEIDON Fahrtbericht / Cruise Report POS493, AUV DEDAVE Test Cruise, Las Palmas - Las Palmas (Spain), 26.01.-01.02.2016, Ed.: Klas Lackschewitz, 17 pp, DOI: 10.3289/GEOMAR_REP_NS_28_2016
29	Integrated German Indian Ocean Study (IGIOS) - From the seafloor to the atmosphere - A possible German contribution to the International Indian Ocean Expedition 2 (IIOE-2) programme – A Science Prospectus, Eds.: Bange, H.W. , E.P. Achterberg, W. Bach, C. Beier, C. Berndt, A. Biastoch, G. Bohrmann, R. Czeschel, M. Dengler, B. Gaye, K. Haase, H. Herrmann, J. Lelieveld, M. Mohtadi, T. Rixen, R. Schneider, U. Schwarz-Schampera, J. Segschneider, M. Visbeck, M. Voß, and J. Williams, 77pp, DOI: 10.3289/GEOMAR_REP_NS_29_2016
30	RV SONNE Fahrtbericht / Cruise Report SO249, BERING – Origin and Evolution of the Bering Sea: An Integrated Geochronological, Volcanological, Petrological and Geochemical Approach, Leg 1: Dutch Harbor (U.S.A.) - Petropavlovsk-Kamchatsky (Russia), 05.06.2016-15.07.2016, Leg 2: Petropavlovsk-Kamchatsky (Russia) - Tomakomai (Japan), 16.07.2016-14.08.2016, Eds.: Reinhard Werner, et al., DOI: 10.3289/GEOMAR_REP_NS_30_2016
31	RV POSEIDON Fahrtbericht/ Cruise Report POS494/2, HIERROSEIS Leg 2: Assessment of the Ongoing Magmatic-Hydrothermal Discharge of the El Hierro Submarine Volcano, Canary Islands by the Submersible JAGO, Valverde – Las Palmas (Spain), 07.02.-15.02.2016, Eds.: Hannington, M.D. and Shipboard Scientific Party, DOI: 10.3289/GEOMAR_REP_NS_31_2016
32	RV METEOR Fahrtbericht/ Cruise Report M127, Extended Version, Metal fluxes and Resource Potential at the Slow-spreading TAG Midocean Ridge Segment (26°N, MAR) – Blue Mining@Sea, Bridgetown (Barbados) – Ponta Delgada (Portugal) 25.05.-28.06.2016, Eds.: Petersen, S. and Shipboard Scientific Party, DOI: 10.3289/GEOMAR_REP_NS_32_2016
33	RV SONNE Fahrtbericht/Cruise Report SO244/1, GeoSEA: Geodetic Earthquake Observatory on the Seafloor, Antofagasta (Chile) – Antofagasta (Chile), 31.10.-24.11.2015, Eds.: Jan Behrmann, Ingo Klaucke, Michal Stipp, Jacob Geersen and Scientific Crew SO244/1, DOI: 10.3289/GEOMAR_REP_NS_33_2016
34	RV SONNE Fahrtbericht/Cruise Report SO244/2, GeoSEA: Geodetic Earthquake Observatory on the Seafloor, Antofagasta (Chile) – Antofagasta (Chile), 27.11.-13.12.2015, Eds.: Heidrun Kopp, Dietrich Lange, Katrin Hannemann, Anne Krabbenhoeft, Florian Petersen, Anina Timmermann and Scientific Crew SO244/2, DOI: 10.3289/GEOMAR_REP_NS_34_2016

For GEOMAR Reports, please visit:
https://oceanrep.geomar.de/view/series/GEOMAR_Report.html

Reports of the former IFM-GEOMAR series can be found under:
https://oceanrep.geomar.de/view/series/IFM-GEOMAR_Report.html

GEOMAR
Helmholtz-Zentrum für Ozeanforschung Kiel

Das GEOMAR Helmholtz-Zentrum für Ozeanforschung Kiel ist Mitglied der Helmholtz-Gemeinschaft Deutscher Forschungszentren e.V.

The GEOMAR Helmholtz Centre for Ocean Research Kiel is a member of the Helmholtz Association of German Research Centres

Helmholtz-Zentrum für Ozeanforschung Kiel / Helmholtz Centre for Ocean Research Kiel
GEOMAR
Dienstgebäude Westufer / West Shore Building
Düsternbrooker Weg 20
D-24105 Kiel
Germany

Helmholtz-Zentrum für Ozeanforschung Kiel / Helmholtz Centre for Ocean Research Kiel
GEOMAR
Dienstgebäude Ostufer / East Shore Building
Wischhofstr. 1-3
D-24148 Kiel
Germany

Tel.: +49 431 600-0
Fax: +49 431 600-2805
www.geomar.de